DEVELOPMENT OF CELLULAR AND MOLECULAR METHODS TO CHARACTERIZE THE MECHANISMS OF COMMON INFECTIOUS- AND NON-INFECTIOUS-BASED DISEASES OF POULTRY

A Dissertation

by

DAN ZHAO

Submitted to the Office of Graduate and Professional Studies of
Texas A&M University
in partial fulfillment of the requirements for the degree of

DOCTOR OF PHILOSOPHY

Chair of Committee,	Morgan Farnell
Co-Chair of Committee,	Yuhua Farnell
Committee Members,	Michael Kogut
	Kenneth Genovese
Head of Department,	Audrey McElroy

May 2021

Major Subject: Poultry Science

ABSTRACT

Poultry production plays an important role in the global economy. Nevertheless, common infectious- and non-infectious-diseases of poultry negatively affect public health and cause economic losses. Salmonellosis is one of the infectious diseases caused by *Salmonella* infection. *Salmonella* Typhimurium (ST) is one of the most common serotypes that cause human gastrointestinal disease globally. Chickens do not show any clinical symptoms after ST infection. What makes the coexistence of ST in chicken gut is not completely understood. The intestinal organoid (IO) model has been widely used for studying molecular mechanisms of host-pathogen interactions in mammals. However, there are limited avian IO studies. The development of long-term avian IO for poultry research is needed. Recently, exosomes are reported to play important roles in host immunity to pathogen infection by regulating exosomal microRNA (miRNA) levels. However, the mechanism of exosomes in host-pathogen in chickens remains to be elucidated. One of the common non-infectious diseases in poultry is wooden breast (WB), a degenerative myopathy. While the etiology of WB is unknown, localized hypoxia and decreased lactate levels in WB indicate the presence of altered lactate metabolism. Therefore, the aims of these studies were to 1) develop avian IO and optimize their culture conditions, 2) elucidate the effects of ST on exosomal miRNA levels in broiler serum, and 3) investigate if altered lactate homeostasis was present in WB muscles.

We have successfully developed and characterized the avian IO that recapitulates intestinal epithelial structure *in vivo*. The finding of up-regulated miRNAs in serum-derived exosomes due to the exposure of ST, while preliminary, suggests that exosomes

may act as potential immunomodulators that are easily delivered to cells of different organs. Wooden breast muscles of broilers exhibited altered major proteins involved in lactate metabolism, suggesting that the development of agents targeting this pathway may provide a potential therapeutic treatment for reducing the incidence of WB myopathy. Ultimately, my work has a considerable impact on the future avian *ex vivo* intestinal study and helps us better understand the mechanism the *Salmonella* infection in poultry and WB, eventually leading to the discovery of pathogen and WB intervention strategies in poultry.

ACKNOWLEDGEMENTS

I would like to thank my committee co-chair, Dr. Yuhua Farnell for supervising my research and editing all my papers. I also would like to thank my committee chair and members, Drs. Morgan Farnell, Michael Kogut, and Kenneth Genovese for their help and guidance with my studies.

I would like to sincerely thank my friends and colleagues for making my time at Texas A&M University a great experience.

Finally, I am so grateful to have the support and understanding from my parents, Xiaoshan Zhao and Jiange Wang, and my little sister, Qing Zhao.

CONTRIBUTORS AND FUNDING SOURCES

Contributors

All of the studies in this dissertation were conducted and supervised by committee chair Dr. Morgan B. Farnell, and co-chair, Dr. Yuhua Z. Farnell at the Texas A&M University Department of Poultry Science, and committee members, Drs. Michael H. Kogut and Kenneth J. Genovese from the Southern Plains Agricultural Research Center, Agricultural Research Service (ARS), US Department of Agriculture (USDA), College Station, TX.

All animal experiments were performed with the help from Dr. Farnell's lab members, Dr. Xi Wang (post-doc), Ms. Megan Pineda, and Ms. Allison Milby. Dr. Haiqi He from USDA-ARS at College Station TX helped blood collection. Small RNA libraries were constructed by Dr. Chuan-Yu Hsu of Institute for Genomics, Biocomputing and Biotechnology at Mississippi State University. Bioinformatic analyses of small RNA sequence data were performed by Dr. Wenli Li of the US Dairy Forage Research Center of USDA-ARS at Madison, WI. Drs. Robert Chapkin and Laurie Davidson from the Program in Integrative Nutrition & Complex Diseases at Texas A&M AgriLife Research provided the all-in-one BZ-X800 Keyence Fluorescence Microscope and BZ X800 Keyence Fluorescence Microscope. Dr. Robert Droleskey of USDA-ARS captured the images of exosomes using a transmission electron microscope.

The Ag Women Excited to Share Opinions, Mentoring & Experiences faculty group in the College of Agriculture and Life Sciences at Texas A&M University offered the assistance with editing the manuscripts. Initial group financial support was through NSF

ADVANCE Institutional Transformation Award 1008385, with continued support from the college.

Funding Sources

Graduate studies were supported by 1) A Merit Fellowship from the Poultry Science Department of College of Agriculture and Life Science at Texas A&M University from Sept. 2016 to Aug. 2019; 2) Department of Poultry Science Dr. Morgan Farnell's start-up funds, and 3) Tom Slick Graduate Research Fellowship from College of Agriculture and Life Science at Texas A&M University from Jan. 2020-Dec. 2020, 4) Department of Poultry Science Dr. Morgan Farnell's start-up funds from Jan. 2021-May. 2021.

All of work in these studies were also supported by the USDA ARS #505584-97090. Its contents are solely the responsibility of the authors and do not necessarily represent the official views of the USDA.

NOMENCLATURE

3’-UTR	3’ untranslated region
3D	Three-dimensional
BMP	Bone morphogenetic protein
cDNA	Complementary DNA
CHIR	CHIR 99021
Ct	Cycle threshold
DE	Differentially expressed
ECL	Enhanced chemiluminescence
EGF	Epidermal growth factor
H&E	Haemotoxylin and eosin
ILVs	Intraluminal vesicles
IO	Intestinal organoids
LDH H	LDH heart subunit
LDH M	LDH muscle subunit
LDHA	Lactate dehydrogenases A
LDHB	Lactate dehydrogenases B
Lgr5	Leucine-rich repeat containing G-protein coupled receptor
MCT1	Monocarboxylate transporters 1
MCT4	Monocarboxylate transporters 4
MiRNA	MicroRNA

MVBs	Multi-vesicular bodies
NB	Normal breast
NN	Nalidixic acid and novobiocin
nts	Nucleotides
NTA	Nanoparticle tracking analysis
OGM	Organoid growth media
Pre-miRNA	Precursor miRNA
Pri-miRNA	Primary miRNA
RIPA	Radioimmunoprecipitation assay
RT-PCR	Reverse transcription polymerase chain reaction
RV	Rappaport-Vassiliadis
ST	*Salmonella* Typhimurium
TBS	Tris-buffered saline
TBST	TBS with 0.1% Tween twenty
TCA	Tricarboxylic acid cycle
TEM	Transmission electron microscope
TLR2	Toll-like receptor 2
TSB	Tryptic soy broth
USDA	United States Department of Agriculture
VA	Valproic acids
WB	Wooden breast

TABLE OF CONTENTS

Page

ABSTRACT ii

ACKNOWLEDGEMENTS iv

CONTRIBUTORS AND FUNDING SOURCES v

NOMENCLATURE vii

TABLE OF CONTENTS ix

LIST OF FIGURES xii

LIST OF TABLES xiv

1. INTRODUCTION 1

1.1. The influence of *Salmonella* Typhimurium in poultry 3
1.2. The traditional models for *Salmonella* studies 4
1.3. Generation of intestinal organoids review 5
1.3.1. Composition of intestinal epithelium 5
1.3.2. Definition of intestinal organoids 7
1.3.3. History of intestinal organoids 8
1.3.4. Development of avian intestinal organoids 9
1.3.5. Establishment of intestinal organoids 10
1.3.6. The application of organoids 14
1.4. Exosomes and microRNAs review 15
1.4.1. Bio-generation and composition of exosomes 15
1.4.2. The roles of host-derived exosomes in health and disease 16
1.4.3. The roles of pathogen-derived outer membrane vesicles in disease 17
1.4.4. The microRNA bio-genesis and mechanism of miRNA-mRNA regulation 18
1.4.5. Regulation of miRNA in host-pathogen interactions 20
1.5. Wooden breast review 21
1.5.1. History of skeletal muscle myopathies in the broiler industry 21
1.5.2. Classification of wooden breast 22
1.5.3. The etiologies of wooden breast 23
1.5.4. The lactate metabolism pathway 24
1.5.5. MicroRNA-375 27
1.6. References 28

2. AVIAN INTESTINAL ORGANOIDS FROM CRYPTS TO ENTEROIDS: ESTABLISHMENT AND CHARACTERIZATION OF AVIAN INTESTINAL ORGANOIDS 45

2.1. Introduction 45
2.2. Materials and methods 48
2.2.1. Experimental birds 48
2.2.2. Crypt isolation 48
2.2.3. The collection of conditioned media (CM) from L-WRN cell cultures 48
2.2.4. Intestinal crypt culture and the generation of organoids 49
2.2.5. Imaging of the avian IO growth 49
2.2.6. Passaging avian organoid cultures 49
2.2.7. Cryopreservation of organoids 49
2.2.8. Histochemistry 50
2.2.9. Immunohistochemistry 50
2.2.10. Protein extraction and western blotting 50
2.2.11. Total RNA extraction and reverse transcription PCR (RT-PCR) 51
2.2.12. The effects of OGM supplemented with VA and CHIR on avian small IO growth 53
2.2.13. Statistical evaluation 53
2.3. Results 53
2.3.1. Isolation of intestinal crypts of avian origin 53
2.3.2. Time course of avian ceca-derived organoid growth 54
2.3.3. Growth development of avian organoids from the ceca and small intestines of broiler, layer, or embryo origins at different ages 56
2.3.4. Immunofluorescence staining of avain cecal organoid 56
2.3.5. Characterization of cell populations of organoids by immunoblotting and RT-PCR 57
2.3.6. The OGM supplemented with both VA and CHIR increased avian IO size 59
2.4. Discussion 61
2.5. References 64

3. CHARACTERIZATION OF THE EFFECT OF *SALMONELLA* TYPHIMURIUM ON SERUM-DERIVED EXOSOMAL MIRNAS IN CHICKS 69

3.1. Introduction 69
3.2. Materials and methods 71
3.2.1. *Salmonella* Typhimurium culture 71
3.2.2. Experimental design and birds 71
3.2.3. Enumeration of *Salmonella* Typhimurium in cecal contents of broilers 72
3.2.4. Blood sample collection and serum isolation 72
3.2.5. Exosome isolation 73
3.2.6. Size distribution and concentration of exosomes by nanoparticle tracking analysis (NTA) 73
3.2.7. Transmission electron microscopy (TEM) 74

3.2.8. Small RNA extraction, quantification, library construction, and sequencing 74
3.2.9. Bioinformatics analysis and differential miRNA expression analysis 76
3.2.10. Statistical analysis 76
3.3. Restults 76
3.3.1. Confirmation of ST colonization in cecal contents of ST-challenged broiler 76
3.3.2. Size distribution and concentration of serum-derived exosomes 77
3.3.3. Characterization of exosome morphology and size by TEM 79
3.3.4. Chicken serum-derived exosomes contain miRNAs 80
3.3.5. Unique exosomal miRNA profiles and prediction of their target gene and biological pathways 81
3.3.6. Differential expression of miRNAs in the ST group compared to the Con group 83
3.3.7. Multiple sequence alignment of the gga-miR-34/449 family 85
3.3.8. The analyses of target gene and biological pathways of the gga-miR-34/449 family with seed sequences 87
3.4. Discussion 90
3.5. References 93

4. ALTERED EXPRESSION OF LACTATE DEHYDROGENASE AND MONOCARBOXYLATE TRANSPORTER INVOLVED IN LACTATE METABOLISM IN BROILER WOODEN BREAST 99

4.1. Introduction 99
4.2. Materials and methods 102
4.2.1. Sample collection 102
4.2.2. Total RNA and small RNA extraction 102
4.2.3. Quantitative reverse transcription polymerase chain reaction (RT-PCR) for mRNAs 103
4.2.4. Quantitative RT-PCR for miR-375 104
4.2.5. Western blotting analysis 105
4.2.6. Specific LDH enzyme activity assay 106
4.2.7. Statistical analysis 107
4.3. Results 107
4.3.1. Expression of the LDHA and LDHB mRNA and protein inWB muscles compared to NB muscles 107
4.3.2. The levels of miR-375 expression in WB did not differ from those of NB tissues 109
4.3.3. WB has decreased specific LDH enzymatic activities that convert pyruvate to lactate 110
4.3.4. Gene expression of MCT1 and MCT4 110
4.4. Discussion 112
4.5. References 119

5. CONCLUSIONS 126

LIST OF FIGURES

Page

Figure 1.1 The intestinal epithelium structure and composition of cells 7

Figure 1.2 Cross section diagram of intestinal organoid structure and cell populations ... 8

Figure 1.3 The generation and composition of exosomes 16

Figure 1.4 Biogenesis of a miRNA 19

Figure 1.5 Regulation of miRNAs 20

Figure 1.6 The appearance of normal and wooden breast 23

Figure 1.7 Schematic representation of the lactate metabolism pathway of a broiler muscle cell 25

Figure 1.8 The tetramers of LDH 26

Figure 2.1 Description of the establishment of crypt-derived 3D avian intestinal organoids 54

Figure 2.2 Time course of avian ceca-derived organoid growth from day-one-old broilers 55

Figure 2.3 Morphology of avian intestinal organoids 56

Figure 2.4 Immunofluorescence staining of avian cecal organoids 57

Figure 2.5 Western blot analysis of different cell types from avian cecal organoids using protein biomarkers 58

Figure 2.6 RT-PCR confirms cell populations of organoids using cell marker genes 58

Figure 2.7 The effect of valproic acid and CHIR99021 on avian small intestinal organoid growth 60

Figure 3.1 Nanoparticle tracking analysis of serum-derived exosomes 78

Figure 3.2 Different size distributions (D10, D50, D90) of serum-derived exosomes from Con (n=4) and ST (n=4) groups 79

Figure 3.3 Negative-staining transmission electron microscopy of serum exosomes 79

Figure 3.4 Size description of small RNA isolated from exosomes 80

Figure 3.5 Venn diagram summary of unique and DE miRNAs in exosomes from serum of Con and ST groups 82

Figure 3.6 DAVID functional GO analysis of KEGG pathway, MF (molecular function), CC (cell component), and BP (biological process) enrichment for the combination of unique gga-mir-1788-5p, 3530-5p, 383-5p in ST group. .. 83

Figure 3.7 Multiple sequence alignment of gga-miR-34/449 family 86

Figure 3.8 DAVID functional GO analysis of biological processes enrichment 88

Figure 3.9 DAVID functional GO analysis of biological process (BP), cell component (CC), molecular function (MF), and KEGG pathway of gga-mir-449a, gga-mir-449b-5p, gga-mir-449c-5p, gga-mir-449d-5p. 89

Figure 3.10 DAVID functional GO analysis of biological processes enrichment for gga-mir-34b-5p, gga-mir-34c-5p, gga-mir-449a, gga-mir-449b-5p, gga-mir-449c-5p, and gga-mir-449d-5p 90

Figure 4.1 The altered mRNA and protein levels of LDHA and LDHB in WB compared to NB tissues 108

Figure 4.2 The levels of miR-375 expression in WB did not differ from those of NB tissues 109

Figure 4.3 LDH enzyme activity that converts lactate to pyruvate is decreased in WB tissue compare to NB tissues 110

Figure 4.4 The altered mRNA and protein levels of MCT1 and MCT4 in WB compared to NB tissues 111

Figure 4.5 Schematic representation of the lactate metabolism pathway of broiler muscle affected with wooden breast (WB) myopathy (B) compared to normal breast muscle (A) 113

LIST OF TABLES

Page

Table 2.1 Summary of primers used for RT-PCR analysis 52

Table 3.1 Evaluation of *Salmonella* Typhimurium colonization in ceca of broiler chickens 77

Table 3.2 Summary of miRNA profiles only found in Con and ST group 82

Table 3.3 Differentially expressed exosomal miRNAs of the ST group compared to the Con group 84

Table 4.1 Primer sequences used for qRT-PCR 104

1. INTRODUCTION

Over the last 20 years, the global poultry industry provided approximately 107 million tons of meat and 1.3 trillion eggs per year, which play an important role in the global economy (FAOSTAT, 2019). In poultry, common infectious and non-infectious diseases cause considerable economic losses and human foodborne illnesses. One of the most common infectious diseases is salmonellosis. The Centers for Disease Control and Prevention (CDC) estimate that *Salmonella* cause 1.35 million cases of human foodborne illness and 420 deaths annually in the United States, including over 2,000 serotypes (CDC, 2021). *Salmonella* Typhimurium (ST) is one of the *Salmonella* serotypes that causes human gastrointestinal disease globally. It is an intracellular pathogen that does not cause any clinical disease symptoms in the infected adult chickens. Thus, the poultry products contaminated with ST are one of the main sources of ST in food production resulting in huge economic losses (Galis et al., 2013). Chicken-ST interaction in the gut is not completely understood. Numerous studies have studied the mechanisms of ST infection in chickens at the cellular and molecular level using the primary chicken gut epithelial cells or human colorectal adenocarcinoma cells (Velge et al., 2002; Martinez-Argudo and Jepson, 2008; Rath et al., 2018). However, the primary cells have a limited lifespan and restricted dividing potential, and human cancer cell lines cannot represent the real nature of the avian intestinal epithelial cells. The appropriate model for avian intestinal study is needed. The intestinal organoid (IO) model has been widely used for studying molecular mechanisms of host-pathogen interactions in mammals but not in avian. Intestinal organoids are three-dimensional structures and are composed of organ-specific cell types,

which can be derived from pluripotent stem cells either from embryonic or adult intestines. They mimic organ-specific structures and functions. Thus, the first project was to establish avian intestinal organoids and characterize their cell populations.

Although the pathogenesis of *Salmonella* has been revealed based on the significant alterations of several proteins and mRNAs involved in avian immune responses by proteomic, kinome array, and RNA sequencing methods (Kogut et al., 2016; Packialakshmi et al., 2016; Li et al., 2018). The mechanism of chicken-ST interactions is still not well understood. Recently, host-derived exosomes consisting of molecular signatures, especially microRNAs (miRNAs), have been implicated as novel mediators in host-pathogen interactions. Exosomes are phospholipid bilayer extracellular vesicles (30 to 150 nm in diameter) consisting of miRNAs, mRNAs, DNAs, proteins, and lipids (Colombo et al., 2014; Li et al., 2014; Zhang et al., 2015). They are secreted by different cell types into a variety of body fluids, including serum, urine, and saliva (Van Niel et al., 2001; Blanchard et al., 2002; Pisikun et al., 2004; Caby et al., 2005; Fauré et al., 2006). MicroRNAs are small non-coding RNAs, ranging from 18 to 25 nucleotides (nts) in length, that are considered as the post-transcriptional regulators by regulating the translation of their target mRNAs. The second project was to investigate the effects of ST challenge on miRNA regulation in serum-derived exosomes of broilers using next-generation sequencing and analyze the target genes and biological pathways of the differential expressed (DE) exosomal miRNA that were involved in the host response to ST.

One of the common non-infectious diseases in the poultry industry is wooden breast (WB), a degenerative myopathy in fast-growing commercial broilers and results in significant economic losses in the broiler industry due to poor meat quality. Wooden

breasts have diffuse hardened areas and pale ridge-like bulges at the caudal end (Sihvo et al., 2014; Bailey et al., 2015; Tasoniero et al., 2016). Sihvo et al. (2014) reported a high incidence of WB for 48-73% in commercial broilers. Several studies have investigated the mechanism of WB using high throughput molecular methods including RNA sequencing, proteomics, and metabolomics methods indicating changes of genes and proteins that were associated with oxidative stress, hypoxia, cellular repair, and metabolic perturbations (Mutryn et al., 2015; Abasht et al., 2016). While the etiology of WB is not fully understood, the presence of localized hypoxia and decreased lactate levels in WB that indicated the presence of altered lactate metabolism (Abasht et al., 2016). Therefore, the third project was to evaluate the expression levels of the major signaling molecules that control the lactate metabolism, including lactate dehydrogenases (LDHA & B) and monocarboxylate transporters (MCT1 & 4) in WB muscles.

In summary, the specific aims of my project were to develop and characterize avian IO model from small intestines and ceca of birds, evaluate the effects of *Salmonella* infection in regulating exosomal miRNA in serum of broilers, and investigate the roles of major genes that were involved in lactate metabolism in WB muscles, which are common infectious- and non-infectious-diseases in poultry, respectively.

1.1. The influence of *Salmonella* Typhimurium in poultry

Salmonella causes foodborne illnesses in approximately 1.2 million people every year in the United States, a major concern for human health, resulting in direct cost of $365 million annually in US (CDC, 2019; Scallan et al., 2011). *Salmonella* Typhimurium is one of the most common *Salmonella* serotypes and causes gastrointestinal disease in humans globally (Scallan et al., 2011; CDC, 2014). It is a Gram-negative, rod-shaped, and

flagellated anaerobe. One of the main sources of ST is poultry products, including meat products from broiler chickens and egg products from layer chickens (Galis et al., 2013). *Salmonella* Typhimurium can infect day-old birds and colonize in ceca without any clinical symptoms, which will be shed and contaminate the other birds (Hur et al., 2012). Zoonotic infections are a big concern because they affect public health and cause significant economic losses for producers and consumers. Understanding the mechanism of ST infection in chickens may effectively decrease or eliminate ST contamination in poultry products.

1.2. The traditional models for *Salmonella* studies

Many experimental models are employed to study *Salmonella* infection, including *in vivo* and *in vitro* models. The *in vivo* models are widely used to investigate alteration of gene expression at mRNA and protein levels in immune tissues that are involved in avian immune response after *Salmonella* infection using microarray analysis (van Hemert et al., 2006), RT-PCR (Haghighi et al., 2008), proteomic (Packialakshmi et al., 2016), kinomic (Kogut et al., 2016), and RNA sequencing methods (Li et al., 2018). Compared to the animal models, the *in vitro* cell line models provide homogeneous cell populations and consistent environment to evaluate the molecular mechanisms of host cell-pathogen interactions. However, suitable *in vitro* models for avian intestinal studies are limited. The majority of published avian studies are based on short-term cultured avian primary cell lines, such as fibroblast cell lines and enterocyte cell lines derived from chicken embryos (Caldwell et al., 1993; Velge et al., 2002; Dimier-Poisson et al., 2004; Rath et al., 2018) or commercial cell lines from different species, including human colorectal adenocarcinoma Caco-2 cells (Martinez-Argudo and Jepson, 2008; Salehi et al., 2017). Primary cells have a

limited lifespan and restricted dividing potential. Immortalized commercial cell lines, which are homogeneous cell populations, normally do not represent the normal cell structures of the avian intestine. Consequently, an available *in vivo* intestinal model is needed for avian intestinal research.

1.3. Generation of intestinal organoids review

1.3.1. Composition of intestinal epithelium

The intestine is a critical site for food digestion, nutrient absorption, and immune response, which consists of villi and crypts as shown in Fig. 1.1. Villi are finger-like structures that are extended into the intestinal lumen. Crypts are invaginations around the villi and are the main location for intestinal stem cells and Paneth cells in mammalian system (Cheng and Leblond, 1974). The spatial properties of the crypt protect the stem cells from the direct connection to the luminal environment containing digestive enzymes and microbial products (Kaiko et al., 2016; Gehart and Clevers, 2018). Cells at the tip of the villus undergo apoptosis and shed into the intestinal lumen after 3 to 4 days in the chicken (Uni et al., 2000). Crypt stem cells are continuously differentiated into progenitor cells to replace worn-out matured cells in the villus.

The intestinal epithelium contains heterogeneous cell populations such as enterocytes, goblet cells, enteroendocrine cells, Paneth cells, and stem cells (Fig. 1.1). Enterocytes, columnar epithelial cells, are the predominant cell type that lines the small and large intestines. One of the main function of the enterocyte is nutrient absorption based on their microvillar membrane, also named as “brush-border”. The microvillar membrane contain thousands of microvilli with digestive enzymes and carrier proteins (McConnell et al., 2011). Goblet cells are named by their goblet-like shape, containing abundant packaged

mucus laden granules in apical section. Goblet cells secret mucus to protect the intestinal epithelium from digestion damage (Klasing, 1999). In the chicken, the mucin 2 (Muc2), the predominant mucin glycoprotein in mucus secreted by goblet cells, are widely used as molecular biomarker for goblet cells (Zhang et al., 2015). Enteroendocrine cells are considered as endocrine cells that secret peptide hormones related to metabolism that maintain the homeostasis of the intestine, including regulation of enzymatic secretion, intestinal peristalsis, appetite and satiety. Chromogranin A is present in secretary vesicles of enteroendocrine cells and normally considered as their cell biomarker (Gunawardene et al., 2011). Paneth cells are positioned adjacent to stem cells of crypts, supporting stem cell proliferation and protecting stem cells by secreting antimicrobial molecules such as lysozyme, which is the marker for Paneth cells (Wang et al., 2016; Gassler, 2017; Gehart and Clevers, 2019). They play a crucial role in maintaining the intestinal organoids by expressing wingless-related integration (Wnt), epidermal growth factor (EGF), and Notch ligands, which are involved in three main signaling pathways (Sato et al., 2011; Clevers and Bevin, 2013). The intestinal stem cells identified by their special gene marker called the leucine-rich repeat containing G-protein coupled receptor 5 (Lgr5 ; Barker et al., 2007), are located in the intestinal crypts, repopulate the intestinal epithelial cells and modulating homeostasis of the intestine (Clevers, 2013; Beumer and Clevers, 2016).

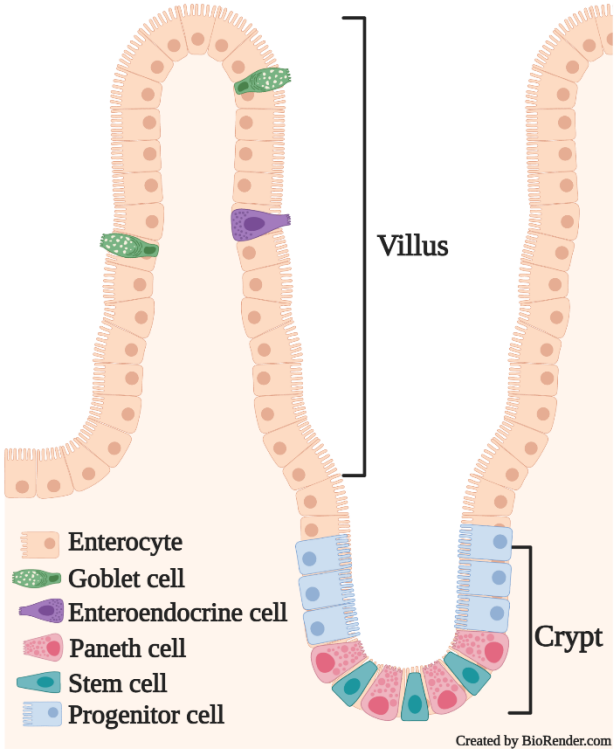

Figure 1.1 The intestinal epithelium structure and composition of cells. The intestinal epithelium is arranged into many villi and crypts. A villus consists of enterocytes, goblet cells, and enteroendocrine cells. The crypt region contains Paneth cells and stem cells, which are normally adjacent to each other. The mature enterocytes on the tip of villi continuously undergo apoptosis and are sloughed off. The stem cells residing in the crypts keep proliferating to produce progenitor cells for different functional mature cells. The figure was created in BioRender by Dan Zhao.

1.3.2. Definition of intestinal organoids

Organoids are defined as a mimic of an organ following three main capabilities: first, they exhibit multiple organ-specific cell types; second, they recapitulate organ-specific functions; third, they are organized into a structure similar to the organ in vivo (Finkbeiner and Spence, 2013; Lancaster and Knoblich, 2014). Accordingly, the gastrointestinal organoid (also named as “mini-gut” or enteroid) is described as a self-

renewing three-dimensional intestinal in vitro model that retains multiple intestinal cell types, basic intestinal structure, and functions (Fig. 1.2).

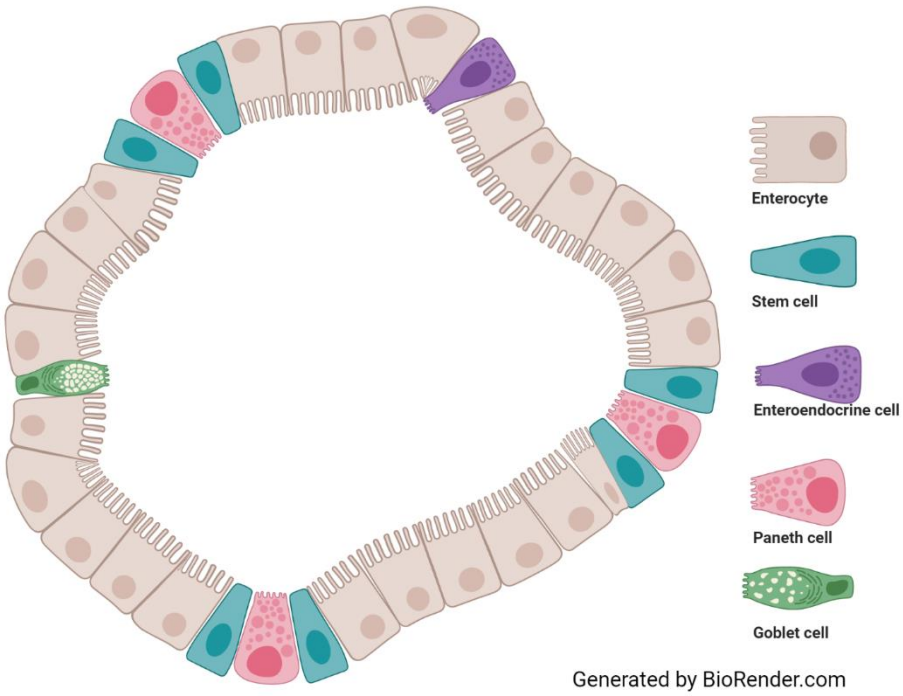

Figure 1.2 Cross section diagram of intestinal organoid structure and cell populations. The intestinal organoids consist of enterocytes, stem cells, enteroendocrine cells, Paneth cells, and goblet cells. The figure was generated in BioRender by Dan Zhao.

1.3.3. History of intestinal organoids

In 1907, Dr. Wilson first demonstrated the self-organization function of sponge cells, which has laid the foundation for *in vitro* organism regeneration. Accordingly, the hypothesis to rebuild a functional organ in vitro was intensely and extensively investigated. A few decades later, stem cell lines were established, including pluripotent stem cells, and embryonic stem cells (Evans, 1981; Martin, 1981; Thomson et al., 1998), which led to the development of a three-dimensional (3D) cell culture system. However, no success was

made in the development of intestinal organoids (IO) until 2009. Sato et al. (2009) isolated pure $Lgr5^+$ stem cells from mouse intestinal crypts and first successfully established the mouse IO using Matrigel^{TM}, containing various intestinal-specific cell types and maintaining crypt-villus structure. Ootani et al. (2009) also described long-term cultures of mice small and large IO in a collagen gel. Compared to conventional homogenous two-dimensional cultures, organoids recapitulate cell composition, architecture, and function of the corresponding tissue or organ, which better represents the real biological processes in vivo (Finkbeiner and Spence, 2013; Behjati et al., 2014; Huch et al., 2015; Li et al., 2016; Duarte et al., 2018). Subsequently, intestinal organoids are widely developed and used in human health and disease.

1.3.4. Development of avian intestinal organoids

To our knowledge, the first avian IO were reported by the Pierzchalska group in Poland in 2012, following the protocol from Sato et al. (2009). They isolated crypts from the small intestine of 18-day-old chicken embryos and established chicken small IO, which consisted of enterocytes, identified by the specific marker villin, and stem cells, characterized by stem cell biomarker Sox-9. The same research team developed the hanging drop culture system for small IO derived from the 18-day-old chicken embryos (Panek et al., 2018). Subsequently, Pierzchalska and colleges demonstrated that probiotic bacteria or the synthetic TLR2 ligands promoted chicken embryonic IO (Pierzchalska et al., 2017) and described the migration and fusion of chicken embryonic intestinal organoids (Pierzchalska et al., 2019). Powell and Behnke (2017) established the long-term culture of cecal IO that can be cultured up to 125 days and passaged 35 times. However, they did not fully characterize cecal-derived organoids. Li et al. (2018) established IO

derived from the jejunum of 2 to 3-week old chickens and identified a villus structure with transmission electron microscopy. Compared to mouse small IO, the crypt-villus structures are barely observed in avian IO (Pierzchalska et al., 2012).

Studies on avian IO are limited, the cell populations in the intestinal organoids are not fully characterized, and the development of long-term cultures of intestinal organoids for poultry research is lacking. Therefore, this study was aimed to generate crypt-derived organoids from chicken intestines, optimize conditions for cell growth and enrichments, passages, cryopreservation, and to characterize avian IO.

1.3.5. Establishment of intestinal organoids

There are three essential elements involved in establishing IO, including the sources of stem cells, extracellular matrix substitutes, growth factors and small molecules that regulate several important signaling pathways described below. The stem cells include pluripotent and adult stem cells, which can be isolated from intestinal crypts. An extracellular matrix substitute, such as Matrigel™, is a 3D microenvironment mimicking an *in vivo* environment. The activation of essential signaling pathways, including Wnt, Notch, EGF, and bone morphogenic protein (BMP) pathways (Miura and Suzuki, 2018), are needed to maintain stem cell proliferation and differentiation.

1.3.5.1. Stem cells for intestinal organoids generation

1.3.5.1.1. Pluripotent stem cells

Pluripotent stem cells can be differentiated into many cell types. Human IO have been established from pluripotent stem cells, including embryonic stem cells and induced pluripotent stem cells (Spence et al., 2011). These human IO isolated from intestinal crypts contained not only epithelial cells, but also mesenchymal cells. *In vivo*, the interaction

between epithelial cells and mesenchymal cells are necessary for intestinal cell proliferation and differentiation (Powell et al., 2011). Organoids derived from pluripotent stem cells must be provided stage-appropriate and -specific medium during cell proliferation and differentiation due to the organoids are developed from directed differentiation of homogeneous cell types (McCracken et al., 2014; Camp et al., 2017; Quadrato et al., 2017). Induced pluripotent stem cell-derived IO are widely used in human studies due to the limitation of availability of human intestinal samples.

1.3.5.1.2. Intestinal adult stem cells

Adult stem cells are capable of self-renewing and generate organ-specific mature cells. They play a crucial role in maintaining organ or tissue homeostasis. Mouse intestinal stem cells reside in crypts and are adjacent to Paneth cells, which were first described by Cheng and Leblond in 1974. Their specific gene marker, Lgr5, a target gene of the Wnt signaling pathway, was identified and was commonly employed to characterize crypt stem cells (Barker et al., 2007). Single sorted $Lgr5^+$ stem cell from mouse small intestine in a defined culture medium formed IO with crypt-villus unit that consisted of various mature intestinal cell types (Sato et al., 2009). The $Lgr5^+$ stem cells have a rapid cell division rate that the average cell cycle time is about 21.5 hr (Schepers et al., 2011). In addition, there are other quiescent and low-cycling stem cells in mammalian system, identified by the several specific markers including Bmi1, Lrig1, Hopx, and mTert in mice (Baker et al., 2012). They are able to be activated and replace damaged Lgr5+ stem cells in mammalian system (Montgomery et al., 2011).

1.3.5.2. Extracellular matrix substitute

In a 3D culture system, cells do not contact the plastic dish directly but in the suspension environment, which can be established with or without scaffold materials. Scaffolds consist of biological or synthetic hydrogels that mimic the *in vivo* extracellular matrix and provide structural support. For instance, Matrigel^{TM} is the most commonly used biological hydrogel that is extracted from the Engelbreth-Holm-Swarm mouse sarcoma. Matrigel consists of laminin, collagen IV, heparin sulfate proteoglycans, entactin/nidogen and a number of growth factors (Orkin et al., 1977; Sato et al., 2009; Shamir and Ewald, 2014). Without scaffold, cells can be cultured in culture medium droplets on a hanging plate (Timmins et al., 2007).

1.3.5.3. Organoid growth media

Organoids are maintained in media containing several factors that are essential for the maintenance, proliferation and differentiation of stem cells, including Wnt, BMP, Notch, and EGF signaling pathways.

The Wnt signaling pathway is crucial to maintain intestinal stem cells, which is involved in the terminal differentiation of Paneth cells (Korinek et al., 1998; Farin et al., 2012). At the bottom of the crypt, the activation of Wnt signals maintain and induce the proliferation of stem cells. Inactivating the downstream transcription factors of the Wnt pathway restricted crypt proliferation in neonatal mice (Korinek et al., 1998). Furthermore, Wnt inhibitor (Dickkopf 1) reduced crypts number and stem cell proliferation in mice (Pinto et al., 2003; Kuhnert et al., 2004). The Wnt ligands are expressed in Paneth cells and mesenchyme neighboring the crypt (Farin et al., 2012; Kabiri et al., 2014). Paneth cells are essential for intestinal organoid organization *in vitro*. The depletion of Paneth cells *in vivo*

didn’t affect the formation of crypts, in which the mesenchyme served as an alternative source of Wnt signaling (Farin et al., 2012).

The BMP signaling pathway contributes to cell differentiation in the crypt. In vivo, the mesenchymal cells neighboring the crypt stem cells secrete BMP inhibitors to prevent the differentiation of stem cells in the crypt (Kosinski et al., 2007). The BMP ligands are highly expressed in villi and promote cell differentiation (Haramis et al., 2004). The BMP inhibition promotes the crypt formation. The BMP inhibitor, Noggin, is essential in the IO culture medium (Sato et al., 2009).

The Notch signaling pathway relies on the Notch receptor of stem cells. The receptor binds ligands presented by cells, such as Paneth cells. Notch activation promotes progenitors differentiate into secretory cells (Ueo et al., 2012). Similar to Notch activation, Notch inhibition causes proliferating cells to differentiate into goblet cells (Milano et al., 2004; van Es et al., 2005; van Es et al., 2010). Notch signaling pathways determine the secretory cells fate.

The EGF signaling pathway is essential for the generation of IO (Sato et al., 2009). The knockout of a negative regulator, Lrig1, for the EGF signaling pathway increased epithelial proliferation in the mouse (Wong et al., 2012). Human IO grew slow in the media supplemented with EGF inhibitor (Matano et al., 2015). The EGF signaling pathway is essential for the generation of intestinal organoids (Sato et al., 2009).

In conclusion, Wnt and EGF signaling pathways are necessary for intestinal stem cell proliferation (Korinek et al., 1998; Dignass et al., 2001; Pinto et al., 2003; Kuhnert et al., 2004; Kim et al., 2005). Notch and BMP signaling pathways are required for cell differentiation (de Santa Barbara et al., 2003; Yin et al., 2014; Chin et al., 2017).

1.3.6. The application of organoids

Organoid technology has been already developed and studied for more than 10 years, and widely used for mammalian studies. Intestinal organoids have been used to study intestine physiology (Schwank et al., 2013; Middendorp et al., 2014), cross-talk between cells (Sato et al., 2011), and functional assay (Dekkers et al., 2013). They are also play a key role in disease modeling, drug screening, and tissue transplant (Yui et al., 2012; Dehia et al., 2016; Drost and Clevers, 2017). For example, human IO were utilized to study intestinal fibrosis induced by inflammatory bowel disease (Angus et al., 2020). Mouse IO were transplanted into a damaged colon and repaired the damaged section (Dedhia et al., 2016; Yin et al., 2016). One of the primary applications of IO is to study host-pathogen interactions. Finkbeiner et al. (2016) first employed human IO to understand the mechanism of rotavirus infection. More studies have been performed in IO derived from various mammalian species infected with bacteria, parasites, and viruses (Finkbeiner et al., 2012; Zhang et al., 2014; Gerbe et al., 2016; Heo et al., 2018; Derricott et al., 2019; Zhou et al., 2020).

Based on all the IO applications in mammalian research, avian IOs have potential applications including bio-banking chicken intestine-derived organoids, nutriention research, intestinal epithelial barrier functions, cross-talk between gut epithelial and immune cells, *ex vivo* inflammation model, microbiota-host interactions, drug discovery and toxicity studies.

1.4. Exosomes and microRNAs review

1.4.1. Bio-generation and composition of exosomes

Exosomes are phospholipid bilayer extracellular vesicles, 30 to 150 nm in diameter, that are secreted from various cell types, such as blood cells, immune cells, neural cells, epithelial cells, and are present in bodily fluids, including serum, urine, saliva, milk, and seminal fluid (Van Niel et al., 2001; Blanchard et al., 2002; Pisikun et al., 2004; Caby et al., 2005; Fauré et al., 2006; Lotvall and Valadi, 2007; Alvarez-Rodriguez et al., 2012). The generation of exosomes is initiated from the inward budding of endosomal membranes into early endosomes (Fig. 1.3). Early endosomes develop into multi-vesicular bodies (MVBs) containing intraluminal vesicles (ILVs). The MVBs can either be digested by lysosomes or be released into the extracellular environment as exosomes (Théry et al., 2002; Huotari et al., 2011; Li et al., 2019). During this generation process, exosomes are packaged with unique biomolecules, including miRNAs, mRNAs, DNAs, proteins, lipids (Colombo et al., 2014; Li et al., 2014). With the protection of a phospholipid bilayer, genes and proteins contained in exosomes are protected from degradation during long-distance transportation in bodily fluids. Exosomes are considered as the messenger for adjacent and distant cell-to-cell communication.

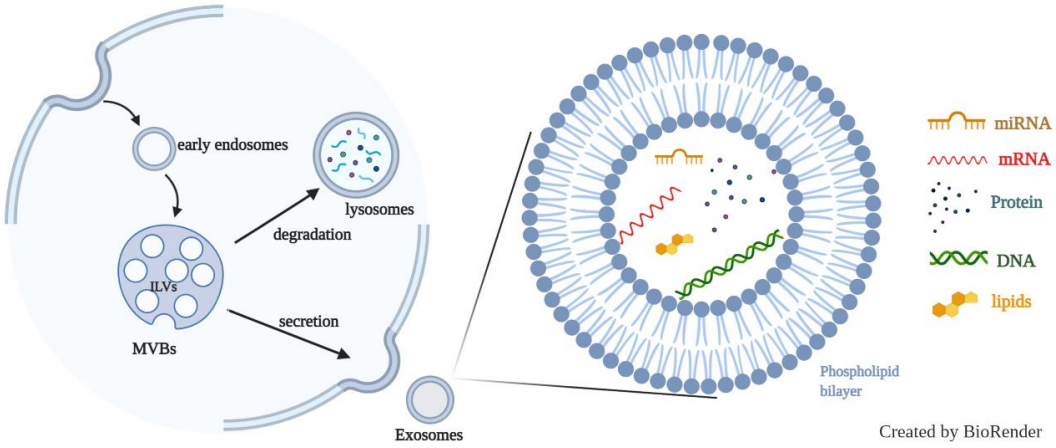

Figure 1.3 The generation and composition of exosomes. Exosomes are generated from the inward budding of endosomal membranes into early endosomes and combined into multi-vesicular bodies (MVBs). The MVBs can be either degraded by lysosomes or secreted into the extracellular space as exosomes that contain miRNAs, mRNAs, proteins, DNAs, and lipids. The figure was generated in BioRender by Dan Zhao.

1.4.2. The roles of host-derived exosomes in health and disease

Exosomes are generated by healthy host cells and are secreted into the extracellular space containing various biomolecules such as miRNA and proteins. Once exosomes are released into extracellular compartments, they can be taken by recipient cells throughout the body via endocytosis, phagocytosis, or micropinocytosis pathways, delivering their effector molecules including miRNA and protein into target cells by facilitating intercellular communications (Mathieu et al., 2019).

Several studies demonstrated that exosomes are involved in intercellular communication and immune response. Proteins or miRNAs inside of exosomes are considered as the potential biomarkers for diseases. For example, miRNA-29c in urinary exosome was proposed to be a biomarker for renal fibrosis (Johnstone et al., 1987; Raposo et al., 1996; Wolfers et al., 2001; Ratajczak et al., 2006; Valadi et al., 2007; Skog et al.,

2008; Lv et al., 2013). Exosomes have been found in the media from several cells including dendritic cells, macrophages, B cells, T cells, and intestinal epithelial cells, and contain major histocompatibility complex (MHC) class molecules (Johansson et al., 2008; Buschow et al., 2009; Buschow et al., 2010; Bakela et al., 2015; Wang et al., 2015). Yang et al. (2012) demonstrated that plasma-derived exosomes, containing MHC class I and MHC class II, from tumor-bearing mice caused immunosuppression in the host. In addition, dendritic cell-secreted exosomes that contained MHC class I and MHC class II had the potential to activate T cells ($CD4^+$ or $CD8^+$) (Utsugi-Kobukai et al., 2003; Luketic et al., 2007). Host-derived exosomes play a crucial role after pathogen infection (Delabranche et al., 2012; Laganà et al., 2013). The exosomal miR-155 has been reported to be involved in the immune response to a *Helicobacter pylori* infection (Wang et al., 2018).

1.4.3. The roles of pathogen-derived outer membrane vesicles in disease

Pathogen-derived nanoparticles released by microbes, called outer membrane vesicles (OMVs), have been reported to help the colonization of microbes in the host (Yonezawa et al., 2009; Olofsson et al., 2010; Yonezawa et al., 2011; Toledo et al., 2012; Rybak and Robatzek, 2019). Bacteria secrete OMVs into their environment (Kulp and Kuehn, 2010; Schwechheimer et al., 2015). The composition and function of OMVs have been demonstrated in several Gram-negative bacteria. For example, the ClyA cytoxin, a pore-forming protein, was found in OMVs extracted from culture of *Escherichia coli* and *Salmonella* Typhimurium (Wai et al., 2003). Outer membrane vesicles were identified in *in vivo* and *in vitro* system after *Salmonella* Typhimurium challenge (Vesy et al., 2000; Bergman et al., 2005). Intracellular and extracellular bacteria derived OMVs are also

detected in several mammalian host cells, including neutrophils, macrophages, and epithelial cells (Srisatjaluk et al., 1999; Qi et al., 2003; Ho et al., 2015). Bacterial OMVs contain genes and proteins, of which some are critical virulence factors that help the pathogen escape the host immune response, promote pathogen infection process, and inhibit the host immune responses (Ellis and Kuehn, 2010; Berleman and Auer, 2013; Feng et al., 2013; Laganà et al., 2013). Bacterial virulence factors can be incorporated into host-derived exosomes which can be delivered to other normal cells. For instance, the key virulence factor (α-toxin, a pore-forming toxin) secreted from *Staphylococcus aureus* or *Helicobacter pylori* was identified in their OMVs (Husmann et al., 2009; Shimoda et al., 2016). Otherwise, host-derived exosomes can enhance the infection process. They serve as bidirectional messengers between host-pathogen interactions.

Investigation of differentially expressed exosomal macromolecules, either miRNA or protein, which are derived from *Salmonella* challenged and non-*Salmonella* challenged chickens could provide the foundation to understand the roles of exosomes in the immune response, which will help to find solutions to reduce *Salmonella* contamination of poultry.

1.4.4. The microRNA bio-genesis and mechanism of miRNA-mRNA regulation

MicroRNA (miRNA) was first reported by Lee et al. in 1993. Numerous researchers have studied the function of miRNAs and have demonstrated that they are involved in diverse biological processes, including cell proliferation, differentiation, metabolism, innate and adaptive immunity and also serve as a biomarker of cancers (Alvarez-Garcia and Miska, 2005; Chen et al., 2006; Johnson et al., 2007; Michael et al., 2010; Xie et al., 2013). MicroRNAs are 18 to 25 nts in length, a single-stranded RNA is generated from endogenous transcripts, which contain a hairpin structure (Ambros et al.,

2003; Bartel, 2004; Cullen et al., 2004; Bartel, 2018). As shown in Fig. 1.4, miRNA biogenesis is initiated by transcribing long double-strand primary transcripts (pri-miRNA, more than 1,000 nts in length) in the nucleus (Lee et al., 2004). The pri-miRNA is split into precursor miRNA (pre-miRNA, about 60 to 120 nts in length) using Drosha, a double-strand RNA-binding protein. Finally, the pre-miRNA is cleaved into mature miRNA (about 22 nts in length) by Dicer, an RNase III family protein, in the cytoplasm (Kim, 2005).

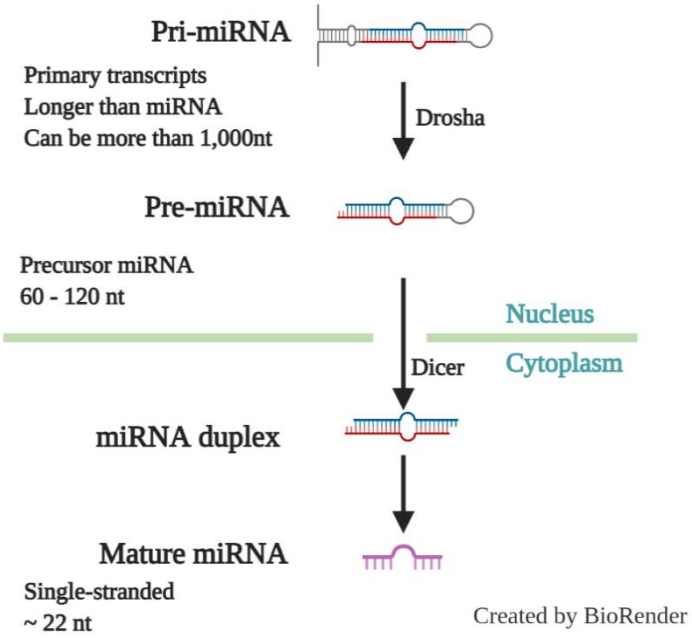

Figure 1.4 Biogenesis of a miRNA. The miRNA genes are transcribed from DNA sequences into primary miRNAs (pri-miRNAs) that have a hairpin structure. The hairpin structure can be recognized by Drosha Rnases and cleaved into precursor miRNAs (pre-miRNAs) in the nucleus. The pre-miRNAs are exported to the cytoplasm and are cut into mature miRNAs by Dicer. The figure was generated in BioRender by Dan Zhao.

1.4.5. Regulation of miRNA in host-pathogen interactions

MicroRNAs, endogenous small non-coding RNAs, do not code for proteins but regulate the post-transcriptional gene expression by binding to the 3' untranslated region (3'-UTR) of their target gene and inducing cleavage or silencing the target mRNAs as showing in Fig. 1.5 (Bartel, 2004; Bartel, 2009; Huntzinger et al., 2011). One miRNA can bind to different target RNAs, and one target RNA can be controlled by several different miRNAs (Lewis et al., 2003).

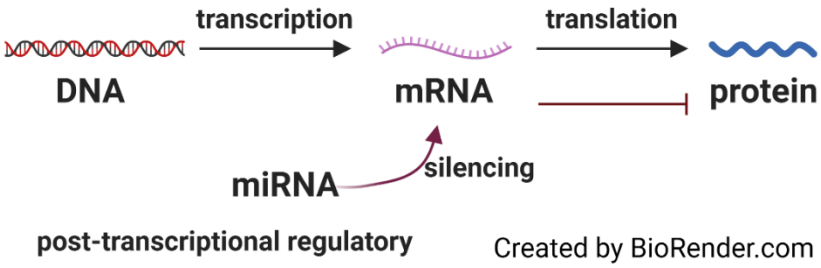

Figure 1.5 Regulation of miRNAs. MiRNAs can silence their target mRNAs and reduce their translation. The figure was generated in BioRender by Dan Zhao.

Labbaye and Testa (2012) has reported the role of miRNAs in modulating innate and adaptive immune responses. The alteration of miRNA expression had been demonstrated in infectious diseases caused by bacteria, viruses, and parasites (Fu et al., 2011; Reynoso et al., 2014; Petrini et al., 2015). For example, the gga-miR-2129, extracted from liver tissue, was considered the predicted miRNA related to resistance to avian leukosis virus subgroup-induced tumor formation in chickens (Zhang et al., 2017), as well as gga-miR-6673-3p (Zhang et al., 2018). The mir-16 and mir-71 were up-regulated in *Heligmosomoides polygyrus* infections (Buck et al., 2014). They found that exosomes

derived from *Heligmosomoides polygyrus* suppress innate immunity in mice by regulating IL-33 levels. Both mir-21 and mir-29a expression levels were up-regulated in exosomes secreted by HBV-infected hepatocytes (Kouwaki et al., 2016). Two exosomal miRNAs extracted from Marek's disease virus-infected chicken serum, gga-mir-146 and gga-mir-21, were proposed to be biomarkers of Marek's disease (Neerukonda et al., 2019). The expression levels of splenic miRNAs to *Salmonella* Enteritidis infection were investigated. Sixteen miRNAs were differentially expressed in the spleen of the challenged group compared to the non-challenged group (Li et al., 2018). Sixty-two miRNAs related to inflammatory process genes were differentially expressed in the ileum of *Salmonella* Typhimurium challenged pigs compared to the control group after a two-day post-infection (Uribe et al., 2016). MicroRNA response to *Salmonella* Enteritidis challenge was investigated in the ceca of white Leghorn layer chickens, where gga-miR-125b-5p and gga-miR-1416-5p were up-regulated, gga-miR-34a-5p and gga-miR-1662 were down-regulated (Wu et al., 2017).

Thus, miRNA-target molecular pathways will significantly improve our understanding of the mechanism of host-pathogen interactions in chicken.

1.5. Wooden breast review

1.5.1. History of skeletal muscle myopathies in the broiler industry

Poultry products are considered as a major human protein sources. The United States is the top broiler meat producer in the world pruducing about 20.51 million metric tons of meat in 2020 (Shahbandeh, 2020). Over the last 58 years in the US, per capita consumption of broilers has increased 290% (National Chicken Council, 2018). To meet the increasing demand for poultry meat, broilers have been selected for fast growth rates,

high feed conversion ratios, and high meat yields (Zuidhof et al., 2014; Petracci et al., 2015; Tallentire et al., 2018). However, the fast-growing and heavy weights of broilers have increased the incidence of degenerative myopathies, severely affecting meat appearance and quality (Kuttappan ett al., 2012, Tijare et al., 2016). One novel muscle myopathy is wooden breast (WB) that was first described by Sihvo et al. in 2014. Wooden breast appears in 2- to 3-week-old broilers and the incidence of WB occurs approximately 48 to 73% (Sihvo et al., 2014 and 2017), resulting in a considerable economic losses in the US due to poor meat quality, such as low water-holding capacity, reduced product yield, decreased myofibrillar protein contents, and poor meat texture (Mazzoni et al., 2015; Mudalal et al., 2015; Kuttappan et al., 2016; Aguirre et al., 2018; Hubert and Athrey, 2020).

1.5.2. Classification of wooden breast

Wooden breast is considered a manifestation of metabolic syndrome in fast-growing broilers, which makes the pectoralis major muscle pale, rigid and bulge outwards as showing in Fig. 1.6 (Sihvo et al., 2014; Bailey et al., 2015; Tasoniero et al., 2016). There are several criteria for determining the severity of WB score. Based on the level of hardness, WB are categorized into normal, mild, moderate, and severe by tactile evaluation (Tijare et al., 2016; Xing et al., 2020). Histologically, WB is characterized morphologically by the development of myofiber necrosis and fibrosis, and high levels of fibrillar collagen in skeletal muscle tissues (Sihvo et al., 2014; Velleman and Clark, 2015; Kuttappan et al., 2016). According to meat quality, WB can be further analyzed by texture, pH value, and water holding ability (Bailey et al., 2015).

Figure 1.6 The appearance of normal and wooden breast (Sihvo et al., 2014). A. Normal breast. B. Wooden breast. The wooden breast muscle is pale, visually rigid, bulge, and covered with clear sticky fluid (Sihvo et al., 2014).

1.5.3. The etiologies of wooden breast

Wooden breast is a novel myopathy that was first described by Sihvo et al (2014). Since then, the etiologies for WB have been studied extensively by researchers globally. The cause for WB is still under investigation, but it is believed to be related to a combination of environmental and genetic factors (Bailey et al., 2015; Griffin et al., 2018; Zampiga et al., 2018). Wooden breast has a high incidence in the fast-growing and heavy weights of broilers. The most common features of WB include increased oxidative stress, abnormal metabolisms (Mutryn et al., 2015; Abasht et al., 2016), decreased capillary density (Dransfield and Sosnicki, 1999; Hoving-Bolink et al., 2000), muscle fiber necrosis, and fibrosis (Wilson et al., 1990; Dransfield and Sosnicki, 1999), and localized hypoxia (Mutryn et al., 2015; Sihvo et al., 2018). Bottje et al. (2021) conducted a proteomic

analysis for feed efficiency broilers (pedigree male) and commercial broilers with or without WB. They found that several potential regulators that may be involved in WB, such as angiopoietin 2 and peroxisome proliferator coactivator 1 in the WB dataset. Besides, Papah et al. (2018) demonstrated the early pathogenesis of WB by RNA-sequencing with commercial broilers. They reported 41, 618, and 39 differentially expressed genes for birds with WB at weeks 2, 3, and 4, respectively. The molecular mechanism of WB is still unknown. Due to the presence of localized hypoxia and decreased lactate levels in WB muscle (Abasht et al., 2016), the pathway related to lactate metabolism may play a critical role in understanding the molecular mechanism of WB.

1.5.4. The lactate metabolism pathway

In cells, pyruvate, the end product of glycolysis, undergoes fermentative glycolysis under hypoxic conditions. As shown in Fig. 1.7, the end-point of fermentative glycolysis is the formation of lactate without additional energy production. Lactate can be transported into the liver, regenerate glucose, and go through the tricarboxylic acid cycle (TCA cycle) to produce more ATP. The key molecules involved in fermentative glycolysis are lactate dehydrogenase (LDH) -A and -B, which inter converse pyruvate and lactate, and monocarboxylate transporter (MCT) -1 and -4 that transport lactate (Urbańska and Orzechowski, 2019).

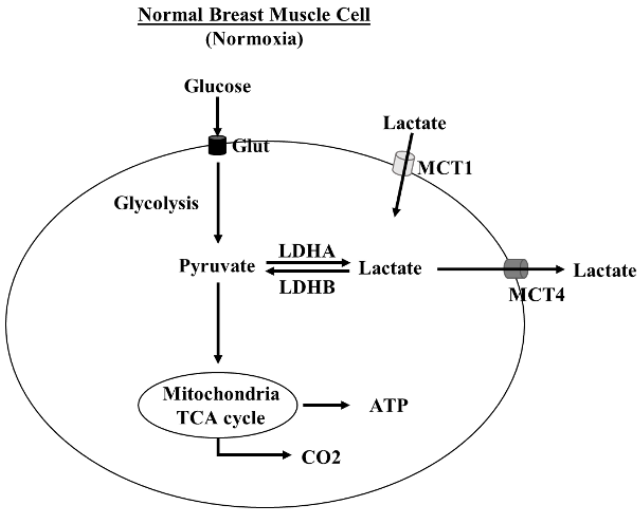

Figure 1.7 Schematic representation of the lactate metabolism pathway of a broiler muscle cell. Glucose is transported to the cell cytosol by glucose transporter (Glut), and then is converted to pyruvate, the end product of glycolysis. Under normoxic conditions, pyruvate enters the mitochondria and produces 38 ATPs per oxidized glucose molecule, including glycolysis, tricarboxylic acid cycle (TCA cycle) and oxidative phosphorylation. The activity of TCA cycle is decreased and the pyruvate switches to the fermentation pathway, resulting in the production of lactate by the action of lactate dehydrogenase A (LDHA). Lactate can be re-oxidized to pyruvate by LDHB activity, or it can be transported out of the cell by the monocarboxylate transporter 4 (MCT4).

1.5.4.1. Lactate dehydrogenase

Lactate dehydrogenase (LDH), a class of oxidoreductases, is a cytoplasmic enzyme that was first detected in skeletal muscle and later found in nearly all living animal cells, composed of tetramers derived from two LDH subunits. It is encoded by LDHA, which converts pyruvate to lactate and LDHB gene which converts lactate to pyruvate in the last step of glycolysis (Cahn et al., 1962; Dawson et al., 1964; Pesce et al., 1964). Studies demonstrated that knockout either LDHA or LDHB could not reduce lactate production (Ždralević et al., 2018). However, a double knockout of LDHA and LDHB resulted in the lack secretion of lactate in human and mouse cell lines (Ždralević et al., 2018). The combination of LDHA and LDHB produce five LDH isoenzymes, categorized as LDH1

(B4), LDH2 (A1B3), LDH3 (A2B2), LDH4 (A3B1) and LDH5 (A4) (Dawson et al., 1964), which is shown in Fig.1.8. These five isoenzymes have differential expression in different tissues (Drent et al., 1996). For example, LDH1, LDH2, LDH3, LDH4, and LDH5 is the major isozymes in heart tissues, the reticuloendothelial system, lungs, kidneys, and skeletal muscles, respectively (Read et al., 2001; Farhana and Lappin, 2020; Khan et al., 2020). The altered level of LDH enzyme in human serum indicates damaged cells and tissues and has become a common marker for tissue injuries and disease (Drent et al., 1996; Kato et al., 2006; Ding et al., 2017).

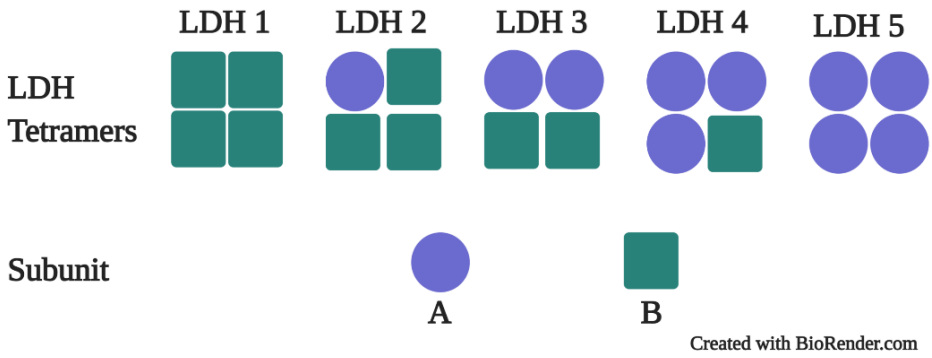

Figure 1.8 The tetramers of LDH. LDH contain two different subunits: LDHA (the purple round) and LDHB (the green square). LDH1 contains 4 LDHB subunits, LDH2 has three LDHB and one LDHA subunits, LDH3 consist of two LDHB subunits and two LDHA subunits, LDH4 includes one LDHB and three LDHA subunits, LDH5 comprises four LDHA subunits. The figure was generated in BioRender by Dan Zhao.

1.5.4.2. Monocarboxylate transporter

Monocarboxylate transporters (MCTs) belong to members of the solute carrier 16 (SLC16) family of transporter that play important roles in shuttling monocarboxylates such as lactate and pyruvate (Poole et al., 1993; Halestrap et al., 2004; Halestrap, 2012; Melanie et al., 2020). Monocarboxylate transporter plays a vital role in cell-to-cell metabolic

communication. Lactates, the end product of anaerobic glycolysis, are transported by MCT1 and MCT4, located on the cell membrane. The existence of MCT1 was first reported in human red blood cells (Halestrap et al., 1974). Monocarboxylate transporter 1 is found in the majority of tissues (Halestrap et al., 2004). Monocarboxylate transporter 4 is widely expressed in glycolytic tissue including white skeletal muscle fibers, white blood cells, and mammal cell lines (Wilson et al., 1998; Bergersen et al., 2002; Halestrap and Meredith, 2004). In the rat, MCT4 is expressed in the neonatal heart but is absent in the adult heart, which have an abundant of MCT1 expression (Wilson et al., 1998; Hatta et al., 2001). Translocation of lactate in skeletal muscles is facilitated by MCT1, which facilitates the uptake of lactate into cells, and MCT4, which exports lactate out of cells (Roth and Brooks, 1990; Halestrap and Price, 1999; Halestrap and Meredith, 2004). The alternation of MCTs was hypothesized to maintain the glycolysis rate and prevent cell apoptosis in several tumor studies (Pinheiro et al., 2008).

1.5.5. MicroRNA-375

MicroRNAs (miRNAs) are small non-coding RNAs that negatively regulate their target gene expression. Micro RNA-375, 22 nts in length, was first identified in human and mice pancreatic cells and related to the regulation of insulin secretion (Poy et al., 2004) and has been reported to be inversely associated with LDHB gene expression in cancer cells including human squamous cell carcinoma, esophageal squamous cancer cells, and Merkel cell carcinoma (Kinoshita et al., 2012; Isozaki et al., 2015; Kumar et al., 2018). Overexpression of gga-miR-375 promoted p53 protein expression which is related to tumor suppression (Zhang et al., 2020). Li et al. (2014) revealed that gga-miR-375 was associated with avian leucosis tumorigenesis using miRNA microarray.

Therefore, the studies of potential roles of LDH and MCT on lactate metabolism will provide a unique molecular elucidation for altered lactate homeostasis in WB muscles of broilers.

1.6. References

Abasht, B., M. F. Mutryn, R. D. Michalek, and W. R. Lee. 2016. Oxidative stress and metabolic perturbations in wooden breast disorder in chickens. PloS One. 11:e0153750.

Aguirre, M. E., C. M. Owens, R. K. Miller, and C. Z. Alvarado. 2018. Descriptive sensory and instrumental texture profile analysis of woody breast in marinated chicken. Poult. Sci. 97:1456-1461.

Alvarez-Garcia, and I., E. A. Miska. 2005. MicroRNA functions in animal development and human disease. Development. 132:4653-4662.

Ambros, V., B. Bartel, B. Bartel, D. P. Burge, C. B. Carrington, J. C. Chen, X. Dreyfuss, G. Eddy, S. R. Griffiths-Jones, S. A. M. Marshall, and M. Matzke. 2003. A uniform system for microRNA annotation. RNA. 9:277-279.

Angus, H. C., A. G. Butt, M. Schultz, and R. A. Kemp. 2020. Intestinal organoids as a tool for inflammatory bowel disease research. Front. Med. 6:334.

Bailey, R. A., K. A. Watson, S. F. Bilgili, and S. Avendano. 2015. The genetic basis of pectoralis major myopathies in modern broiler chicken lines. Poult. Sci. 94:2870-2879.

Barker, N., A. van Oudenaarden, and H. Clevers. 2012. Identifying the stem cell of the intestinal crypt: strategies and pitfalls. Cell stem cell. 11:452-460.

Barker, N., J. H. Van Es, J. Kuipers, P. Kujala, M. Van Den Born, M. Cozijnsen, A. Haegebarth, J. Korving, H. Begthel, P. J. Peters, and H. Clevers. 2007. Identification of stem cells in small intestine and colon by marker gene Lgr5. Nature. 449:1003-1007.

Bartel, D. P. 2004. MicroRNAs: genomics, biogenesis, mechanism, and function. Cell. 116:281-297.

Bartel, D. P. 2009. MicroRNAs: target recognition and regulatory functions. Cell. 136:215-233.

Bartel, D. P. 2018. Metazoan micrornas. Cell. 173:20-51.

Behjati, S., M. Huch, R. van Boxtel, W. Karthaus, D. C. Wedge, A. U. Tamuri, I. Martincorena, M. Petljak, L. B. Alexandrov, G. Gundem, and P. S. Tarpey. 2014. Genome sequencing of normal cells reveals developmental lineages and mutational processes. Nature. 513:422-425.

Bergman, M. A., L. A. Cummings, S. L. R. Barrett, K. D. Smith, J. C. Lara, A. Aderem, and B. T. Cookson. 2005. CD4+ T cells and toll-like receptors recognize *Salmonella* antigens expressed in bacterial surface organelles. Infect. Immun. 73:1350-1356.

Berleman, J., and M. Auer. 2013. The role of bacterial outer membrane vesicles for intra- and interspecies delivery. Environ. Microbiol. 15:347-354.

Beumer, J., and H. Clevers. 2016. Regulation and plasticity of intestinal stem cells during homeostasis and regeneration. Development. 143:3639-3649.

Bjerre, A., B. Brusletto, E. Rosenqvist, E. Namork, P. Kierulf, R. Øvstebø, G. B. Joø, and P. Brandtzæg. 2000. Cellular activating properties and morphology of membrane-bound and purified meningococcal lipopolysaccharide. J. Endotoxin Res. 6:437-445.

Blanchard, N., D. Lankar, F. Faure, A. Regnault, C. Dumont, G. Raposo, and C. Hivroz. 2002. TCR activation of human T cells induces the production of exosomes bearing the TCR/CD3/ζ complex. J. Immunol. 168:3235-3241.

Buck, A. H., G. Coakley, F. Simbari, H. J. McSorley, J. F. Quintana, T. Le Bihan, S. Kumar, C. Abreu-Goodger, M. Lear, Y. Harcus, and A. Ceroni. 2014. Exosomes secreted by nematode parasites transfer small RNAs to mammalian cells and modulate innate immunity. Nat. Commun. 5:1-2.

Caby, M. P., D. Lankar, C. Vincendeau-Scherrer, G. Raposo, and C. Bonnerot. 2005. Exosomal-like vesicles are present in human blood plasma. Int. Immunol. 17:879-887.

Caldwell, D. J., R. E. Droleskey, M. H. Elissalde, M. H. Kogut, J. R. DeLoach, and B. M. Hargis. 1993. Isolation and primary culture of chicken intestinal epithelial cells retaining normal in vivo-like morphology. J. Tissue Cult. Methods. 15:15-18.

Cahn, R. D., E. Zwilling, N. O. Kaplan, and L. Levine. 1962. Nature and development of lactic dehydrogenase: the two major types of this enzyme from molecular hybrids which change in makeup during development. Science. 136:962-969.

Camp, J. G., K. Sekine, T. Gerber, H. Loeffler-Wirth, H. Binder, M. Gac, S. Kanton, J. Kageyama, G. Damm, D. Seehofer, and L. Belicova. 2017. Multilineage

communication regulates human liver bud development from pluripotency. Nature. 546:533-538.

Centers for Disease Control and Prevention (CDC). 2013. National *Salmonella* surveillance annual report, 2011. US Department of Health and Human Services, CDC, Atlanta, GA.

Center for Disease Control and Prevention. 2021. *Salmonella*. Accessed Apr. 2021. https://www.cdc.gov/salmonella/

Chen, J. F., E. M. Mandel, J. M. Thomson, Q. Wu, T. E. Callis, S. M. Hammond, F. L. Conlon, and D. Z. Wang. 2006. The role of microRNA-1 and microRNA-133 in skeletal muscle proliferation and differentiation. Nat. Genet. 38:228-233.

Cheng, H., and C. P. Leblond. 1974. Origin, differentiation and renewal of the four main epithelial cell types in the mouse small intestine. Columnar cell. J. Anat. 141:461-479.

Chin, A. M., D. R. Hill, M. Aurora, and J. R. Spence. 2017. Morphogenesis and maturation of the embryonic and postnatal intestine. Semin. Cell Dev. Biol. 66:81-93.

Clevers, H. 2013. The intestinal crypt, a prototype stem cell compartment. Cell. 154:274-284.

Clevers, H. C., and C. L. Bevins. 2013. Paneth cells: maestros of the small intestinal crypts. Annu. Rev. Physiol. 75:289-311.

Colombo, M., G. Raposo, and C. Théry. 2014. Biogenesis, secretion, and intercellular interactions of exosomes and other extracellular vesicles. Annu. Rev. Cell Dev. Biol. 30:255-289.

Cullen, B. R. 2004. Transcription and processing of human microRNA precursors. Mol. Cell. 16:861-865.

Dawson, D. M., T. L. Goodfriend, and N. O. Kaplan. 1964. Lactic dehydrogenases: Functions of the two types rates of synthesis of the two major forms can be correlated with metabolic differentiation. Science. 143: 929-933.

Dedhia, P. H., N. Bertaux-Skeirik, Y. Zavros, and J. R. Spence. 2016. Organoid models of human gastrointestinal development and disease. Gastroenterology. 150:1098-1112.

Dekkers, J. F., C. L. Wiegerinck, H. R. De Jonge, I. Bronsveld, H. M. Janssens, K. M. De Winter-de Groot, A. M. Brandsma, N. W. De Jong, M. J. Bijvelds, B. J. Scholte,

and E. E. Nieuwenhuis. 2013. A functional CFTR assay using primary cystic fibrosis intestinal organoids. Nat. Med. 19:939-945.

Derricott, H., L. Luu, W. Y. Fong, C. S. Hartley, L. J. Johnston, S. D. Armstrong, N. Randle, C. A. Duckworth, B. J. Campbell, J. M. Wastling, and J. L. Coombes. 2019. Developing a 3D intestinal epithelium model for livestock species. Cell Tissue Res. 375:409-424.

Dedhia, P. H., N. Bertaux-Skeirik, Y. Zavros, and J. R. Spence. 2016. Organoid models of human gastrointestinal development and disease. Gastroenterology. 150:1098-1112.

de Santa Barbara, P., G. R. Van Den Brink, and D. J. Roberts. 2003. Development and differentiation of the intestinal epithelium. Cell. Mol. Life Sci. 60:1322-1332.

Dignass, A. U., and A. Sturm. 2001. Peptide growth factors in the intestine. Eur. J. Gastroenterol. Hepatol. 13:763-770.

Ding, J., J. E. Karp, and A. Emadi. 2017. Elevated lactate dehydrogenase (LDH) can be a marker of immune suppression in cancer: Interplay between hematologic and solid neoplastic clones and their microenvironments. Cancer Biomark. 19:353-363.

Dransfield, E., A. A. Sosnicki. 1999. Relationship between muscle growth and poultry meat quality. Poult. Sci. 78:743-746.

Drent, M., N. A. Cobben, R. F. Henderson, E. F. Wouters, and M. van Dieijen-Visser. 1996. Usefulness of lactate dehydrogenase and its isoenzymes as indicators of lung damage or inflammation. Eur. Respir. J. 9:1736-1742.

Drost, J., and H. Clevers. 2017. Translational applications of adult stem cell-derived organoids. Development. 144:968-975.

Duarte, A. A., E. Gogola, N. Sachs, M. Barazas, S. Annunziato, J. R. de Ruiter, A. Velds, S. Blatter, J. M. Houthuijzen, M. Van De Ven, and H. Clevers. 2018. BRCA-deficient mouse mammary tumor organoids to study cancer-drug resistance. Nat. Methods. 15:134.

Ellis, T. N., and M. J. Kuehn. 2010. Virulence and immunomodulatory roles of bacterial outer membrane vesicles. Microbiol. Mol. Biol. Rev. 74:81-94.

Evans, M. 1981. Origin of mouse embryonal carcinoma cells and the possibility of their direct isolation into tissue culture. Reproduction. 62:625-631.

Food and Agriculture Organisation of the United Nations. 2019. Database Collection of the Food and Agriculture Organization of the United Nations. Accessed on Apr. 2021. http://www.fao.org/faostat/en/#data (FAOSTAT).

Farin, H. F., J. H. Van Es, and H. Clevers. 2012. Redundant sources of Wnt regulate intestinal stem cells and promote formation of Paneth cells. Gastroenterology. 143:1518-1529.

Fauré, J., G. Lachenal, M. Court, J. Hirrlinger, C. Chatellard-Causse, B. Blot, J. Grange, G. Schoehn, Y. Goldberg, V. Boyer, and F. Kirchhoff. 2006. Exosomes are released by cultured cortical neurones. Mol. Cell. Neurosci. 31:642-648.

Feng, Z., L. Hensley, K. L. McKnight, F. Hu, V. Madden, L. Ping, S. H. Jeong, C. Walker, R. E. Lanford, and S. M. Lemon. 2013. A pathogenic picornavirus acquires an envelope by hijacking cellular membranes. Nature. 496:367-371.

Finkbeiner, S. R., and J. R. Spence. 2013. A gutsy task: generating intestinal tissue from human pluripotent stem cells. Dig. Dis. Sci. 58:1176-1184.

Finkbeiner, S. R., X. L. Zeng, B. Utama, R. L. Atmar, N. F. Shroyer, and M. K. Estes. 2012. Stem cell-derived human intestinal organoids as an infection model for rotaviruses. MBio. 3:e00159-12.

Fu, Y., Z. Yi, X. Wu, J. Li, and F. Xu. 2011. Circulating microRNAs in patients with active pulmonary tuberculosis. J. Cline. Microbiol. 49:4246-4251.

Galiş, A. M., C. Marcq, D. Marlier, D. Portetelle, I. Van, Y. Beckers, and A. Théwis. 2013. Control of *Salmonella* contamination of shell eggs—Preharvest and postharvest methods: A review. Compr. Rev. Food. Sci. Food. Saf. 12:155-182.

Gassler, N. 2017. Paneth cells in intestinal physiology and pathophysiology. World J. Gastrointest. Pathophysiol. 8:150.

Gerbe, F., E. Sidot, D. J. Smyth, M. Ohmoto, I. Matsumoto, V. Dardalhon, P. Cesses, L. Garnier, M. Pouzolles, B. Brulin, and M. Bruschi. 2016. Intestinal epithelial tuft cells initiate type 2 mucosal immunity to helminth parasites. Nature. 529:226-230.

Gehart, H., and H. Clevers. 2019. Tales from the crypt: new insights into intestinal stem cells. Nat. Rev. Gastroenterol. Hepatol. 16:19-34.

Griffin, J. R., L. Moraes, M. Wick, and M. S. Lilburn. 2018. Onset of white striping and progression into wooden breast as defined by myopathic changes underlying Pectoralis major growth. Estimation of growth parameters as predictors for stage of myopathy progression. Avian Pathol. 47:2–13.

Gunawardene, A. R., B. M. Corfe, and C. A. Staton. 2011. Classification and functions of enteroendocrine cells of the lower gastrointestinal tract. Int. J. Clin. Exp. Pathol. 92:219-231.

Haghighi, H. R., M. F. Abdul-Careem, R. A. Dara, J. R. Chambers, and S. Sharif. 2008. Cytokine gene expression in chicken cecal tonsils following treatment with probiotics and *Salmonella* infection. Vet. Microbiol. 126:225-233.

Halestrap, A. P., and D. Meredith. 2004. The SLC16 gene family—from monocarboxylate transporters (MCTs) to aromatic amino acid transporters and beyond. Pflügers Archiv. 447:619-628.

Halestrap, A. P., and N. T. Price. 1999. The proton-linked monocarboxylate transporter (MCT) family: structure, function and regulation. Biochem. J. 343: 281-99.

Haramis, A. P., H. Begthel, M. Van Den Born, J. Van Es, S. Jonkheer, G. J. Offerhaus, and H. Clevers. 2004. De novo crypt formation and juvenile polyposis on BMP inhibition in mouse intestine. Science. 303:1684-1686.

Heo, I., D. Dutta, D. A. Schaefer, N. Iakobachvili, B. Artegiani, N. Sachs, K. E. Boonekamp, G. Bowden, A. P. Hendrickx, R. J. Willems, and P. J. Peters. 2018. Modelling Cryptosporidium infection in human small intestinal and lung organoids. Nat. Microbiol. 3:814-823.

Hubert, S. M., and G. Athrey. 2020. Energy metabolism and sources of oxidative stress in wooden breast-a review. F1000 Research. 9:319.

Huch, M., H. Gehart, R. Van Boxtel, K. Hamer, F. Blokzijl, M. M. Verstegen, E. Ellis, M. Van Wenum, S. A. Fuchs, J. de Ligt, and M. van de Wetering. 2015. Long-term culture of genome-stable bipotent stem cells from adult human liver. Cell. 160:299-312.

Huntzinger, E., and E. Izaurralde. 2011. Gene silencing by microRNAs: contributions of translational repression and mRNA decay. Nat. Rev. Genet. 12:99-110.

Huotari, J., and A. Helenius. 2011. Endosome maturation. The EMBO J. 30:3481-3500.

Hur, J., C. Jawale, and J. H. Lee. 2012. Antimicrobial resistance of *Salmonella* isolated from food animals: A review. Int. Food Res. 45:819-830.

Husmann, M., E. Beckmann, K. Boller, N. Kloft, S. Tenzer, W. Bobkiewicz, C. Neukirch, H. Bayley, and S. Bhakdi. 2009. Elimination of a bacterial pore-forming toxin by sequential endocytosis and exocytosis. FEBS letters. 583:337-344.

Isozaki, Y., I. Hoshino, N. Nohata, T. Kinoshita, Y. Akutsu, N. Hanari, M. Mori, Y. Yoneyama, N. Akanuma, N. Takeshita, T. Maruyama, N. Seki, N. Nishino, M. Yoshida, and H. Matsubara. 2012. Identification of novel molecular targets regulated by tumor suppressive miR-375 induced by histone acetylation in esophageal squamous cell carcinoma. Int. J. Oncol. 41:985–994.

Johnson, C. D., A. Esquela-Kerscher, G. Stefani, M. Byrom, K. Kelnar, D. Ovcharenko, M. Wilson, X. Wang, J. Shelton, J. Shingara, and L. Chin. 2007. The let-7 microRNA represses cell proliferation pathways in human cells. Cancer Res. 67:7713-7722.

Johnstone, R. M., M. Adam, J. R. Hammond, L. Orr, and C. Turbide. 1987. Vesicle formation during reticulocyte maturation. Association of plasma membrane activities with released vesicles (exosomes). J. Biol. Chem. 262:9412-9420.

Kabiri, Z., G. Greicius, B. Madan, S. Biechele, Z. Zhong, H. Zaribafzadeh, J. Aliyev, Y. Wu, R. Bunte, B. O. Williams, and J. Rossant. 2014. Stroma provides an intestinal stem cell niche in the absence of epithelial Wnts. Development. 141:2206-2215.

Kaiko, G. E., S. H. Ryu, O. I. Koues, P. L. Collins, L. Solnica-Krezel, E. J. Pearce, E. M. Oltz, and T. S. Stappenbeck. 2016. The colonic crypt protects stem cells from microbiota-derived metabolites. Cell. 165.

Kato, G. J., V. McGowan, R. F. Machado, J. A. Little, J.Taylor, C. R. Morris, J. S. Nichols, X. Wang, M. Poljakovic, S. M. Morris, and M. T. Gladwin. 2006. Lactate dehydrogenase as a biomarker of hemolysis-associated nitric oxide resistance, priapism, leg ulceration, pulmonary hypertension, and death in patients with sickle cell disease. Blood. 7:2279–2285.

Kim, K. A., M. Kakitani, J. Zhao, T. Oshima, T. Tang, M. Binnerts, Y. Liu, B. Boyle, E. Park, P. Emtage, and W. D. Funk. 2005. Mitogenic influence of human R-spondin1 on the intestinal epithelium. Science. 309:1256-1259.

Kim, V. N. 2005. MicroRNA biogenesis: coordinated cropping and dicing. Nat. Rev. Mol. Cell Biol. 6:376-385.

Kinoshita, T., N. Nohata, H. Yoshino, T. Hanazawa, N. Kikkawa, L. Fujimura, T. Chiyomaru, K. Kawakami, H. Enokida, M. Nakagawa, Y. Okamoto, and N. Seki. 2012. Tumor suppressive microRNA-375 regulates lactate dehydrogenase B in maxillary sinus squamous cell carcinoma. Int. J. Oncol. 40:185-193.

Klasing, K. C. 1999. Avian gastrointestinal anatomy and physiology. Semin. Avian Exot. Pet. 8:42-50.

Korinek, V., N. Barker, P. Moerer, E. van Donselaar, G. Huls, P. J. Peters, and H. Clevers. 1998. Depletion of epithelial stem-cell compartments in the small intestine of mice lacking Tcf-4. Nat. Genet. 19:379-383.

Kosinski, C., V. S. Li, A. S. Chan, J. Zhang, C. Ho, W. Y. Tsui, T. L. Chan, R. C. Mifflin, D. W. Powell, S. T. Yuen, and S. Y. Leung. 2007. Gene expression patterns of human colon tops and basal crypts and BMP antagonists as intestinal stem cell niche factors. Proc. Natl. Acad. Sci. 104:15418-15423.

Kouwaki, T., Y. Fukushima, T. Daito, T. Sanada, N. Yamamoto, E. J. Mifsud, C. R. Leong, K. Tsukiyama-Kohara, M. Kohara, M. Matsumoto, and T. Seya. 2016. Extracellular vesicles including exosomes regulate innate immune responses to hepatitis B virus infection. Front. Immunol. 7:335.

Kuhnert, F., C. R. Davis, H. T. Wang, P. Chu, M. Lee, J. Yuan, R. Nusse, and C. J. Kuo. 2004. Essential requirement for Wnt signaling in proliferation of adult small intestine and colon revealed by adenoviral expression of Dickkopf-1. Proc. Natl. Acad. Sci. 101:266-271.

Kulp, A., and M. J. Kuehn. 2010. Biological functions and biogenesis of secreted bacterial outer membrane vesicles. Annu. Rev. Microbiol. 64:163-184.

Kumar, S., H. Xie, P. Scicluna, L. Lee, V. Björnhagen, A. Höög, C. Larsson, and W. O. Lui. 2018. MiR-375 regulation of LDHB plays distinct roles in polyomavirus-positive and -negative Merkel cell carcinoma. Cancers.10:e443.

Kuttappan, V. A., B. M. Hargis, and C. M. Owens. 2016. White striping and woody breast myopathies in the modern poultry industry: a review. Poult Sci. 95:2724-2733.

Kuttappan, V.A., V. B. Brewer, J. K. Apple, P. W. Waldroup, and C. M. Owens. 2012. Influence of growth rate on the occurrence of white striping in broiler breast fillets. Poult Sci. 91:2677-2685.

Labbaye, C., and U. Testa. 2012. The emerging role of MIR-146A in the control of hematopoiesis, immune function and cancer. J. Hematol. Oncol. 5:1-10.

Laganà, A., F. Russo, D. Veneziano, S. Di Bella, A. Pulvirenti, R. Giugno, C. M. Croce, and A. Ferro. 2013. Extracellular circulating viral microRNAs: current knowledge and perspectives. Front.Genet. 4:120.

Lancaster, M. A., and J. A. Knoblich. 2014. Organogenesis in a dish: modeling development and disease using organoid technologies. Science. 345:6194.

Lewis, B. P., I. H. Shih, M. W. Jones-Rhoades, D. P. Bartel, and C. B. Burge. 2003. Prediction of mammalian microRNA targets. Cell. 115:787-798.

Li, H., H. Shang, D. Shu, H. Zhang, J. Ji, B. Sun, H. Li, and Q. Xie. 2014. gga-miR-375 plays a key role in tumorigenesis post subgroup J avian leukosis virus infection. PLoS One. 9:e90878.

Li, J., J. Li, S. Y. Zhang, R. X. Li, X. Lin, Y. L. Mi, and C. Q. Zhang. 2018. Culture and characterization of chicken small intestinal crypts. Poult. Sci. 97:1536-1543.

Li, M., E. Zeringer, T. Barta, J. Schageman, A. Cheng, and A. V. Vlassov. 2014. Analysis of the RNA content of the exosomes derived from blood serum and urine and its potential as biomarkers. Philos. Trans. R. Soc. Lond. B. Biol. Sci. 369:20130502.

Li, X., A. L. Corbett, E. Taatizadeh, N. Tasnim, J. P. Little, C. Garnis, M. Daugaard, E. Guns, M. Hoorfar, and I. T. Li. 2019. Challenges and opportunities in exosome research—Perspectives from biology, engineering, and cancer therapy. APL Bioeng. 3:011503.

Li, Z., T. Araoka, J. Wu, H. K. Liao, M. Li, M. Lazo, B. Zhou, Y. Sui, M. Z. Wu, I. Tamura, and Y. Xia. 2016. 3D culture supports long-term expansion of mouse and human nephrogenic progenitors. Cell Stem Cell. 19:516-529.

Martin, G. R. 1981. Isolation of a pluripotent cell line from early mouse embryos cultured in medium conditioned by teratocarcinoma stem cells. Proc. Natl. Acad. Sci. 78:7634-7638.

Martinez-Argudo, I., and M. A. Jepson. 2008. *Salmonella* translocates across an in vitro M cell model independently of SPI-1 and SPI-2. Microbiology. 154:3887-3894.

Matano, M., S. Date, M. Shimokawa, A. Takano, M. Fujii, Y. Ohta, T. Watanabe, T. Kanai, and T. Sato. 2015. Modeling colorectal cancer using CRISPR-Cas9–mediated engineering of human intestinal organoids. Nat. Med. 21:256-262.

Mathieu, M., L. Martin-Jaular, G. Lavieu, and C. Thery. 2019. Specificities of secretion and uptake of exosomes and other extracellular vesicles for cell-to-cell communication. Nat. Cell Biol. 21:9-17.

Mazzoni, M., M. Petracci, A. Meluzzi, C. Cavani, P. Clavenzani, and F. Sirri. 2015. Relationship between pectoralis major muscle histology and quality traits of chicken meat. Poult. Sci. 94:123-130.

McConnell, R. E., A. E. Benesh, S. Mao, D. L. Tabb, and M. J. Tyska. 2011. Proteomic analysis of the enterocyte brush border. Am. J. Physiol. Gastr. L. 300:914-926.

McCracken, K.W., E. M. Catá, C. M. Crawford, K. L. Sinagoga, M. Schumacher, B. E. Rockich, Y. H. Tsai, C. N. Mayhew, J. R. Spence, Y. Zavros, and J. M. Wells.

2014. Modelling human development and disease in pluripotent stem-cell-derived gastric organoids. Nature. 516:400-404.

Michael, A., S. D. Bajracharya, P. S. Yuen, H. Zhou, R. A. Star, G. G. Illei, and I. Alevizos. 2010. Exosomes from human saliva as a source of microRNA biomarkers. Oral Dis. 16:34-38.

Middendorp, S., K. Schneeberger, C. L. Wiegerinck, M. Mokry, R. D. Akkerman, S. van Wijngaarden, H. Clevers, and E. E. Nieuwenhuis. 2014. Adult stem cells in the small intestine are intrinsically programmed with their location‐specific function. Stem cells. 32:1083-1091.

Milano, J., J. McKay, C. Dagenais, L. Foster-Brown, F. Pognan, R. Gadient, R. T. Jacobs, A. Zacco, B. Greenberg, and P. J. Ciaccio. 2004. Modulation of notch processing by γ-secretase inhibitors causes intestinal goblet cell metaplasia and induction of genes known to specify gut secretory lineage differentiation. Toxicol. Sci. 82:341-358.

Miura, S., and A. Suzuki. 2018. Brief summary of the current protocols for generating intestinal organoids. Dev. Growth Differ. 60:387-392.

Montgomery, R. K., D. L. Carlone, C. A. Richmond, L. Farilla, M. E. Kranendonk, D. E. Henderson, N. Y. Baffour-Awuah, D. M. Ambruzs, L. K. Fogli, S. Algra, and D. T. Breault. 2011. Mouse telomerase reverse transcriptase (mTert) expression marks slowly cycling intestinal stem cells. Proc. Natl. Acad. Sci. 108:179-184.

Mudalal, S., M. Lorenzi, F. Soglia, C. Cavani, and M. Petracci. 2015. Implications of white striping and wooden breast abnormalities on quality traits of raw and marinated chicken meat. Animal. 9:728-734.

Mutryn, M. F., E. M. Brannick, W. Fu, W. R. Lee, and B. Abasht. 2015. Characterization of a novel chicken muscle disorder through differential gene expression and pathway analysis using RNA-sequencing. BMC Genomics. 16:399.

Namork, E., and P. Brandtzaeg. 2002. Fatal meningococcal septicaemia with “blebbing” meningococcus. The Lancet. 360:1741.

National Chicken Council. 2018. Per capita consumption of poultry and livestock, 1965 to estimated 2018, in pounds. http://www.nationalchickencouncil.org/about-the-industry/statistics/per-capita-consumption-of-poultry-and-livestock-1965-to-estimated-2012-in-pounds/.

Neerukonda, S. N., N. A. Egan, J. Patria, I. Assakhi, P. Tavlarides-Hontz, S. Modla, E. R. Muñoz, M. B. Hudson, and M. S. Parcells. 2019. Comparison of exosomes purified via ultracentrifugation (UC) and Total Exosome Isolation (TEI) reagent from the

serum of Marek's disease virus (MDV)-vaccinated and tumor-bearing chickens. J. Virol. Methods. 263:1-9.

Ootani, A., X. Li, E. Sangiorgi, Q. T. Ho, H. Ueno, S. Toda, H. Sugihara, K. Fujimoto, I. L. Weissman, M. R. Capecchi, and C. J. Kuo. 2009. Sustained in vitro intestinal epithelial culture within a Wnt-dependent stem cell niche. Nat. Med. 15:701.

Orkin, R. W., P. Gehron, E. B. Mcgoodwin, G. R. Martin, T. Valentine, and R. Swarm. 1977. A murine tumor producing a matrix of basement membrane. J. Exp. Med. 145:204-220.

Panek, M., M. Grabacka, and M. Pierzchalska. 2018. The formation of intestinal organoids in a hanging drop culture. Cytotechnology. 70:1085-1095.

Pesce, A., R. H. McKay, F. Stolzenbach, R. D. Cahn, and N. O. Kaplan. 1964. The comparative enzymology of lactic dehydrogenases: I. properties of the crystalline beef and chicken enzymes. J. Biol. Chem. 239:1753-1761.

Petracci, M., S. Mudalal, F. Soglia, and C. Cavani. 2015. Meat quality in fast-growing broiler chickens. Worlds Poult. Sci. J. 71:363-374.

Petrini, E., G. P. Caviglia, M. L. Abate, S. Fagoonee, A. Smedile, and R. Pellicano. 2015. MicroRNAs in HBV-related hepatocellular carcinoma: functions and potential clinical applications. Panminerva Med. 57:201-209.

Pierzchalska, M., M. Grabacka, M. Michalik, K. Zyla, and P. Pierzchalski. 2012. Prostaglandin E2 supports growth of chicken embryo intestinal organoids in Matrigel matrix. Biotechniques. 52:307-315.

Pierzchalska, M., M. Panek, and M. Grabacka. 2019. The migration and fusion events related to ROCK activity strongly influence the morphology of chicken embryo intestinal organoids. Protoplasma. 256:575-581.

Pierzchalska, M., M. Panek, M. Czyrnek, A. Gielicz, B. Mickowska, and M. Grabacka. 2017. Probiotic Lactobacillus acidophilus bacteria or synthetic TLR2 agonist boost the growth of chicken embryo intestinal organoids in cultures comprising epithelial cells and myofibroblasts. Comp. Immunol Microbiol Infect Dis. 53:7-18.

Pierzchalska, M., M. Panek, M. Czyrnek, and M. Grabacka. 2016. The three-dimensional culture of epithelial organoids derived from embryonic chicken intestine. Organoids. 135-144.

Pinheiro, C., A. Longatto-Filho, L. Ferreira, S. M. M. Pereira, D. Etlinger, M. A. Moreira, L. F. Jube, G. S. Queiroz, F. Schmitt, and F. Baltazar. 2008. Increasing expression of monocarboxylate transporters 1 and 4 along progression to invasive cervical carcinoma. Int. J. Gynecol. Pathol. 27:568-574.

Pinheiro, C., A. Longatto-Filho, C. Scapulatempo, L. Ferreira, S. Martins, L. Pellerin, M. Rodrigues, V. A. Alves, F. Schmitt, and F. Baltazar. 2008. Increased expression of monocarboxylate transporters 1, 2, and 4 in colorectal carcinomas. Virchows Arch. 452:139-146.

Pinto, D., A. Gregorieff, H. Begthel, and H. Clevers. 2003. Canonical Wnt signals are essential for homeostasis of the intestinal epithelium. Genes Dev. 17:1709-1713.

Pisitkun, T., R. F. Shen, and M. A. Knepper. 2004. Identification and proteomic profiling of exosomes in human urine. Proc. Natl. Acad. Sci. 101:13368-13373.

Powell, D. W., I. V. Pinchuk, J. I. Saada, X. Chen, and R. C. Mifflin. 2011. Mesenchymal cells of the intestinal lamina propria. Annu. Rev. Physiol. 73:213-237.

Powell, R. H., and M. S. Behnke. 2017. WRN conditioned media is sufficient for in vitro propagation of intestinal organoids from large farm and small companion animals. Biol. Open. 6:698-705.

Quadrato, G., T. Nguyen, E. Z. Macosko, J. L. Sherwood, S. M. Yang, D. R. Berger, N. Maria, J. Scholvin, M. Goldman, J. P. Kinney, and E. S. Boyden. 2017. Cell diversity and network dynamics in photosensitive human brain organoids. Nature. 545:48-53.

Raposo, G., H. W. Nijman, W. Stoorvogel, R. Liejendekker, C. V. Harding, C. J. Melief, and H. J. Geuze. 1996. B lymphocytes secrete antigen-presenting vesicles. J. Exp. Med. 183:1161-1172.

Ratajczak, J., K. Miekus, M. Kucia, J. Zhang, R. Reca, P. Dvorak, and M. Z. Ratajczak. 2006. Embryonic stem cell-derived microvesicles reprogram hematopoietic progenitors: evidence for horizontal transfer of mRNA and protein delivery. Leukemia. 20:847-856.

Reynoso, R., N. Laufer, M. Hackl, S. Skalicky, R. Monteforte, G. Turk, M. Carobene, J. Quarleri, P. Cahn, R. Werner, and H. Stoiber. 2014. MicroRNAs differentially present in the plasma of HIV elite controllers reduce HIV infection in vitro. Sci. Rep. 4:5915.

Roth, D. A., and G. A. Brooks. 1990. Lactate transport is mediated by a membrane-bound carrier in rat skeletal muscle sarcolemmal vesicles. Arch Biochem Biophys. 279:377-385.

Salehi, S., K. Howe, M. L. Lawrence, J. P. Brooks, R. H. Bailey, and A. Karsi. 2017. *Salmonella* Enterica serovar Kentucky flagella are required for broiler skin adhesion and Caco-2 cell invasion. Appl. Environ. 83:e02115-16.

Sato, T., R. G. Vries, H. J. Snippert, M. Van De Wetering, N. Barker, D. E. Stange, J. H. Van Es, A. Abo, P. Kujala, P. J. Peters, and H. Clevers. 2009. Single Lgr5 stem cells build crypt-villus structures in vitro without a mesenchymal niche. Nature. 459:262-265.

Sato, T., J. H. Van Es, H. J. Snippert, D. E. Stange, R. G. Vries, M. Van Den Born, N. Barker, N. F. Shroyer, M. Van De Wetering, and H. Clevers. 2011. Paneth cells constitute the niche for Lgr5 stem cells in intestinal crypts. Nature. 469:415-418.

Scallan, E., R. M. Hoekstra, F. J. Angulo, R. V. Tauxe, M. A. Widdowson, S. L. Roy, J. L. Jones, and P. M. Griffin. 2011. Foodborne illness acquired in the United States—major pathogens. Emerg. Infect. Dis. 17:7.

Schepers, A. G., R. Vries, M. Van Den Born, M. Van De Wetering, and H. Clevers. 2011. Lgr5 intestinal stem cells have high telomerase activity and randomly segregate their chromosomes. EMBO J. 30:1104-1109.

Schwank, G., A. Andersson-Rolf, B. K. Koo, N. Sasaki, and H. Clevers. 2013. Generation of BAC transgenic epithelial organoids. PloS One. 8:e76871.

Schwechheimer, C., and M. J. Kuehn. 2015. Outer-membrane vesicles from Gram-negative bacteria: biogenesis and functions. Nat. Rev. Microbiol. 13:605-619.

Shahbandeh, M. 2020. Global broiler meat production 2020, by selected country. Accessed on Apr. 2021. https://www.statista.com/statistics/237597/leading-10-countries-worldwide-in-poultry-meat-production-in-2007/#statisticContainer

Shamir, E. R., and A. J. Ewald. 2014. Three-dimensional organotypic culture: experimental models of mammalian biology and disease. Nat. Rev. Mol. Cell Biol. 15:647-664.

Shimoda, A., K. Ueda, S. Nishiumi, N. Murata-Kamiya, S. A. Mukai, S. I. Sawada, T. Azuma, M. Hatakeyama, and K. Akiyoshi. 2016. Exosomes as nanocarriers for systemic delivery of the Helicobacter pylori virulence factor CagA. Sci. Rep. 6:1-9.

Sihvo, H. K., J. Lindén, N. Airas, K. Immonen, J. Valaja, and E. Puolanne. 2017. Wooden breast myodegeneration of pectoralis major muscle over the growth period in broilers. Vet. Pathol. 54:119-128.

Sihvo, H. K., K. Immonen, and E. Puolanne. 2014. Myodegeneration with fibrosis and regeneration in the pectoralis major muscle of broilers. Vet. Pathol. 51:619-623.

Sihvo, H. K., N. Airas, J. Lindén, and E. Puolanne. 2018. Pectoral vessel density and early ultrastructural changes in broiler chicken wooden breast myopathy. J. Comp. Pathol. 161:1-10.

Skog, J., T. Würdinger, S. Van Rijn, D. H. Meijer, L. Gainche, W. T. Curry, B. S. Carter, A. M. Krichevsky, and X. O. Breakefield. 2008. Glioblastoma microvesicles transport RNA and proteins that promote tumour growth and provide diagnostic biomarkers. Nat. Cell Biol. 10:1470-1476.

Spence, J. R., C. N. Mayhew, S. A. Rankin, M. F. Kuhar, J. E. Vallance, K. Tolle, E. E. Hoskins, V. V. Kalinichenko, S. I. Wells, A. M. Zorn, and N. F. Shroyer. 2011. Directed differentiation of human pluripotent stem cells into intestinal tissue in vitro. Nature. 470:105-109.

Tallentire, C. W., I. Leinonen, and I. Kyriazakis. 2018. Artificial selection for improved energy efficiency is reaching its limits in broiler chickens. Sci. Rep. 8:1168.

Tasoniero, G., M. Cullere, M. Cecchinato, E. Puolanne, and A. Dalle Zotte. 2016. Technological quality, mineral profile, and sensory attributes of broiler chicken breasts affected by White Striping and Wooden Breast myopathies. Poult. Sci. 95:2707-2714.

Théry, C., L. Zitvogel, and S. Amigorena. 2002. Exosomes: composition, biogenesis and function. Nat. Rev. Immunol. 2:569-579.

Thomson, J. A., J. Itskovitz-Eldor, S. S. Shapiro, M. A. Waknitz, J. J. Swiergiel, V. S. Marshall, and J. M. Jones. 1998. Embryonic stem cell lines derived from human blastocysts. Science. 282:1145-1147.

Tijare, V. V., F. L. Yang, V. A. Kuttappan, C. Z. Alvarado, C. N. Coon, and C. M. Owens. 2016. Meat quality of broiler breast fillets with white striping and woody breast muscle myopathies. Poult. Sci. 95:2167-2173.

Timmins, N. E., and L. K. Nielsen. 2007. Generation of multicellular tumor spheroids by the hanging-drop method. Methods Mol. Med. 140:141-151.

Ueo, T., I. Imayoshi, T. Kobayashi, T. Ohtsuka, H. Seno, H. Nakase, T. Chiba, and R. Kageyama. 2012. The role of Hes genes in intestinal development, homeostasis and tumor formation. Development. 139:1071-1082.

Uni, Z., A. Geyra, H. Ben-Hur, and D. Sklan. 2000. Small intestinal development in the young chick: crypt formation and enterocyte proliferation and migration. Br. Poult. Sci. 41:544-551.

Urbańska, K., and A. Orzechowski. 2019. Unappreciated role of LDHA and LDHB to control apoptosis and autophagy in tumor cells. Int. J. Mol. Sci. 20:2085.

Uribe, J. H., M. Collado-Romero, S. Zaldívar-López, C. Arce, R. Bautista, A. Carvajal, S. Cirera, M. G. Claros, and J. J. Garrido. 2016. Transcriptional analysis of porcine intestinal mucosa infected with *Salmonella* Typhimurium revealed a massive inflammatory response and disruption of bile acid absorption in ileum. Vet. Res. 47:1-10.

Valadi, H., K. Ekström, A. Bossios, M. Sjöstrand, J. J. Lee, and J. O. Lötvall. 2007. Exosome-mediated transfer of mRNAs and microRNAs is a novel mechanism of genetic exchange between cells. Nat. Cell Biol. 9:654-659.

van Es, J. H., N. De Geest, M. Van De Born, H. Clevers, and B. A. Hassan. 2010. Intestinal stem cells lacking the Math1 tumour suppressor are refractory to Notch inhibitors. Nat. Commun. 1:1-5.

van Es, J. H., M. E. van Gijn, O. Riccio, M. van den Born, M. Vooijs, H. Begthel, M. Cozijnsen, S. Robine, D. J. Winton, F. Radtke, and H. Clevers. 2005. Notch/γ-secretase inhibition turns proliferative cells in intestinal crypts and adenomas into goblet cells. Nature. 435:959-963.

van Hemert, S., A. J. Hoekman, M. A. Smits, and J. M. Rebel. 2006. Gene expression responses to a *Salmonella* infection in the chicken intestine differ between lines. Vet. Immunol. Immunopathol. 114:247-258.

van Niel, G., G. Raposo, C. Candalh, M. Boussac, R. Hershberg, N. Cerf–Bensussan, and M. Heyman. 2001. Intestinal epithelial cells secrete exosome–like vesicles. Gastroenterology. 121:337-349.

Velleman, S. G., and D. L. Clark. 2015. Histopathologic and myogenic gene expression changes associated with wooden breast in broiler breast muscles. Avian Dis. 59:410-418.

Vesy, C. J., R. L. Kitchens, G. Wolfbauer, J. J. Albers, and R. S. Munford. 2000. Lipopolysaccharide-binding protein and phospholipid transfer protein release lipopolysaccharides from gram-negative bacterial membranes. Infect. Immun. 68:2410-2417.

Wai, S. N., B. Lindmark, T. Söderblom, A. Takade, M. Westermark, J. Oscarsson, J. Jass, A. Richter-Dahlfors, Y. Mizunoe, and B. E. Uhlin. 2003. Vesicle-mediated export and assembly of pore-forming oligomers of the enterobacterial ClyA cytotoxin. Cell. 115:25-35.

Wang, S., L. Ye, M. Li, J. Liu, C. Jiang, H. Hong, H. Zhu, and Y. Sun. 2016. GSK-3β inhibitor CHIR-99021 promotes proliferation through upregulating β-catenin in neonatal atrial human cardiomyocytes. J. Cardiovasc Pharmacol. 68:425-432.

Wilson, H. V. 1907. A new method by which sponges may be artificially reared. Science. 25:912-915.

Wong, V. W., D. E. Stange, M. E. Page, S. Buczacki, A. Wabik, S. Itami, M. Van De Wetering, R. Poulsom, N. A. Wright, M. W. Trotter, and F. M. Watt. 2012. Lrig1 controls intestinal stem-cell homeostasis by negative regulation of ErbB signalling. Nat. Cell. Biol. 14:401-408.

Wolfers, J., A. Lozier, G. Raposo, A. Regnault, C. Théry, C. Masurier, C. Flament, S. Pouzieux, F. Faure, T. Tursz, and E. Angevin. 2001. Tumor-derived exosomes are a source of shared tumor rejection antigens for CTL cross-priming. Nat. Med. 7:297-303.

Wu, L., J. Guo, Q. Wang, S. Lu, X. Dai, Y. Xiang, and D. Fan. 2017. Sensitivity enhancement by using few-layer black phosphorus-graphene/TMDCs heterostructure in surface plasmon resonance biochemical sensor. Sensor Actuat. B-Chem. 249:542-548.

Xie, Z., G. Chen, X. Zhang, D. Li, J. Huang, C. Yang, P. Zhang, Y. Qin, Y. Duan, B. Gong, and Z. Li. 2013. Salivary microRNAs as promising biomarkers for detection of esophageal cancer. PloS One. 8:e57502.

Xing, T., X. Zhao, L. Zhang, J. L. Li, G. H. Zhou, X. L. Xu, and F. Gao. 2020. Characteristics and incidence of broiler chicken wooden breast meat under commercial conditions in China. Poult. Sci. 99:620-628.

Yin, X., H. F. Farin, J. H. Van Es, H. Clevers, R. Langer, and J. M. Karp. 2014. Niche-independent high-purity cultures of Lgr5+ intestinal stem cells and their progeny. Nat. Methods. 11:106.

Yin, X., B. E. Mead, H. Safaee, R. Langer, J. M. Karp, and O. Levy. 2016. Engineering stem cell organoids. Cell Stem Cell. 18:25-38.

Yui, S., T. Nakamura, T. Sato, Y. Nemoto, T. Mizutani, X. Zheng, S. Ichinose, T. Nagaishi, R. Okamoto, K. Tsuchiya, and H. Clevers. 2012. Functional engraftment of colon epithelium expanded in vitro from a single adult Lgr5+ stem cell. Nat. Med. 18:618-623.

Zampiga, M., J. Flees, A. Meluzzi, S. Dridi, and F. Sirri. 2018. Application of omics technologies for a deeper insight into quali-quantitative production traits in broiler chickens: A review. J. Anim. Sci. Biotechnol. 9:61.

Ždralević, M., A. Brand, L. Di Ianni, K. Dettmer, J. Reinders, K. Singer, K. Peter, A. Schnell, C. Bruss, S. M. Decking, and G. Koehl. 2018. Double genetic disruption

of lactate dehydrogenases A and B is required to ablate the “Warburg effect” restricting tumor growth to oxidative metabolism. J. Biol. Chem. 293:15947-15961.

Zhang, S., B. Saremi, E. R. Gilbert, and E. A. Wong. 2017. Physiological and biochemical aspects of methionine isomers and a methionine analogue in broilers. Poult. Sci. 96:425-439.

Zhang, Y. G., S. Wu, Y. Xia, and J. Sun. 2014. *Salmonella*-infected crypt-derived intestinal organoid culture system for host-bacterial interactions. Physiol. Rep. 2:e12147.

Zhou, J., C. Li, X. Liu, M. C. Chiu, X. Zhao, D. Wang, Y. Wei, A. Lee, A. J. Zhang, H. Chu, and J. P. Cai. 2020. Infection of bat and human intestinal organoids by SARS-CoV-2. Nat. Med. 26:1077-1083.

Zuidhof, M. J., B. L. Schneider, V. L. Carney, D. R. Korver, and F. E. Robinson. 2014. Growth, efficiency, and yield of commercial broilers from 1957, 1978, and 20051. Poult. Sci. 93:2970-2982.

2. AVIAN INTESTINAL ORGANOIDS FROM CRYPTS TO ENTEROIDS: ESTABLISHMENT AND CHARACTERIZATION OF AVIAN INTESTINAL ORGANOIDS

2.1. Introduction

Functional and heterogeneous intestinal organoids (IO), also known as “mini gut” or “enteroids”, are self-organized three-dimensional (3D) organ-like constructs. Intestinal organoids have been well developed and are used to study gastrointestinal diseases, intestinal physiology, and host-pathogen interaction in human medicine (Forbester et al., 2015; Thorne et al., 2018; Chandra et al., 2019). Sato et al. (2009) described a long-term Matrigel^{TM}-based culture system to establish 3D IO using a single stem cell (Lgr5^{+}) from mouse small intestines without losing phenotype and karyotype for eight months. These organoids fully recapitulate the physiology of intestinal epithelium, containing stem cells and differentiated cells (enterocytes, goblet cells, Paneth cells and enteroendocrine cells (Antfolke and Jensen, 2020). Intestinal organoids are established from intestinal crypts containing pluripotent stem cells or adult stem cells (Sato et al., 2009; Sato et al., 2011; Forbester et al., 2015). They are maintained in the culture media containing various growth factors relating to several critical signaling pathways. The Wnt signals are required for stem cell proliferation and Paneth cell terminal differentiation (Korinek et al., 1998; Farin et al., 2012). Notch signals serve as the enterocyte-secretory switch (van Es et al., 2005). The epidermal growth factor (EGF) assists the mitosis of stem cells (Wong et al., 2012). The bone morphogenetic protein (BMP) supports the villus formation (Haramis et al., 2004). Compared to traditional two-dimensional cell lines, 3D IO grown in organoid

growth media (OGM) containing these factors preserve natural intestine morphology and cell polarity, more accurately represent the in vivo environment, and increase cell-to-cell interactions (Simian and Bissell, 2016).

This beneficial IO culture system is widely studied in mammalian systems but not extensively in avian research although there are also various gastrointestinal diseases and pathogen infections affecting the quality and quantity of poultry products. Currently, avian intestinal epithelial cells as *in vitro* model systems are not available for studying the mechanism of host-microbe interaction and screening nutrients to improve overall gut health. The majority of the avian studies are based on short-term studies of avian primary enterocyte cultures (Velge et al., 2002; Dimier-Poisson et al., 2004; Rath et al., 2018) or commercial mammalian cell lines as proxy. In the past 10 years, six papers reported the establishment of IO from chickens, of which four described organoids derived from small intestines of chick embryos by a research team in Poland (Pierzchalska et al., 2012, 2017, and 2019; Panek et al., 2018). They demonstrated that prostaglandin E2 played an important role for the growth of small IO in 18-day-old chicken embryos. The probiotic bacteria and synthetic Toll like receptor 2 (TLR2) ligands also had positive influence on IO derived from the small intestine of 19-day-old chicken embryos (Pierzchalska et al., 2017). The migration and fusion of IO originated from the small intestine of 19-day-old chicken embryos were demonstrated (Pierzchalska et al., 2019). Li et al. (2018) established organoids from the jejunum of 2- to 3-week-old layer chickens and demonstrated the villus structure using transmission electron microscopy. However, the establishment of organoids from avian ceca has not been studied extensively. Powell and Behnke (2017) collected chicken ceca from processing plants and established a culture of chicken cecum organoids.

However, they did not fully characterize cellular and molecular components of cecum-derived organoids. The generation of avian species-specific IO will further benefit basic and applied poultry research on mechanisms of intestinal disease, host-pathogen interactions, metabolic crosstalk between host epithelium and pathogens, gut immune responses, and as a model for screening different nutritional effects on the host.

In the development of an organoid culture system, new functional growth factors are selected to optimize the organoid growth. Valproic acids (VA) play an essential role in Notch activation as a histone deacetylase inhibitor (Stockhausen et al., 2005; Greenblatt et al., 2007). CHIR99021 (CHIR), an activator of Wnt signaling pathway, can inhibit GSK3β-mediated β-catenin degradation as a specific GSK3 inhibitor (Bain et al., 2007). Valproic acids and CHIR have been proved to increase stem cell proliferation in mice and human IO cultures (Ye et al., 2012; Wang et al., 2016; Langlands et al., 2018). However, studies of the effects of VA and CHIR on avian IO development and growth are not known.

Therefore, this research aims to establish crypt-derived IO in laminin-rich Matrigel^{TM} surrounded by organoid growth media (OGM), to observe the development of changes in IO morphology, to characterize cellular compositions via western blotting, reverse transcription polymerase chain reaction (RT-PCR) and immunofluorescence, and to evaluate the effects of small molecules, CHIR and VA, on the growth and development of organoids.

2.2. Materials and methods

2.2.1. Experimental birds

Layer chickens at embryonic day 19 (n = 20) and layer and broiler chickens with ages ranging from day one to twenty weeks (n = 15) were used. The animal use protocol was approved by Institutional Animal Care and Use Committee of Texas A&M University (IACUC.2016-0270 and 2019-0171).

2.2.2. Crypt isolation

Isolation of crypts followed the previously protocol described by Fujii et al. (2015) with some modifications. Briefly, the intestinal tissues were collected from birds, opened longitudinally and washed 3 times with cold PBS to remove luminal contents. The cleaned intestinal tissues were then cut into 2 to 4 cm pieces and incubated with 2.5 mM EDTA in PBS for 30 min on a shaker with a speed of 300 rpm at 4°C to release crypts. Supernatant fractions enriched in crypts were collected, filtered through a 100-um and 70-um cell strainer (Fisher Science), and centrifuged at 300 x g for 5 min at 4°C to collect the crypts. The crypt pellet was washed in cold PBS at 300 x g for 5 min, 150 x g for 5 min, and 70 x g for 5 min to remove small debris and single cells.

2.2.3. The collection of conditioned media (CM) from L-WRN cell cultures

L-WRN cells (ATCC, #CRL-3276), producing Wnt-3A, R-spondin, and noggin factors, were cultured in high glucose DMEM (Gibco, Grand Island, NY) supplemented with 1X penicillin/streptomycin (Gibco) and 10% fetal bovine serum (FBS; HyClone, Logan, UT). The L-WRN CM was collected following the large-scale L-WRN CM production protocol described by Miyoshi and Stappenbeck (2013) and stored at -80°C.

2.2.4. Intestinal crypt culture and the generation of organoids

Approximately 500 crypts were suspended in 30 µL of growth factor reduced phenol-free Matrigel™ (BD Biosciences, San Jose, CA), as shown in Fig. 1A. The Matrigel™/crypt mix was placed in the center well of a 24-well plate. After 10 min of polymerization, 500 µL of OGM was added to the wells and was changed every other day. The OGM contains advanced DMEM/F12 (Gibco, Grand Island, NY) supplemented with 1X antibiotic-antimycotic (Gibco, Grand Island, NY), 10 mM HEPES (Sigma), 1X Glutamax (Gibco), 1 mM N-Acetyl-L-Cysteine (ACROS), 50 ng/ml EGF (Gibco), 500 nM A83-01 (AdooQ), 10 µM SB202190 (AdooQ), 10 µM Y-27632 (AdooQ), 0.02 µM PGE2, and 50% L-WRN cell-derived conditioned media (CM).

2.2.5. Imaging of the avian IO growth

Live images of the avian IO were captured with the all-in-one BZ-X800 Keyence Fluorescence Microscope (Osaka; Osaka Prefecture, Japan).

2.2.6. Passaging avian organoid cultures

Organoids were split every 4-5 days at a 1:4 ratio using TrypLE Express (Gibco) with 10nm Y-27632 (AdooQ) and plated in 24 well plates.

2.2.7. Cryopreservation of organoids

Organoids were suspended in OGM by pipetting up and down gently and transferred to 1.5 mL tubes. The suspension was centrifuged at 200 x g for 5 min at room temperature. Organoids were resuspended in 500 µL of freezing medium (OGM: FBS: DMSO = 8:1:1) and kept at -80°C. Subsequently, frozen organoids were transferred and stored in a liquid nitrogen tank.

2.2.8. Histochemistry

Cecum sections before and after EDTA chelation were fixed in 4% paraformaldehyde for 48 h and washed with PBS twice, then dehydrated in 70% ethanol and embedded in paraffin. The paraffin blocks were cut into 5-µm sections. The sections were deparaffinized and stained with hematoxylin and eosin (H&E).

The avian IO were rinsed three times in ice-cold PBS, fixed with 4% paraformaldehyde for 30 min at room temperature in the wells, and rinsed with ice-cold PBS. The fixed organoids with Matrigel™ were embedded in paraffin and cut into 5-µm sections. The sections were deparaffinized and stained with hematoxylin and eosin.

2.2.9. Immunohistochemistry

The sections of avian IO were washed with Tris-buffered saline (TBS) containing 0.1% Tween 20 (TBST) and blocked using 10% normal goat serum (Vector Laboratories) in TBST for one hour at room temperature, incubated with mouse anti E-cadherin (1:250, ab76055, Abcam) overnight at 4°C. After three washes with TBST, the secondary antibody Alexa Fluor® 555 goat anti-mouse IgG (1:1000, ab150118, Abcam) was added and incubated at room temperature for one hour followed by three times washed with TBST. The stained slides were mounted with one drop of Prolong Diamond Antifade DAPI (Invitrogen, P36966) and overlaid with a cover glass. The images were captured by all in one BZ X800 Keyence Fluorescence Microscope (Osaka, Osaka Prefecture, Japan).

2.2.10. Protein extraction and western blotting

Radioimmunoprecipitation assay (RIPA) buffer (Thermo Fisher Scientific, Waltham, MA) was used to extract protein from avian IO. Protein concentration was quantified by a BCA Protein Assay Kit (Thermo Fisher Scientific, Waltham, MA). Fifty

micrograms of protein from each sample was resolved onto 4-12% SDS-PAGE gradient gels (Bio-Rad, Hercules, CA). After electrophoresis, proteins were transferred to polyvinylidene difluoride (PVDF) membranes by a semi-dry electroblotting system (Bio-Rad, Hercules, CA) at 50 mA for 2 h. The PVDF membranes were blocked in TBST and 5% non-fat milk overnight at 4°C. Membranes were washed 4 times for 10 min in TBST, and then incubated with primary antibody for 4 h. The following primary antibodies were all from Abcam (Cambridge, MA) and used at the indicated dilutions: rabbit anti-Lgr5 (ab75732; 1:500), mouse anti-E cadherin (ab76055; 1:1,000), rabbit anti-lysozyme (ab391; 1:1,000), mouse anti-chromogranin A (1:500, Dr. Luc Berghman), mouse anti-GAPDH ab8245; 1:10,000). The membrane was washed 4 times in TBST, followed by incubation with a secondary antibody for 1 hour at room temperature. The following secondary antibodies were used: horseradish peroxidase (HRP)-conjugated goat anti-rabbit IgG (ab205718; 1:20,000), HRP-conjugated goat anti-mouse IgG (ab97040; 1:20,000). Enhanced chemiluminescence (ECL) detection reagents (Amersham Pharmacia Biotech, Piscataway, NJ) were employed. The chemiluminescent signals were captured and analyzed by a ChemiDocTM MP Image System (Bio-Rad, Hercules, CA). Immunoblot images were quantified by Quantity One-4.6.1 software (Bio-Rad, Hercules, CA).

2.2.11. Total RNA extraction and reverse transcription PCR (RT-PCR)

The avian IO were collected into a 15 mL low-binding centrifuge tube (STEMFULL, Sbio, Cat MS-90150) with a total 2 mL of TrypLE Express (Gibco, Grand Island, NY). Tubes were placed in a 37°C water bath for 5 min to dissolve the Matrigel^{TM}. Pellets of IO were collected by sequential centrifugations at 400 x g for 5 min at 4°C and at 1,000 x g for 5 min at 4°C. Total RNA was extracted from purified avian IO using the

mirVana miRNA isolation kit (Ambion, Austin, TX) following the manufacturer's manual. Total RNA concentrations were measured by NanoDrop 1000. One microgram of total RNA was reverse transcribed using SuperScript III First-Strand Synthesis System (Invitrogen, Carlsbad, CA) following the manufacturer's protocol. Reverse transcription polymerase chain reaction (RT-PCR) was conducted using Powerup SYBR Green Master Mix according to the manufacturer's instruction. The primer sequences used for qRT-PCR are listed in Table 1. Briefly, Power up SYBR Green Master Mix was combined with 10 µM primers and 10 ng cDNA template and loaded onto a 384-well plate. Then, RT-PCR was performed at 50°C for 2 min, 95°C for 10 min, following 40 cycles of 95°C for 15 s and 60°C for 1 min. PCR products were separated on a 2% agarose gel in Tris-acetate-EDTA (TAE) buffer. To determine the size of PCR products, a 100 bp DNA ladder was loaded onto the gel. The agarose gel image was captured by the PhotoDoc-It Imaging System (UVP, Upland, CA).

Table 2.1 Summary of primers used for RT-PCR analysis

Target gene		Primer Sequence (5' to 3')	Amplicons (bp)	Reference
LGR5	For	CCTTTATCAGCCCAGAAGTGA	338	Li et al., 2018
	Rev	TGGAACAAATGCTACGGATG		
E-cadherin	For	ACTGGTGACATTATTACCGTAGCA	226	Tiwari et al., 2013
	Rev	TAGCCACTATGACATCCACTCTGT		
Lysozyme	For	GACGATGTGAGCTGGCAG	225	Wang et al., 2016
	Rev	GGATGTTGCACAGGTTCC		
Chromogranin A	For	TGAATAAAGGGGACACTAAGG	337	Dr. Berghman
	Rev	AGCTCAGCCAGGGATG		
Muc2	For	CAGCACCAACTTCTCAGTTCC	102	Zhang et al., 2015
	Rev	TCTGCAGCCACACATTCTTT		
OlfM4	For	GACTGGCTCTCTGGATGACC	108	Li et al., 2018
	Rev	AGCGTTGTGGCTATCACTTG		
Alpha-SMA	For	AGGACAGCACTGCCCTTGTTT	136	Tavares et al., 2017
	Rev	CCCATACCAACCATCACACCCT		
Vimentin	For	GAAGCTGCTAACTACCAGGACACT	184	Tiwari et al., 2013
	Rev	TAGGCATGTTAATCCTGCTCTCTT		

Table 2.1 Continued

GAPDH	For	AGAACATCATCCCAGCGT	182	Shang et al.,
	Rev	AGCCTTCACTACCCTCTTG		2014
Beta-Actin	For	TGCTGTGTTCCCATCTATCG	470	Bai et al.,
	Rev	TTGGTGACAATACCGTGTTCA		2017

2.2.12. The effects of OGM supplemented with VA and CHIR on avian small IO growth

Crypts were isolated from small intestines of 19-day-old chicken embryos (n=20) and 500 crypts were embedded in Matrigel™ that were cultured in OGM only (Con) and OGM supplemented with 1mM VA (AdooQ), 3 μM CHIR (AdooQ), and combination of 1 mM VA and 3 μM CHIR for 7 days. Live cultures of the avian IO were imaged with the all-in-one BZ-X800 Keyence Fluorescence Microscope (Osaka; Osaka Prefecture, Japan). The size of the avian IO was measured using ImageJ. The experiments were repeated twice at different days, each time with four biological replicates for each group.

2.2.13. Statistical evaluation

The statistical significance of differences in the mean number and size of the avian IO maintained in various conditions was calculated and analyzed by one way ANOVA using JMP14, P-values ≤ 0.05 were considered statistically significant.

2.3. Results

2.3.1. Isolation of intestinal crypts of avian origin

Crypts were isolated and purified from the small intestines of chicken embryos, the ceca of day-old-broilers and layers. The crypts were then seeded in Matrigel™ cultured in OGM, as shown in Fig. 2.1A. The presences of crypts in the intestine were stained using H&E and are shown in Fig. 2.1B, highlighted by the black arrows. After EDTA chelation,

most of the crypts were released from the intestine (Fig. 2.1C). The released crypts were purified by differential centrifugation and filtration (Fig. 2.1D).

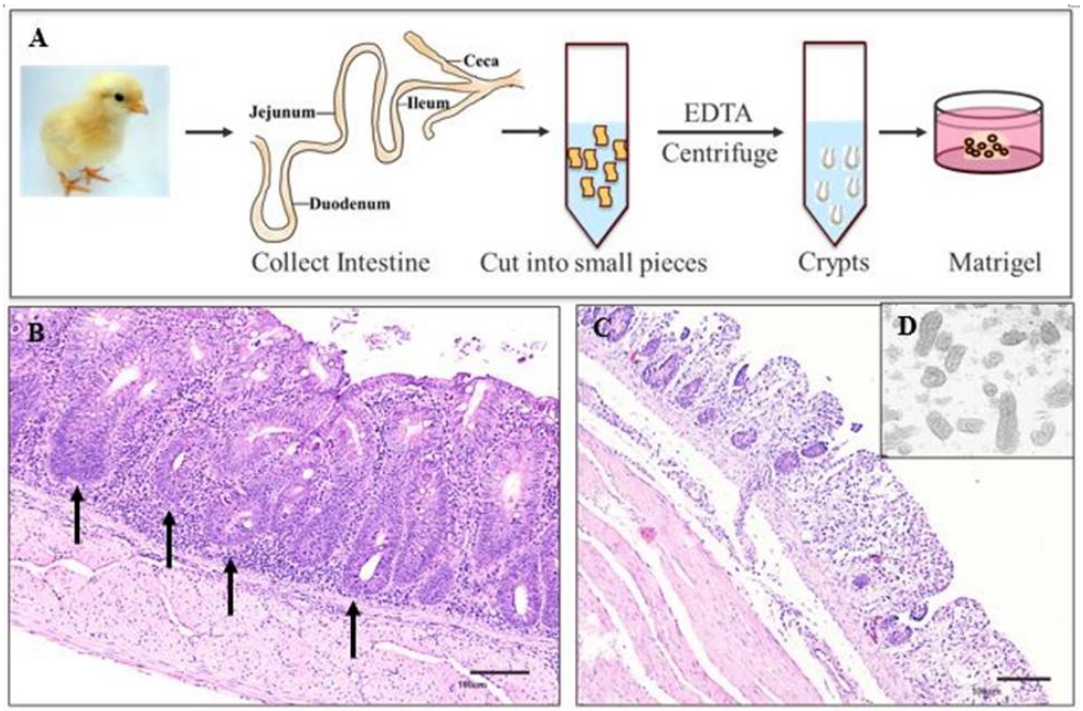

Figure 2.1 Description of the establishment of crypt-derived 3D avian intestinal organoids. (A) Schematic diagram showing avian intestinal crypts isolated from a broiler chicken. The avian intestines were collected, cut open longitudinally, washed three times in cold PBS, cut into small pieces, and incubated in EDTA to release the crypts. The crypts were purified through differential centrifugation and filtration with 100 µm and 70 µm filters. Purified crypts were embedded in Matrigel™ surrounded in organoid growth media. (B) Representative ceca-cross section stained with hematoxylin-eosin (H&E). Black arrows indicate examples of crypts. Scale bar = 100 µm. (C) Representative image of ceca cross-section stained with H&E after the removal of most crypts following EDTA chelation. Scale bar = 100 µm. (D) Purified crypts after differential centrifugation and filtration.

2.3.2. Time course of avian ceca-derived organoid growth

The crypts that were isolated from day-old broilers were seeded in Matrigel™ on a 24 well-plate with OGM that contained growth factors for stem cell proliferation and

differentiation. The live culture images of the avian IO were captured from day 1 to 14 (Fig. 2.2) using an all-in-one BZ-X800 Keyence Fluorescence Microscope. Observation of growth of avian IO in the first 24 h revealed that the majority of the stem cells in the crypts proliferated rapidly to sphere-shaped 3D organoids. The organoids simultaneously transformed into spherical shapes covered with epithelial cells. The organoids continually enlarged during the following seven days. From day 10 to 14 of culture, the organoids developed branches (Fig. 2.2). The cultured organoids were passaged at least 5 times and cryopreserved successfully.

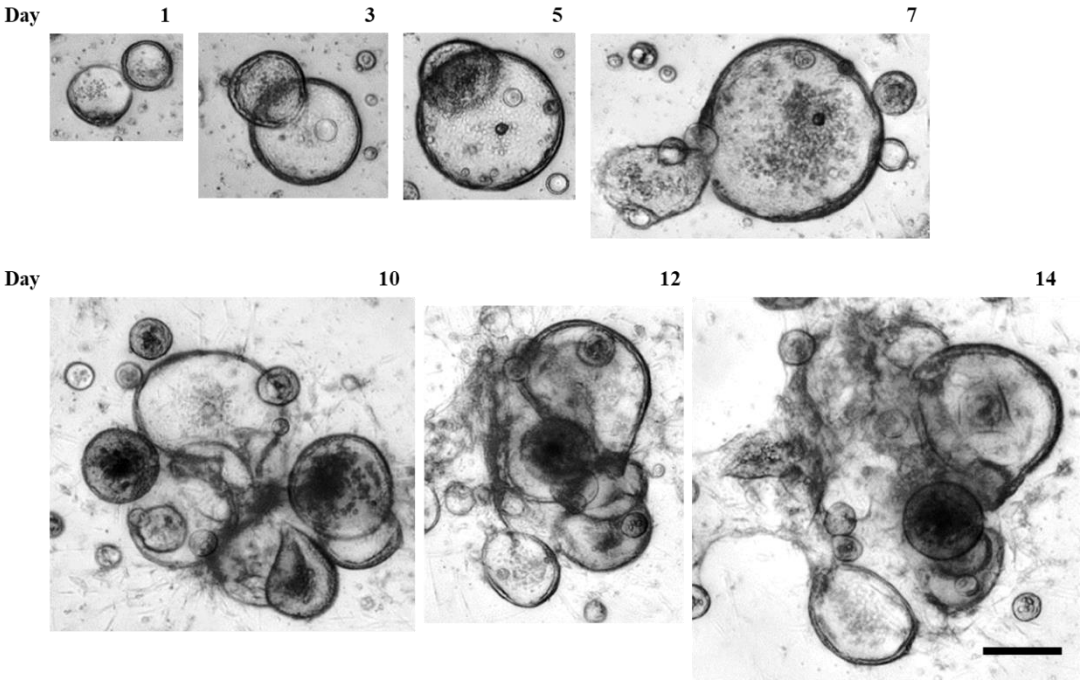

Figure 2.2 Time course of avian ceca-derived organoid growth from day-one-old broilers. Crypts were collected from the ceca of day of hatch broiler chicks and seeded in Matrigel^{TM} on a 24-well plate with organoid culture medium. The growth of live organoids was monitored, and images were captured using an all-in-one BZ-X800 Keyence Fluorescence Microscope on the day indicated as numbered. Scale bar = 200 µm.

2.3.3. Growth development of avian organoids from the ceca and small intestines of broiler, layer, or embryo origins at different ages

We also established the organoids from the ceca of layer (20-week-old; Fig. 2.3A) and broiler chickens (4-day-old; Fig. 2.3B) showing live organoid image with spherical structures. Those IO obtained from the small intestine of chicken embryo (embryonic day 19) are shown in Fig. 2.3C, revealing the same spherical structure.

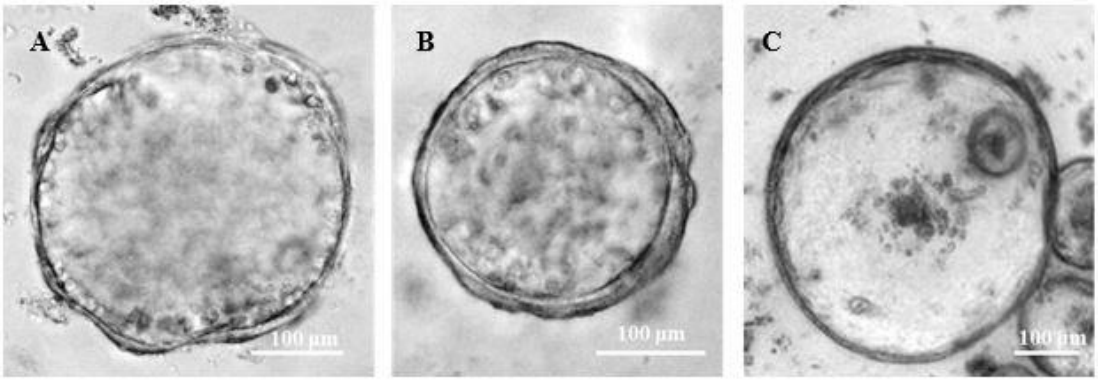

Figure 2.3 Morphology of avian intestinal organoids. A representative bright-field image of an organoid derived from 20-week-old layers (A), cecal crypts of 4-day-old broilers (B), and small intestines of 19-day-old chick embryos (C) are shown. Image (A) and (B) were captured with an Olympus FV 1000 confocal microscope, and image (C) was recorded with an all-in-one BZ-X800 Keyence Fluorescence Microscope. All organoids were cultured in the media for 5 days. Scale bar = 100 µm.

2.3.4. Immunofluorescence staining of avian cecal organoid

Immunofluorescent staining of the cross-section of an organoid showed the population of intestinal enterocytes (red) using E-cadherin for epithelial cell markers (Fig. 2.4A). These organoids had single cell layers and a closed-loop hollow lumen (Fig. 2.4).

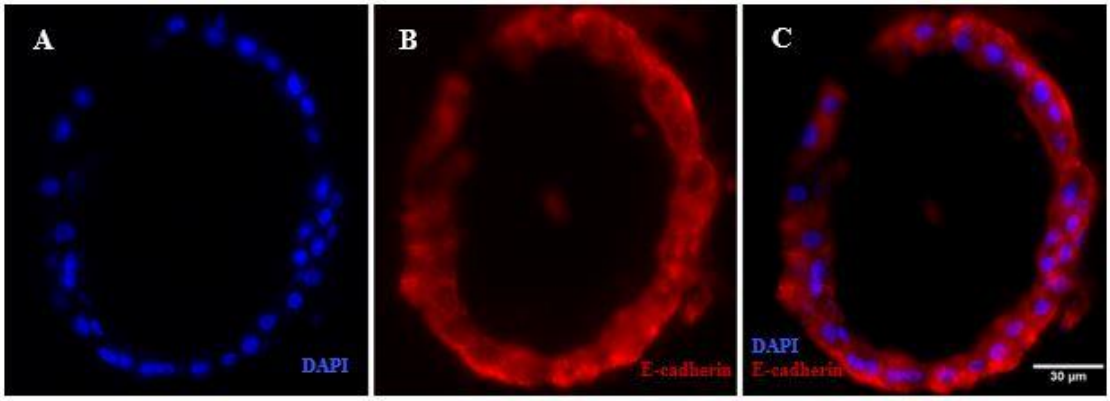

Figure 2.4 Immunofluorescence staining of avian cecal organoids. Representative images of immunofluorescence staining of a cecal organoid cross-section using E-cadherin showing a single cell layer, including nuclei of cells stained in blue (DAPI, A). E-cadherin in red (B). Merge image (C). Scale bar = 30 µm. The images were captured by an all-in-one BZ-X800 Keyence Fluorescence Microscope.

2.3.5. Characterization of cell populations of organoids by immunoblotting and RT-PCR

To identify cell populations in the cultured avian IO, their protein and total RNA were extracted. Western blotting revealed the presence of lysozyme (the marker for Paneth cells), chromogranin A (the marker for enteroendocrine cells), E-cadherin (the marker for enterocytes), and Lgr5 (the marker of stem cells; Fig. 2.5). The expression of these genes at mRNA levels was also verified by RT-PCR (Fig. 2.5). Therefore, crypt-derived organoids were epithelial cells that contained stem cells, enteroendocrine and Paneth cells. Furthermore, the RT-PCR results confirmed the expression of Muc2 (a goblet cell marker), OlfM4 (a stem cell marker), alpha-SMA (a marker of myofibroblast), and vimentin (a marker of mesenchymal cell; Fig. 2.6), confirming the presence of goblet cells, fibroblasts, and mesenchymal cells.

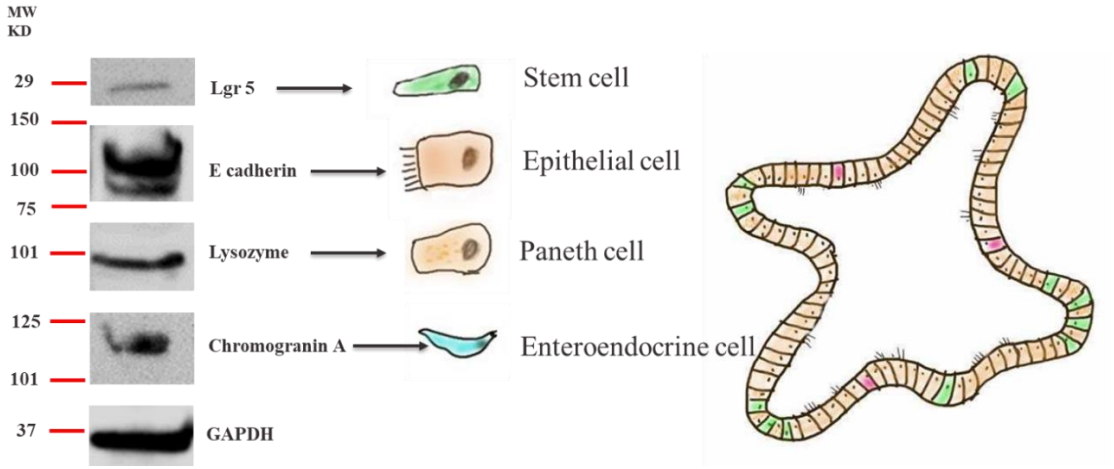

Figure 2.5 Western blot analysis of different cell types from avian cecal organoids using protein biomarkers. Cecal organoids in a Matrigel™ were collected with TrypLE Express and washed with ice-cold PBS. Total protein from organoids was extracted with radioimmunoprecipitation assay buffer (RIPA). Fifty micrograms of protein from cecal organoids were resolved in the 4-12% SDS-PAGE gradient gels. Immunoblotting of whole organoid protein extracts showed the presence of Lgr5 (a stem cell marker), E-cadherin (an epithelial cell marker), lysozyme (a Paneth cell marker), and chromogranin A (an enteroendocrine cell marker).

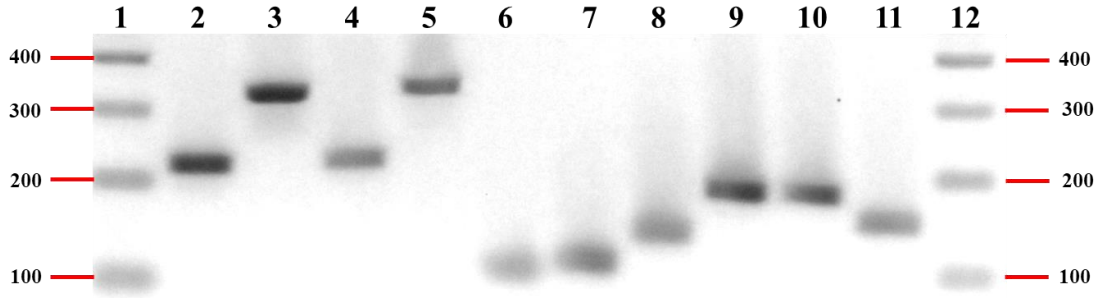

Figure 2.6 RT-PCR confirms cell populations of organoids using cell marker genes. Cell populations of avian small intestinal organoids were identified by RT-PCR with their biomarker genes. A representative image of RT-PCR results from lane 1 to lane 12 were 100 bp DNA ladder, E-cadherin (an epithelial cell marker, 226 bp), Lgr5 (a stem cell marker, 338 bp), lysozyme (a Paneth cell marker, 225 bp), chromogranin A (an enteroendocrine cell marker, 337 bp), Muc2 (a goblet cell marker, 102 bp), OlfM4 (a stem cell marker, 108 bp), alpha-SMA (a myofibroblast marker, 136 bp), vimentin (a mesenchymal cell marker, 184 bp), GAPDH (182 bp), actin (470 bp), and 100 bp DNA ladder, respectively.

2.3.6. The OGM supplemented with both VA and CHIR increased avian IO size

Valproic acid and CHIR were used to improve the efficiency of organoid formation in mammalian models. The concentrations of VA and CHIR used in this study were followed from previous reports in mammalian species (Yin et al., 2014). To determine how these two growth factors influenced avian IO growth, avian IO derived from 19-day embryos were cultured for 7 days in OGM control medium (Con; Fig. 2.7A), OGM supplemented with VA (Fig. 2.7B), CHIR (Fig. 2.7C), or the combined treatment of VA and CHIR (Fig. 2.7D). We found that VA treatment decreased the numbers of organoids, 1.2-fold lower than those organoid numbers in the Con group (Fig. 2.7B and 2.7E; $P < 0.0001$). The treatment of CHIR alone did not change the numbers of organoids (Fig. 2.7E). However, the mean number of organoids in combined treatment of VA and CHIR group was 1.3-fold lower ($P = 0.0013$) than those in the CHIR group (Fig. 2.7E). In addition, the size of the IO was measured by calculating mean surface area. The average size of the organoids in VA group was not significantly different compared to those from Con group, but the average size of organoids in CHIR group was 0.4-fold larger ($P = 0.0087$) than the Con group. The combination of VA and CHIR increased the mean area of organoids 2.3-fold larger ($P < 0.0001$) than those from the CHIR group.

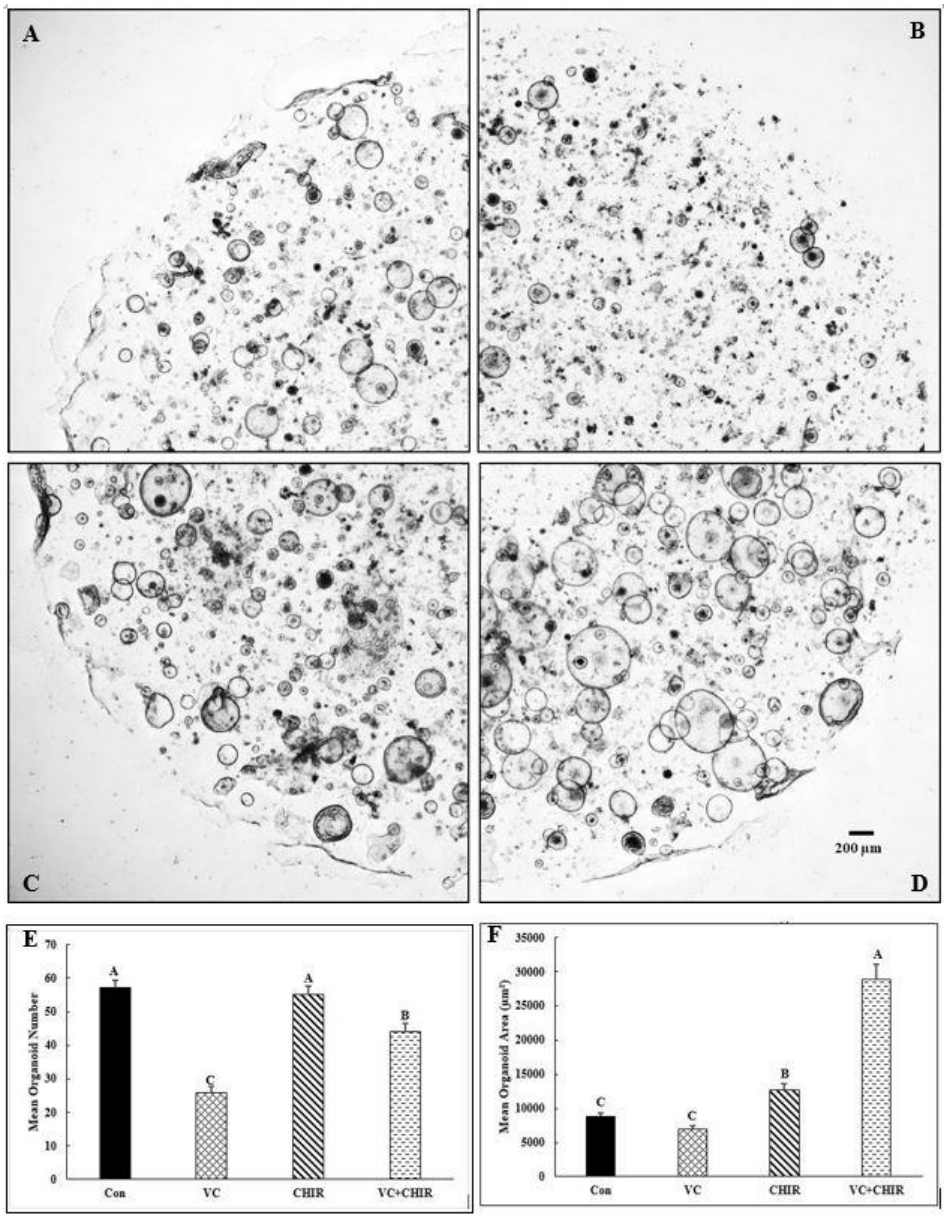

Figure 2.7 The effect of valproic acid and CHIR99021 on avian small intestinal organoid growth. Crypts were isolated from small intestines of 19-day-old chicken embryos and embedded in Matrigel that were cultured in OGM only (Con) and OGM supplemented with valproic acid (VA), CHIR99021 (CHIR), and a combination of VA and CHIR. Representative images of organoids from 7-day cultures are shown for the Con group (A), VA (B), CHIR (C) and VA+CHIR (D). Scale bars represent 200 µm. Effect of media supplemented with VA and CHIR on the mean organoid numbers (E) and mean area of organoids (F) are shown. The experiments were repeated twice on different days, each time with four biological replicates for each group. A total of 20 chicken embryos was used. Results are presented as mean ± SEM. The means with a different superscript letter are significantly different from each other ($P < 0.05$).

2.4. Discussion

Intestinal organoids are multicellular 3D *in vitro* constructs that recapitulated the structure and functions of intestine *in vivo*. Based on the IO culture protocols for human and mouse (Miyoshi and Stappenbeck, 2013; Mahe et al., 2014; Fujii et al., 2015; Pierzchalska et al., 2016), we have successfully generated crypt-derived organoids from chicken small intestines and ceca and optimized the conditions for IO growth, passages and cryopreservation. The cell populations in crypt-derived IO were characterized, confirming the presences of enterocytes, stem cells, enteroendocrine, Paneth cells, and goblet cells.

The IO can be derived from adult stem cells (Sato et al., 2009) or pluripotent stem cells (Spence et al., 2011), which are located at the bottom of the intestinal crypts. Sato et al. (2009) purified the intestinal stem cells from mouse intestinal crypts and established IO with a single stem cell. Nevertheless, several experiments demonstrated that cell contact between stem cells and Paneth cells promote organoids forming efficiency (Snippert et al., 2010; Sato et al., 2011; Farin et al., 2012; Yilmaz et al., 2012). Similar to other reports (Pierzchalska et al., 2012, 2017, 2019; Li et al., 2018), we demonstrated the establishment of 3D organoids by growing purified intestinal crypts that consisted of stem cells and Paneth cells. Compared to the single sorted stem cells, isolated crypts are time- and cost-efficient, and easier handle.

The maintenance of self-renewing stem cells in culture requires three major growth factors, Wnt3a, R-spondin, and Noggin (Sato et al., 2009; Clevers, 2016), which can be provided as commercial products (Sato et al., 2009; Pierzchalska et al., 2012; Li et al., 2018), or secreted by the L-WRN (ATCC CRL-3276) cell lines (Miyoshi et al., 2013) that

produce all three factors. The highly replicable activity of the L-WRN CM was validated over time and between laboratories (VanDussen et al., 2019). The L-WRN CM have been widely used in research to establish mouse and human IO (Miyoshi and Stappenbeck, 2013; Powell and Behnke, 2017; VanDussen et al., 2019). The L-WRN CM supports a cost-effective approach to organoid culture. We established avian IO with L-WRN CM produced by ATCC CRL-3276 cell lines.

The morphology of IO derived from ceca of broiler, layer, and small intestine of chicken embryos all take a sphere shape with a hollow lumen in the center. The morphology of avian IO is similar to the early stage of mouse small intestine IO. Nevertheless, they did not have the regular bud structure that is considered as the crypt section in the mouse small intestine IO (Yin et al., 2014; Lindeboom et al., 2018).

Avian organoids contain heterogeneous cell populations in our studies. The presence of Lgr5-positive and OlfM4-postive stem cells, Paneth cells, enteroendocrine cells, enterocytes, and goblet cells were identified by their gene products, detected using western blotting and RT-PCR. Furthermore, the RT-PCR results confirmed the presences of myofibroblast cells (alpha-SMA) and mesenchymal cells (Vimentin). Sato et al. (2009) also revealed the presence of non-epithelial cells in the mouse IO that were derived from intestinal crypts. We identified the presence of myofibroblast cells in our organoid culture system, which was consistent with previous reports (Pierzchalska et al. 2017 and 2019). They found that the amount of myofibroblasts increased over time more rapidly than the epithelial cells and demonstrated that the presence of myofibroblasts has the potential to promote IO survival and migration. *In vivo*, myofibroblasts adjacent to the crypt were reported to regulate the neighboring intestinal stem cells by activating paracrine signals

(Williams et al., 1992; Li and Xie, 2005; Crosnier et al., 2006). In addition, co-cultured the intestinal crypts with mesenchymal/stromal cells has been found to promote the intestinal cells growth (Ootani et al., 2009; Lahar et al., 2011; Spence et al., 2011; Li et al., 2016).

The two main signaling pathways for the IO culture system are the Wnt and Notch pathways. Valproic acid, a histone deacetylase inhibitor, and CHIR99021, a glycogen synthase kinase 3β inhibitor, are reported to be the activators for these two pathways, respectively (Stockhausen et al., 2005; Greenblatt et al., 2007; Yin et al., 2014; Langlands, et al., 2018; Mead et al., 2018). In this study, we measured the effects of VA and CHIR on the mean number and surface area of the avian IO. We found that VA did not change the size of organoids but decreased the numbers of organoids, and CHIR significantly increased the mean size of organoids without any effect on organoid numbers. It is interesting to note that synergistic effect of CHIR and VA, resulting in the largest mean size of organoids. We speculate that the combined treatment of VA and CHIR increase organoid size by promoting more stem cell formation, as demonstrated by Yin et al. (2014) that the supplementation with CHIR induced larger average size of the mice IO, and the combination of CHIR and VA increased the intensity of stem cells in mice. Ye et al. (2012) revealed the self-renewing promotion of CHIR on mouse embryo stem cells at the molecular level. Lindeboom et al. (2018) generated the stem cell enriched mouse IO with supplements of CHIR and VA in the organoid culture medium. CHIR alone upregulated mRNA expressions of Olfm4 and Lgr5 (stem cell biomarker) in organoids from jejunum-derived crypts of 3-week-old Hyline chickens (Li et al., 2018). The larger the organoid diameter, the more stem cells proliferate in the organoids. The stem cell enriched IO offers a powerful in vitro model to study the mechanism of differentiation of stem cells.

In summary, the avian IO represent a valuable in-vitro model for the study of the avian intestinal system and have the potential to replace the use of animals in experiments. Our results show that organoids can be derived from intestines from any age of chicken, and they consist of main cell types from avian intestines and recapitulate the structure and function of the avian intestine. We anticipate the organoid model will play important roles in advance our knowledge in antimicrobial drug screening, molecular mechanism of crosstalk between gut epithelial and immune cells, dietary supplement screening to improve gut health in poultry, and vaccine development.

2.5. References

Antfolk, M., and K. B. Jensen. 2020. A bioengineering perspective on modelling the intestinal epithelial physiology in vitro. Nat. Commun. 11:1-11.

Bain, J., L. Plater, M. Elliott, N. Shpiro, C. J. Hastie, H. Mclauchlan, I. Klevernic, J. S. Arthur, D. R. Alessi, and P. Cohen. 2007. The selectivity of protein kinase inhibitors: a further update. Biochem. 408:297-315.

Chandra, L., D. C. Borcherding, D. Kingsbury, T. Atherly, Y. M. Ambrosini, A. Bourgois-Mochel, W. Yuan, M. Kimber, Y. Qi, Q. Wang, and M. Wannemuehler. 2019. Derivation of adult canine intestinal organoids for translational research in gastroenterology. BMC Biol. 17:33.

Clevers, H. 2016. Modeling development and disease with organoids. Cell. 165:1586-1597.

Crosnier, C., D. Stamataki, and J. Lewis. 2006. Organizing cell renewal in the intestine: stem cells, signals and combinatorial control. Nat. Rev. Genet. 7:349-359.

Dimier-Poisson, I. H., D. T. Bout, and P. Quéré. 2004. Chicken primary enterocytes: inhibition of Eimeria tenella replication after activation with crude interferon-γ supernatants. Avian Dis. 48:617-624.

Farin, H. F., J. H. Van Es, and H. Clevers. 2012. Redundant sources of Wnt regulate intestinal stem cells and promote formation of Paneth cells. Gastroenterology. 143:1518-1529.

Forbester, J. L., D. Goulding, L. Vallier, N. Hannan, C. Hale, D. Pickard, S. Mukhopadhyay, and G. Dougan. 2015. Interaction of *Salmonella* Enterica serovar

Typhimurium with intestinal organoids derived from human induced pluripotent stem cells. Infect. Immun. 83:2926-2934.

Fujii, M., M. Matano, K. Nanki, and T. Sato. 2015. Efficient genetic engineering of human intestinal organoids using electroporation. Nat. Protoc. 10:1474.

Greenblatt, D. Y., A. M. Vaccaro, R. Jaskula-Sztul, L. Ning, M. Haymart, M. Kunnimalaiyaan, and H. Chen. 2007. Valproic acid activates notch-1 signaling and regulates the neuroendocrine phenotype in carcinoid cancer cells. Oncologist. 12:942-951.

Haramis, A. P., H. Begthel, M. Van Den Born, J. Van Es, S. Jonkheer, G. J. Offerhaus, and H. Clevers. 2004. De novo crypt formation and juvenile polyposis on BMP inhibition in mouse intestine. Science. 303:1684-1686.

Korinek, V., N. Barker, P. Moerer, E. van Donselaar, G. Huls, P. J. Peters, and H. Clevers. 1998. Depletion of epithelial stem-cell compartments in the small intestine of mice lacking Tcf-4. Nat. Genet. 19:379-383.

Lahar, N., N. Y. Lei, J. Wang, Z. Jabaji, S. C. Tung, V. Joshi, M. Lewis, M. Stelzner, M. G. Martín, and J. C. Dunn. 2011. Intestinal subepithelial myofibroblasts support in vitro and in vivo growth of human small intestinal epithelium. PloS One. 6:e26898.

Langlands, A. J., T. D. Carroll, Y. Chen, and I. Näthke. 2018. Chir99021 and Valproic acid reduce the proliferative advantage of Apc mutant cells. Cell Death Dis. 9:1-10.

Li, J., J. Li, S. Y. Zhang, R. X. Li, X. Lin, Y. L. Mi, and C. Q. Zhang. 2018. Culture and characterization of chicken small intestinal crypts. Poult. Sci. 97:1536-1543.

Li, L., and T. Xie. 2005. Stem cell niche: structure and function. Annu. Rev. Cell Dev. Biol. 21:605-631.

Li, X., A. Ootani, and C. Kuo. 2016. An air–liquid interface culture system for 3D organoid culture of diverse primary gastrointestinal tissues. Methods Mol. Biol. 1422:33-40.

Lindeboom, R. G., L. van Voorthuijsen, K. C. Oost, M. J. Rodríguez-Colman, M. V. Luna-Velez, C. Furlan, F. Baraille, P. W. Jansen, A. Ribeiro, B. M. Burgering, and H. J. Snippert. 2018. Integrative multi-omics analysis of intestinal organoid differentiation. Mol. Syst. Biol. 14:e8227.

Mahe, M. M., E. Aihara, M. A. Schumacher, Y. Zavros, M. H. Montrose, M. A. Helmrath, T. Sato, and N. F. Shroyer. 2013. Establishment of gastrointestinal epithelial organoids. Curr. Protoc. Mouse Biol. 3:217-240.

Mead, B. E., J. Ordovas-Montanes, A. P. Braun, L. E. Levy, P. Bhargava, M. J. Szucs, D. A. Ammendolia, M. A. MacMullan, X. Yin, T. K. Hughes, and M. H. Wadsworth.

2018. Harnessing single-cell genomics to improve the physiological fidelity of organoid-derived cell types. BMC Biol. 16:1-24.

Miyoshi, H., and T. S. Stappenbeck. 2013. In vitro expansion and genetic modification of gastrointestinal stem cells in spheroid culture. Nat. Protoc. 8:2471-2482.

Ootani, A., X. Li, E. Sangiorgi, Q. T. Ho, H. Ueno, S. Toda, H. Sugihara, K. Fujimoto, I. L. Weissman, M. R. Capecchi, and C. J. Kuo. 2009. Sustained in vitro intestinal epithelial culture within a Wnt-dependent stem cell niche. Nat. Med. 15:701.

Panek, M., M. Grabacka, and M. Pierzchalska. 2018. The formation of intestinal organoids in a hanging drop culture. Cytotechnology. 70:1085-1095.

Pierzchalska, M., M. Grabacka, M. Michalik, K. Zyla, and P. Pierzchalski. 2012. Prostaglandin E2 supports growth of chicken embryo intestinal organoids in Matrigel matrix. Biotechniques. 2:307-315.

Pierzchalska, M., M. Panek, M. Czyrnek, A. Gielicz, B. Mickowska, and M. Grabacka. 2017. Probiotic Lactobacillus acidophilus bacteria or synthetic TLR2 agonist boost the growth of chicken embryo intestinal organoids in cultures comprising epithelial cells and myofibroblasts. Comp. Immunol. Microbiol. Infect. Dis. 53:7-18.

Pierzchalska, M., M. Panek, M. Czyrnek, and M. Grabacka. 2016. The three-dimensional culture of epithelial organoids derived from embryonic chicken intestine. Organoids. 1576:135-144.

Pierzchalska, M., M. Panek, and M. Grabacka. 2019. The migration and fusion events related to ROCK activity strongly influence the morphology of chicken embryo intestinal organoids. Protoplasma. 256:575-581.

Powell, R. H., and M. S. Behnke. 2017. WRN conditioned media is sufficient for in vitro propagation of intestinal organoids from large farm and small companion animals. Biol. Open. 6:698-705.

Rath, N. C., R. Liyanage, A. Gupta, B. Packialakshmi, and J. O. Lay. 2018. A method to culture chicken enterocytes and their characterization. Poult. Sci. 97:4040-4047.

Sato, T., J. H. Van Es, H. J. Snippert, D. E. Stange, R. G. Vries, M. Van Den Born, N. Barker, N. F. Shroyer, M. Van De Wetering, and H. Clevers. 2011. Paneth cells constitute the niche for Lgr5 stem cells in intestinal crypts. Nature. 469:415-418.

Sato, T., R. G. Vries, H. J. Snippert, M. Van De Wetering, N. Barker, D. E. Stange, J. H. Van Es, A. Abo, P. Kujala, P. J. Peters, and H. Clevers. 2009. Single Lgr5 stem cells build crypt-villus structures in vitro without a mesenchymal niche. Nature. 459:262-265.

Simian, M., and M. J. Bissell. 2017. Organoids: a historical perspective of thinking in three dimensions. J. Cell Biol. 216:31-40.

Snippert, H. J., L. G. Van Der Flier, T. Sato, J. H. Van Es, M. Van Den Born, C. Kroon-Veenboer, N. Barker, A. M. Klein, J. Van Rheenen, B. D. Simons, and H. Clevers. 2010. Intestinal crypt homeostasis results from neutral competition between symmetrically dividing Lgr5 stem cells. Cell. 143:134-144.

Spence, J. R., C. N. Mayhew, S. A. Rankin, M. F. Kuhar, J. E. Vallance, K. Tolle, E. E. Hoskins, V. V. Kalinichenko, S. I. Wells, A. M. Zorn, and N. F. Shroyer. 2011. Directed differentiation of human pluripotent stem cells into intestinal tissue in vitro. Nature. 470:105-109.

Stockhausen, M. T., J. Sjölund, C. Manetopoulos, and H. Axelson. 2005. Effects of the histone deacetylase inhibitor valproic acid on Notch signalling in human neuroblastoma cells. Br. J. Cancer. 92:751-759.

Thorne, C. A., I. W. Chen, L. E. Sanman, M. H. Cobb, L. F. Wu, and S. J. Altschuler. 2018. Enteroid monolayers reveal an autonomous WNT and BMP circuit controlling intestinal epithelial growth and organization. Dev. Cell. 44:624-633.

van Es, J. H., M. E. van Gijn, O. Riccio, M. van den Born, M. Vooijs, H. Begthel, M. Cozijnsen, S. Robine, D. J. Winton, F. Radtke, and H. Clevers. 2005. Notch/γ-secretase inhibition turns proliferative cells in intestinal crypts and adenomas into goblet cells. Nature. 435:959-963.

VanDussen, K. L., N. M. Sonnek, and T. S. Stappenbeck. 2019. L-WRN conditioned medium for gastrointestinal epithelial stem cell culture shows replicable batch-to-batch activity levels across multiple research teams. Stem Cell Res. 37:101430.

Velge, P., E. Bottreau, P. Quéré, P. Pardon, J. C. Nicolle, M. Morisson, D. Bout, and I. Dimier. 2002. Establishment and characterization of partially differentiated chicken enterocyte cell clones. Eur. J. Cell Biol. 81:203-212.

Wang, S., L. Ye, M. Li, J. Liu, C. Jiang, H. Hong, H. Zhu, and Y. Sun. 2016. GSK-3β inhibitor CHIR-99021 promotes proliferation through upregulating β-catenin in neonatal atrial human cardiomyocytes. J. Cardiovasc. Pharmacol. 68:425-432.

Williams, E. D., A. P. Lowes, D. Williams, and G. T. Williams. 1992. A stem cell niche theory of intestinal crypt maintenance based on a study of somatic mutation in colonic mucosa. Am. J. Pathol. 141:773.

Wong, V. W., D. E. Stange, M. E. Page, S. Buczacki, A. Wabik, S. Itami, M. Van De Wetering, R. Poulsom, N. A. Wright, M. W. Trotter, and F. M. Watt. 2012. Lrig1 controls intestinal stem-cell homeostasis by negative regulation of ErbB signalling. Nat. Cell Biol. 14:401-408.

Ye, S., L. Tan, R. Yang, B. Fang, S. Qu, E. N. Schulze, H. Song, Q. Ying, and P. Li. 2012. Pleiotropy of glycogen synthase kinase-3 inhibition by CHIR99021 promotes self-renewal of embryonic stem cells from refractory mouse strains. PloS One. 7:e35892.

Yilmaz, Ö. H., P. Katajisto, D. W. Lamming, Y. Gültekin, K. E. Bauer-Rowe, S. Sengupta, K. Birsoy, A. Dursun, V. O. Yilmaz, M. Selig, and G. P. Nielsen. 2012. mTORC1 in the Paneth cell niche couples intestinal stem-cell function to calorie intake. Nature. 486:490-495.

Yin, X., H. F. Farin, J. H. Van Es, H. Clevers, R. Langer, and J. M. Karp. 2014. Niche-independent high-purity cultures of Lgr5+ intestinal stem cells and their progeny. Nat. Methods. 11:106.

3. CHARACTERIZATION OF THE EFFECT OF *SALMONELLA* TYPHIMURIUM ON SERUM-DERIVED EXOSOMAL MIRNAS IN CHICKS

3.1. Introduction

Salmonella causes foodborne illnesses in approximately 1.2 million people every year in the United States. It is a major concern for human health, resulting in estimated spending of $365 million directly in medical costs per year (Scallan et al., 2011). *Salmonella* Typhimurium (*ST*) is one of the most common *Salmonella* serotypes and causes gastrointestinal disease in humans globally (Scallan et al., 2011; CDC, 2021), and it is a Gram-negative, rod-shaped, flagellated anaerobe. One of the main sources of ST is poultry products, including meat from broiler chickens and eggs from layer chickens (Galis et al., 2013). Reducing contamination of ST is a critical need for reducing foodborne illnesses and decreasing the economic losses for the poultry industry. Understanding host-ST interactions in chickens will improve strategies to reduce contamination of poultry products. Numerous studies correlate the pathogenesis to significant alterations of proteins and mRNAs that were involved in immune responses of chickens using high-throughput assessments, including proteomic, kinome array, and RNA sequencing methods (Kogut et al., 2016; Packialakshmi et al., 2016; Li et al., 2018). The exact mechanisms for host-*Salmonella* interactions are not still well understood in chicks. Studies in mammalian system have reported the vital role of circulating extracellular vesicles (EV) in host-bacteria interaction (Schorey et al., 2015; Hong et al., 2021).

Exosomes are phospholipid bilayer nanoscale extracellular vesicles that are 30 to 150 nm in diameter. Previous studies have demonstrated that exosomes are released by a

variety of cell types, including neuronal cells, red blood cells, immune cells, epithelial cells, and are present in serum, urine, and saliva (Van Niel et al., 2001; Blanchard et al., 2002; Pisikun et al., 2004; Caby et al., 2005; Fauré et al., 2006). The formation of exosomes is initiated from the inward budding of endosomal membranes that come into the early endosomes. Early endosomes develop into multi-vesicular bodies and release into the extracellular environment as exosomes (Théry et al., 2002; Huotari et al., 2011; Li et al., 2019). During this processing, exosomes are packed with miRNAs, mRNAs, DNA, protein, and lipids (Colombo et al., 2014; Li et al., 2014; Zhang et al., 2015). Due to their cell-origin-unique, circulating feature, and composition, they can be easily taken up by the target cells and execute several biological functions, facilitating intercellular communication and modulating immune responses (Mathivanan et al., 2010; Lässer et al., 2011; Bellingham et al., 2012; Yáñez-Mó et al., 2015; Kim et al., 2019). The molecular fingerprints inside exosomes have been widely studied as potential biomarkers in diagnosing a disease. For instance, two exosomal micro RNAs (miRNAs) in Marek's disease virus-infected chicken serum, gga-mir-146 and gga-mir-21, were proposed to be the potential biomarkers of Marek's disease (Neerukonda et al., 2019). Exosomes derived from lipopolysaccharide challenged chicken macrophage cells up-regulated gene expression of cytokines and chemokines, such as IL-4 and CCL4, of chicken macrophage HD 11 cells (Hong et al., 2021).

MicroRNAs, 18-25 nucleotides (nts) in length, are small non-coding RNAs that regulate the translation of their target mRNAs by binding to their 3'-untranslated regions (Bartel, 2004; Guarnieri and DiLeone, 2008). As the post-transcriptional regulators, miRNAs are involved in several physiological and pathologic processes, such as immune

responses, cell proliferation and differentiation, and biomarkers for disease (Lai, 2002; Ambros, 2004; Croce and Calin, 2005; Esquela-Kerscher and Slack, 2006; Hunter et al., 2008; Yates et al., 2013; Maudet et al., 2014; Das et al., 2016; da Rocha et al., 2020). However, the role of miRNAs in host *Salmonella* interactions of chickens is poorly understood. Whether and how ST infection modulates exosomal miRNA expression in the circulatory system of birds is still unknown.

This study aims to elucidate the effects of epizootic bacteria, ST, on non-coding small RNAs derived from exosomes in the peripheral circulation system by small RNA sequencing. We have isolated and characterized exosomes from serum of broilers of control (Con) group and challenged with ST by nanoparticle tracking analysis (NTA) and transmission electron microscope (TEM). Small RNAs were extracted from exosomes, and small RNA libraries were constructed and sequenced by the Illumina NovaSeq 6000. Differential expression (DE) analyses of miRNAs were carried out to identify significantly differentially expressed miRNA panels in ST challenged birds compared to birds from the Con group. Our discoveries about miRNA-target molecular pathways from serum-derived exosomes significantly improves our understanding of the mechanism of ST in chickens.

3.2. Materials and Methods

3.2.1. *Salmonella* Typhimurium culture

The strain of ST, culture method of ST, and concentration determination of ST were previously described by Pineda et al. (2021).

3.2.2. Experimental design and birds

A total of 373 day of hatche non-vaccinated Cobb broiler chicks were purchased from a commercial hatchery and were fed a balanced unmedicated starter ration that met or

exceeded industry recommendations for nutrition (Cobb-Vantress, 2018) and water ad libitum. Birds were randomly divided into two treatment groups and housed in two rooms (190 birds for Con group and 183 birds for ST group). Upon arrival, fecal samples were collected from chick tray papers and cultured to confirm that the chicks were negative for ST. After three days of acclimatization, the chicks were challenged orally by gavage with 0.5 ml of sterile (TSB) for the Con group (n = 190) and 0.5 ml of 10^9 cfu/ml of ST in TSB for ST-challenged group (n = 183). On day one post-challenge, all birds were humanely euthanized. All animal care procedures were approved by the USDA Institutional Animal Care and Use Committee Protocol (IACUC.2016-0270 and 2019-0171).

3.2.3. Enumeration of *Salmonella* Typhimurium in cecal contents of broilers

The ceca from each chick were removed aseptically, and cecal contents (0.25g) were added to 2.25 ml of PBS (stock solution) that were serially diluted to 1:10, 1:100, 1:1,000, and 1:10,000 in PBS. The stock solution (100 µL) was added to 10 mL Rappaport-Vassiliadis (RV) medium for enrichment. The diluents were plated onto xylose lysine tergitol 4-NN (XLT4-NN; Hardy Diagnostics, Santa Maria, CA) plates that were incubated at 37°C for 48 h. The enrichment tubes were incubated at 41°C for 24 h and 100 µL of the enrichment media was plated on XLT4-NN plates, which were incubated at 37°C for 24 h. The enumeration of ST per gram of cecal contents was measured by colony counts on the XLT4-NN plates. Rappaport-Vassiliadis enrichments were also used to determine the presence of low levels of ST.

3.2.4. Blood sample collection and serum isolation

Blood samples were drawn from each recently euthanized bird by cardiac puncture via a 18 -gauge needle. Blood was collected into a 2 mL tube and kept at room temperature

for at least 2 h and centrifuged at 2,000 x g for 10 mins at 4°C. Then, the top clear serum was transferred into a 2 ml centrifuge tube and was stored at -80°C until further use.

3.2.5. Exosome isolation

Exosomes were isolated and purified from serum using differential ultracentrifugation combined with a filtration method (Simpson et al., 2008). Briefly, serum was centrifuged at 10,000 x g for 15 mins at 4°C to remove any cell debris. Supernatant was collected and diluted with the same volume of PBS that was filtrated through a 0.45 µm pore size filter and a 0.22 µm pore size filter, separately (Celltreat Scientific Products, Pepperell, MA). The filtrate was transferred to ultracentrifuge polyallomer tube (Beckman Coulter, Brea, CA, USA) and centrifuged at 100,000 x g for 6 h at 4°C with a Type 70 Ti rotor (Beckmann Optima XPN90; Beckman Coulter, Brea, CA, USA). Exosome pellets were washed once with ice-cold PBS and centrifuged at 100,000 x g for 6 h at 4°C. The exosome pellets were stored at -80°C for downstream applications including nanoparticle tracking analysis (NTA), transmission electron microscopy (TEM), and small RNA isolation, as shown below.

3.2.6. Size distribution and concentration of exosomes by nanoparticle tracking analysis (NTA)

Size determination and concentration measurements of the serum-derived exosomes were performed on a NanoSight LM14 (NanoSight, Malvern, UK) equipped with a 488 nm laser. The serum-derived exosome pellets were diluted with PBS to an available concentration (10^8 particles/mL) for NTA. The diluted exosomes were loaded into the sample chamber using a one mL sterile syringe until the liquid reached the chamber outlet. Images were visually evaluated, and the gain and shutter time was adjusted

to allow for detection of small particles. Afterward, the NTA 3.4 software was used to track all particles in the visual field throughout the captured video. All measurements were performed at room temperature. Size distribution diagrams, mean/mode size value, and standard deviations were calculated within the NTA 3.4 software and used for downstream analysis.

3.2.7. Transmission electron microscopy (TEM)

Transmission electron microscopy was employed to characterize the morphology of exosomes. Exosomes were fixed with 2% glutaraldehyde for about 1 h. One drop (15 ul) of the fixed exosomes was added on a carbon-coated 300-mesh copper grid and negatively stained with 1% uranyl acetate solution for 10 min at room temperature. Exosomes were imaged in a Hitachi H7000 transmission electron microscope (Hitachi High Technologies America, Schaumburg, IL).

3.2.8. Small RNA extraction, quantification, library construction, and sequencing

Small RNAs from serum-derived exosomes was extracted with a Total Exosome RNA and Protein Isolation Kit, according to the instructions from the manufacture (Invitrogen, Carlsbad, CA). Concentrations of isolated small RNAs were estimated with a NanoDrop 1000 (NanoDrop Technologies, Wilmington, DE). Since the length of small RNA is below 200 nt and concentration of exosomal small RNA was low in each sample, the concentration, integrity, and composition of small RNA were examined by an Agilent Bioanalyzer 2100 on an Agilent Small RNA kit (Agilent Technologies, Santa Clara, CA, USA).

Five small RNA libraries for Con group and seven small RNA libraries for ST group were constructed using NEBNext® Small RNA Library Prep Set for Illumina®

(Multiplex Compatible; NEB#: E7330S, New England Biolabs, Ipswich, MA) and NEBNext® Multiplex Oligos for Illumina® (Index Primers Set 1 and 2, NEB #: E7335S and E7500S) in accordance with the manufacturer's instructions. Briefly, 100 ng of small RNA was used for each library preparation. Input small RNAs were ligated by 3’ adapters first, and then the reverse transcription primer was hybridized to prevent adaptor-dimer formation. After primer hybridization, input small RNAs with 3’ adapters were ligated by 5’ adapters. Reverse transcription was performed following both adapters ligation to synthesize the first strand cDNA. Complementary DNA was amplified with PCR using 5’-universal primer and 3’-index primer. Each enriched small RNA library was then indexed with a unique barcoded sequence, which was used for the multiplexing purposes. All enriched small libraries were purified by QIAQuick PCR Purification Kit and eluted in 28 µl nuclease-free Water. AMPure XP beads (Beckman Coulter, Brea, CA) were performed to remove large fragments following the size selection protocol from the manufacturer’s instruction. Final library samples were quantified by the Qubit flourometer using Qubit dsDNA HS Assay Kit (Life Technologies, Carlsbad, CA) and validated by Agilent Bioanalyzer 2100 system using DNA 1000 assay kit (Agilent Technologies, Santa Clara, CA).

To multiplex library samples, all small RNA library samples (5 Con group and 7 for ST group) were diluted to equal concentration and pooled together with equal amounts, which was considered as one sequencing sample. Pooled library samples were sequenced on an Illumina NovaSeq 6000 (Illumina, San Diego, CA) using a 50 base pair single read, at the NUSeq Core facility of Northwestern University, Chicago, IL, USA.

3.2.9. Bioinformatics analysis and differential miRNA expression analysis

Pooled samples were de-multiplexed into individual files according to different indexes. Only reads with an index sequence were reserved. Raw reads were trimmed by removing the bad quality sequence, index sequence, Illumina adapter sequence, and sequence reads shorter than 15 nts. The resulting set of trimmed reads were then mapped against the miRNA database of *Gallus gallus* in miRBase (http://www.mirbase.org). EdgeR can moderate common dispersion of miRNA-Seq data and was used to analyze DE of miRNA. Differential expression of miRNAs between Con and ST groups were assessed in EdgeR by calculating an exact test p-value analogous to the Fisher's exact test (Juhila et al. 2011). The criteria for identifying DE miRNAs are based on 1) read count value was more than 50; 2) log2 (fold-change) > 1; and 3) $P < 0.05$.

Functional annotation of miRNAs and pathway enrichment analysis were examined by DAVID Bioinformatics Resources 6.8 (https://david.ncifcrf.gov/).

3.2.10. Statistical analysis

The data of ST colonization, exosome nanoparticle analysis were evaluated statistically. The t-test determined statistical differences between Con and ST groups using JMP15 software (SAS Institute Inc., Cary, NC). A p-value of < 0.05 was considered a significant difference.

3.3. Results

3.3.1. Confirmation of ST colonization in cecal contents of ST-challenged broiler

We first evaluated and confirmed the colonization of ST in broiler chicks that were challenged by a single oral gavage of 0.5 mL of 10^9 cfu/ml. One day post-challenge, quantitative analysis of ST colonization in each broiler demonstrated that the ST group had

CFU of 7.23 ± 0.74 Log10 CFU/g compared to 0 Log10 CFU/g in the Con group (Table 4.1). No ST colony was found in the cecal contents of the Con group using enrichment. In the ST group, 100% of birds were positive for *Salmonella* colonization in ceca contents, as shown in Table 3.1.

Table 3.1. Evaluation of *Salmonella* Typhimurium colonization in ceca of broiler chickens. Cecal contents of each broiler from the unchallenged Con (n=190) and ST-challenged (ST, n=183) groups were evaluated for *Salmonella* colonization.

	Log_{10} (CFU of ST /g cecal contents of chicken)	Percent positive ceca (# positive/total)
	Day 1 post-infection	Day 1 post-infection
Con	0	0 (0/190)
ST	7.23 ± 0.74	100 (183/183)

The value for colony-forming units (CFU) represents the mean ± standard error of the mean of broilers in each treatment. Percentage positive cecum is expressed as the number of positive ST (*Salmonella* growth after enrichment) / total broilers in the group.

3.3.2. Size distribution and concentration of serum-derived exosomes

Exosomes were isolated and purified from serum using combined differential ultracentrifugation and filtration. The concentration and size distribution of exosomes were measured by NTA, as shown in Fig. 3.1. The representative images of NTA data shown in Fig. 3.1A, which exported the mean size (nm), mode size (nm), and concentration (numbers of particles / mL) of diluted exosomes. The serum-derived exosome's mean size was 100.25 ± 2.87 nm and 106.58 ± 2.96 nm for the Con group and the ST group, respectively (Fig. 3.1B, P = 0.18). The mode size, known as the most common size, of the

isolated exosome from Con birds and ST infected birds was 81.13 ± 5.62 nm and 84.48 ± 2.63 nm, individually (Fig. 3.1C, P = 0.62). On average, approximately (3.5 ± 0.48) x 10^{10} and (4.8 ± 1.26) x 10^{10} exosome particles were recovered from 1 mL of serum from the Con group and ST group, respectively (Fig. 3.1D, P = 0.39). In summary, the exosome's median size was 92.7 ± 3.29 nm for the Con group and 99.7 ± 2.73 nm for the ST group. About 80% of exosomes were in the size range of 61.6 – 149.2 nm for the Con birds and 65.3 – 156.9 nm for the ST-infected birds (Fig. 3.2).

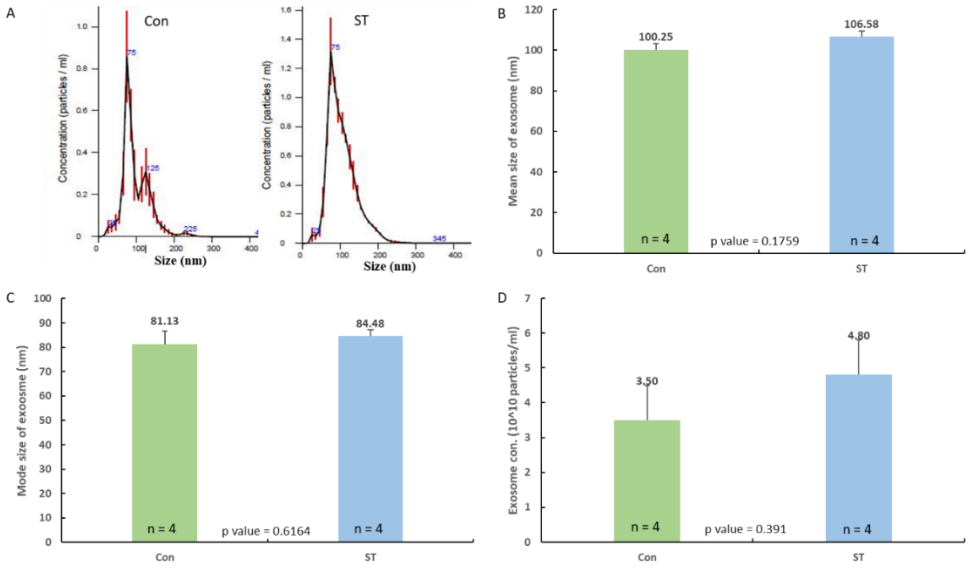

Figure 3.1 Nanoparticle tracking analysis of serum-derived exosomes.
(A) Representative images of the concentration of serum-derived exosomes according to the size of exosomes for Con and ST-infected groups. The X-axis represents the size (nm) and the Y-axis is the concentration of particles (particles / ml). The mean size (B), the mode size (C), and the concentration of exosomes (D) are shown in the serum of the Con (n = 4) and ST-infected group (n = 4), respectively.

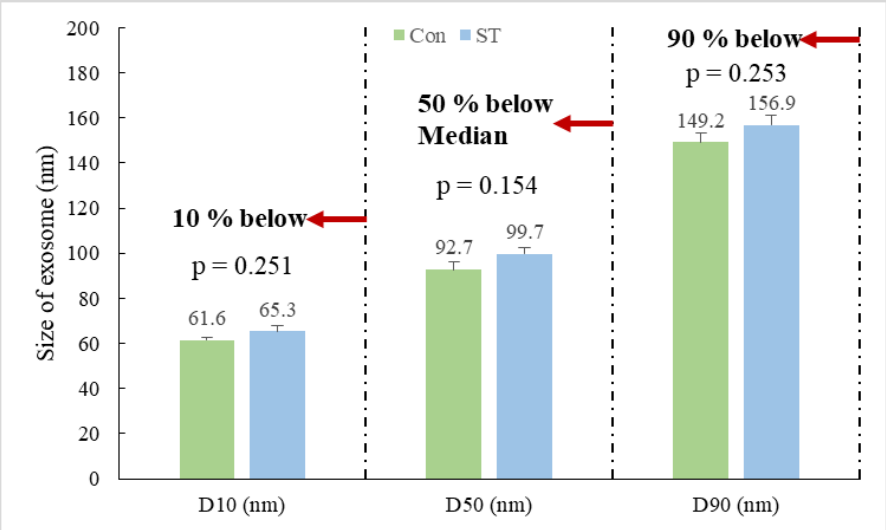

Figure 3.2 Different size distributions (D10, D50, D90) of serum-derived exosomes from Con (n = 4) and ST (n = 4) groups. The D10, D50 and D90 indicates that 10%, 50% and 90% exosomes are below the size as D10, D50 and D90, respectively.

3.3.3. Characterization of exosome morphology and size by TEM

Transmission electron microscope confirmed the presence of exosomes and demonstrated that the size of serum-derived exosomes, which were isolated from Con birds and ST infected birds, were in the size of range of 50 - 100 nm in diameter with a sphere-like shape (Fig. 3.3).

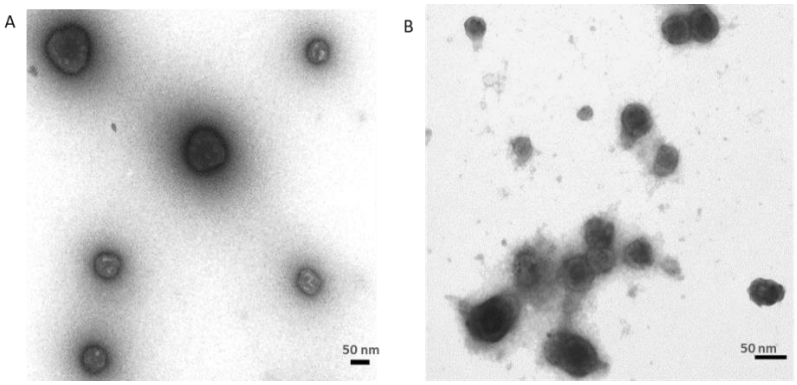

Figure 3.3 Negative-staining transmission electron microscopy of serum exosomes. (A) Representative image of exosomes from the Con group. (B) Representative image of exosomes from the ST-infected group. Scale bar = 50 nm.

3.3.4. Chicken serum-derived exosomes contain miRNAs

The quality and quantity of small RNA extracted from serum-derived exosomes were measured by NanoDrop 1000 and Agilent 2100 Bioanalyzer with a small RNA kit. As shown in Fig. 4.4, miRNA was the majority of the RNA population from isolated small RNAs in exosomes.

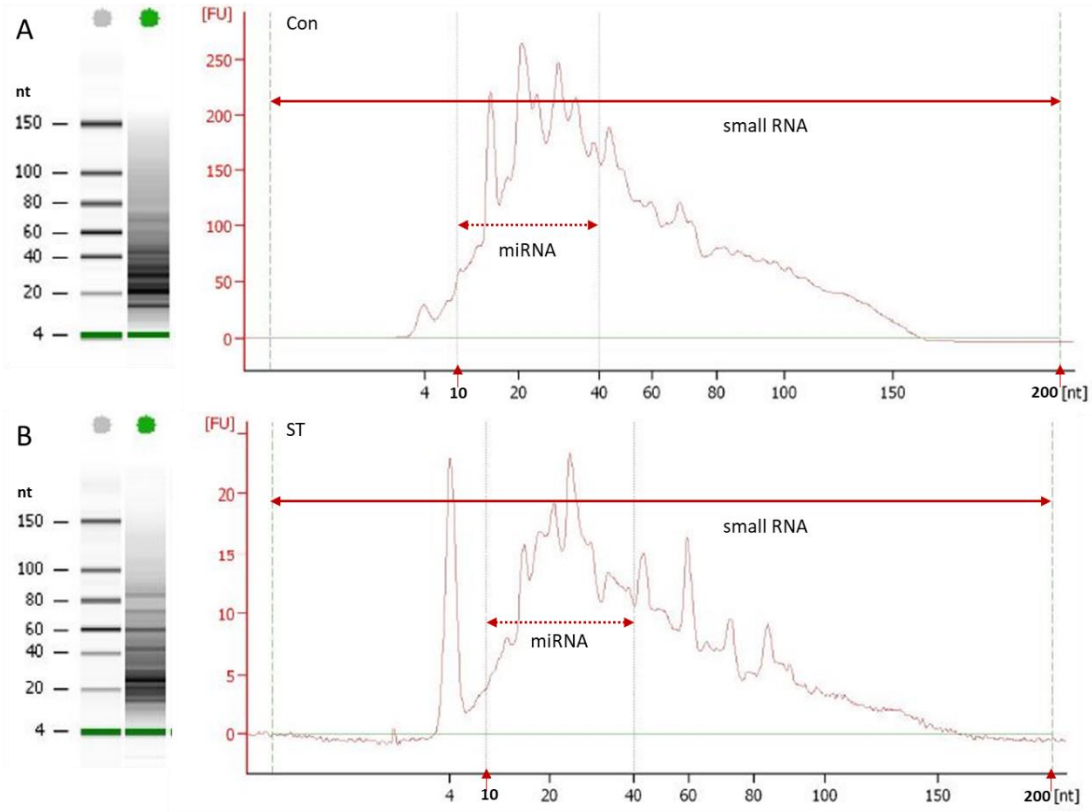

Figure 3.4 Size description of small RNA isolated from exosomes. An Agilent 2100 Bioanalyzer was employed to measure the size distribution verse the concentrations as well as small RNA electrophoresis of small RNA extracted from the serum-derived exosomes of the Con group (A) and ST-infected (B) group. The miRNAs ranged from 10 to 40 nts as indicated by the red dotted lines. The small RNA region covers the size of nucleotides up 150 nts, indicated by the straight red lines. The X-axis indicates the length of small RNA molecules in nucleotides and the Y-axis represents the fluorescence units (FU).

3.3.5. Unique exosomal miRNA profiles and prediction of their target gene and biological pathways

Small RNA sequence data showed that a total of 292 mature miRNAs were identified from the Con group and the ST group (Fig. 3.5). In the Con group, 284 mature miRNAs were identified, of which 11unique miRNAs, gga-miR-1664-3p, miR-101-1-5p, miR-12266-5p, miR-1454, miR-148b-5p, miR-1786, miR-214b-5p, miR-29b-1-5p, miR-301b-3p, miR-6582-5p, miR-9-4-3p were only found in the Con group (Fig. 3.5, Table 3.2). In ST group, total 281 mature miRNAs were detected, including 8 unique miRNAs distinct from the Con birds, gga-let-7g-3p, miR-16-1-3p, miR-1744-3p, miR-1788-5p, miR-3530-5p, miR-383-5p, miR-6542-3p, miR-6710-3p (Fig. 3.5, Table 3.2).

In order to classify unique miRNAs from different treatment groups in any functional class, DAVID functional GO analysis was utilized to export their molecular function, biological process, and biological pathways (Fig. 3.6). The top 3 unique exosomal miRNAs, gga-miR-1788-5p, gga-miR-3530-5p, and gga-miR-383-5p in the ST group, were predicted to target many genes that were involved in FoxO signaling pathway, positive regulation for apoptotic signaling pathway, transferase and phosphotransferase activities.

Table 3.2 Summary of miRNA profiles only found in Con and ST group.

Unique miRNAs	
Con group	ST group
gga-miR-1664-3p	gga-let-7g-3p
gga-miR-101-1-5p	gga-miR-16-1-3p
gga-miR-12266-5p	gga-miR-1744-3p
gga-miR-1454	gga-miR-1788-5p
gga-miR-148b-5p	gga-miR-3530-5p
gga-miR-1786	gga-miR-383-5p
gga-miR-214b-5p	gga-miR-6542-3p
gga-miR-29b-1-5p	gga-miR-6710-3p
gga-miR-301b-3p	
gga-miR-6582-5p	
gga-miR-9-4-3p	

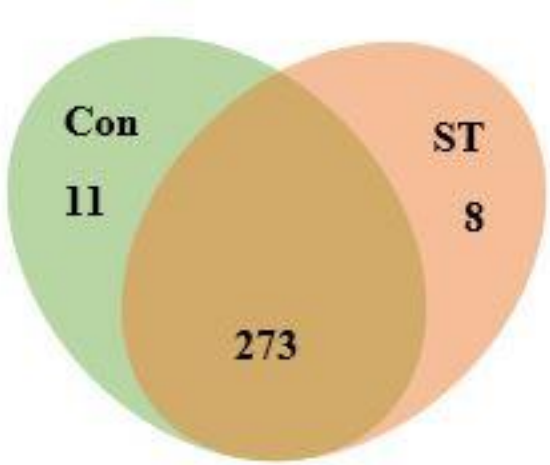

Figure 3.5 Venn diagram summary of unique and DE miRNAs in exosomes from serum of Con and ST groups. The Venn plot shows the number of unique DE miRNA and shared miRNAs in Con (n =5) and ST (n =7).

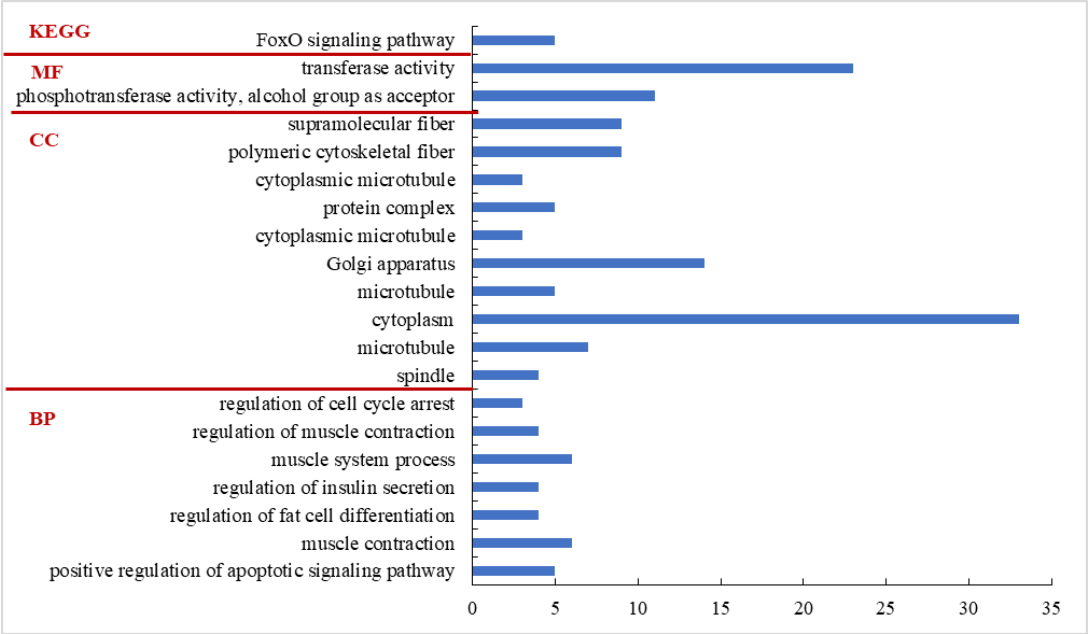

Figure 3.6 DAVID functional GO analysis of KEGG pathway, MF (molecular function), CC (cell component), and BP (biological process) enrichment for the combination of unique gga-mir-1788-5p, 3530-5p, 383-5p in ST group. X-axis represents the count of target genes involved in the functional annotation (Y-axis). $P < 0.05$.

3.3.6. Differential expression of miRNAs in the ST group compared to the Con group

Total 273 miRNAs were found in both Con and ST groups (Fig. 3.5). However, the expression levels of DE miRNAs differed significantly between the Con and ST groups (Table 3.3). Criteria for identifying DE miRNAs are based on 1) read count value was more than 50; 2) log2 (fold-change)>1 (two-fold change); and 3) $P < 0.05$. Compared to the exosomal miRNA profiles from Con group (n = 5), 17 miRNAs were significantly increased, and 12 miRNAs were significant downregulated in the ST group (n = 7). Upregulated 17 miRNA profiles included gga-miR-34c-3p/5p, gga-miR-449c-5p/3p, gga-miR -34b-3p/5p, gga-miR -449b-5p, gga-miR-449a, gga-miR-449d-5p/3p, gga-miR-1569, gga-miR-203a, gga-miR-216a, gga-miR-184-3p, gga-miR-200a-5p, gga-miR-200b-5p,

gga-miR -217-5p, showing the fold change in the range of 2.6 - 45.3 ($P < 0.05$; Table 3.3). Expression levels of 12 miRNAs, gga-miR-454-3p, gga-miR-1662, gga-miR-2954, gga-miR-222a, gga-miR-490-5p, gga-miR-122-3p, gga-miR-7477-3p, gga-miR-1306-5p, gga-miR-190a-5p, gga-miR-12218-3p, gga-miR-3535, gga-miR-137-3p, were significantly decreased in the ST group compared to the Con group ($P < 0.05$; Table 3.2).

Table 3.3 Differentially expressed exosomal miRNAs of the ST group compared to the Con group. Seventeen DE miRNAs were upregulated, and 12 DE miRNAs were downregulated in the ST group compared to the Con group. The criteria for identifying DE miRNAs are 1) read count value > 50; 2) Log2(fold-change)>1 (two-fold change); and 3) $P < 0.05$).

miRNA ID	log2FC*	P value
gga-miR-34c-3p	5.5	0.00000000644
gga-miR-449c-5p	4.7	0.0000352
gga-miR-34b-3p	4.6	0.000000000681
gga-miR-449c-3p	4.3	0.00011225
gga-miR-34b-5p	4.2	0.00000000403
gga-miR-34c-5p	4.2	0.000000007
gga-miR-449b-5p	3.6	0.000804281
gga-miR-449a	3.6	0.0000521
gga-miR-449d-5p	3.2	0.000607765
gga-miR-449d-3p	2.7	0.041257281
gga-miR-1569	2.6	0.018833841
gga-miR-203a	2.0	0.002048079
gga-miR-216a	1.9	0.035300746
gga-miR-184-3p	1.9	0.024440046
gga-miR-200a-5p	1.7	0.007801087
gga-miR-200b-5p	1.4	0.029861782
gga-miR-217-5p	1.4	0.002928658
gga-miR-454-3p	-1.0	0.04421431
gga-miR-1662	-1.0	0.034451637
gga-miR-2954	-1.0	0.003714751
gga-miR-222a	-1.1	0.001791979
gga-miR-490-5p	-1.2	0.04412838
gga-miR-122-3p	-1.6	0.02091287
gga-miR-7477-3p	-1.8	0.035523977
gga-miR-1306-5p	-1.8	0.025534461

Table 3.3 Continued

gga-miR-190a-5p	-1.8	0.001679319
gga-miR-12218-3p	-2.0	0.017454384
gga-miR-137-3p	-2.2	0.03393985
gga-miR-3535	-2.2	0.037312843

*log2FC: Logarithm to the base 2 of fold change.

3.3.7. Multiple sequence alignment of the gga-miR-34/449 family

The DE miRNA analysis of exosomes derived from serum samples indicated that the top 10 upregulated exosomal miRNAs in ST birds belonged to both the gga-miR-34b/c family and gga-miR-449d/a/b/c family. The expression levels of the gga-miR-34b/c family, including gga-miR-34c-3p, gga-miR-34b-3p, gga-miR-34c-5p, and gga-miR-34b-5p, showed a fold increase with a range from 18 to 45 in ST-challenged birds compared with those from the Con birds (Table 4.3). We have found a strong functional relationship between the miR-34b/c family and miR-449d/a/b/c family from the literature reports (Otto et al., 2017; Lv et al., 2019) in human medicine, which was called the miR-34/449 family. Therefore, we analyzed these ten gga-miR-34b/c and gga-miR-449d/a/b/c to see if they share common seed sequences, which could be an indication that they may share the common target genes.

The cluster of precursors, gga-miR-34b/c, map to chicken chromosome 24, while the cluster for precursors of gga-449-d/a/b/c is located on chromosome Z (Fig. 3.7A). The distance between gga-miR-34b and gga-miR-34c was 654-nts in length (data are not shown). The member of gga-449-d/a/b/c cluster are in close proximity with 784-nt-span between precursor gga-miR-449d to gga-miR-449a, 8-nt-span between precursor gga-miR-449a to gga-miR-449b, and 910-nt-span between precursor gga-miR-449b to gga-miR-

449c (data are not shown). The alignment of the precursor of gga-miR-34b/c and 449d/a/b/c showed conserved two seeding sequences in the 5' arm of precursor sequence among them, GGCAGUGU and GUUAGCUG), as shown in Fig. 3.7B. The sequence alignment between mature gga-miR-34b-5p and mature gga-miR-34c-5p showed 95% similarity (Fig. 3.7C). Mature gga-miR-449c-5p has one base difference in the seed sequence (GGCAGUGU) compared to other mature 5p of gga-miR-34b/c and gga-miR-449d/a/b. Mature gga-miR-449d-5p and gga-miR-449b-5p have two, and one base difference in the seed sequence (GUUAGCUG) compared to other mature 5p of gga-miR-34b/c and gga-miR-449a/c (Fig. 3.7C).

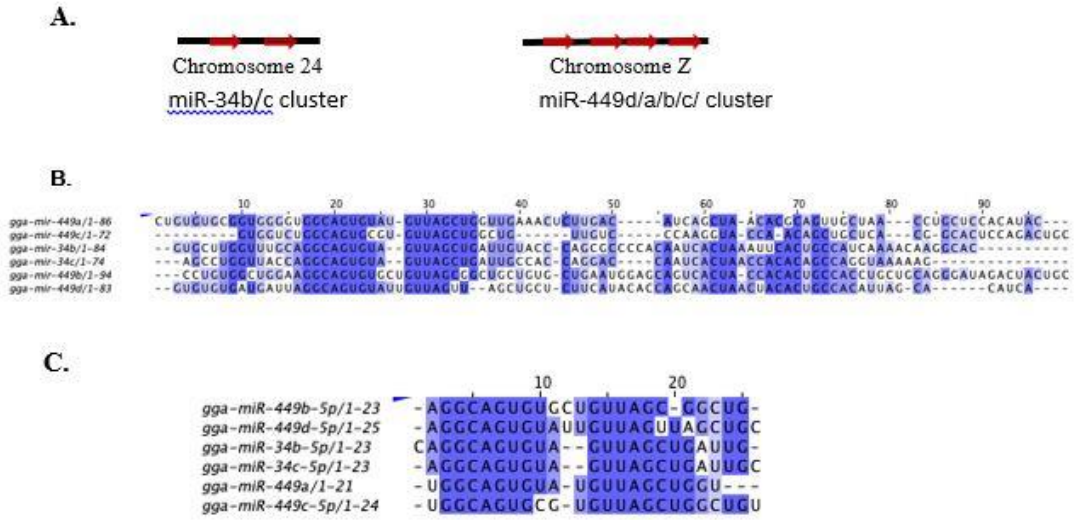

Figure 3.7 Multiple sequence alignment of gga-miR-34/449 family. The location of precursor sequences of gga-miR-34/449 family on chromosomes (A) and precursor sequence alignment of gga-miR-34/449 family (B), and mature sequence alignment for 5p strands of gga-miR-34/339 (C) are shown. Multiple sequence alignments were analyzed by Clustal Omega from EMBL- EBI (https://www.ebi.ac.uk), which was uploaded for visualization using Jalview 2.11.1.3. Aligned sequences are highlighted in dark purple.

3.3.8. The analyses of target gene and biological pathways of the gga-miR-34/449 family with seed sequences

DAVID functional GO analysis of biological processes enrichment and KEGG pathway enrichment were performed to analyze the target genes as well as their biological pathways for both gga-mir-34b-5p and gga-mir-34c-5p, two significantly up-regulated miRNAs in the ST-challenged birds compared to the Con birds. They also share two common seed sequences with the gga-miR-449d/c/b/a family. As shown in Fig. 4.8A, both gga-34b-5p and gga-34c-5p were predicted to target genes that were involved in innate/adaptive/humoral immune responses, cytokine-mediated signaling pathways, B cell differentiation, T cell/nature killer cell activation involved in immune response, positive regulation of Notch signaling pathways, and positive regulation of peptidyl-serine phosphorylation of STAT proteins ($P < 0.05$). Cytosolic DNA-sensing pathways, Toll-like receptor signaling pathways, Herpes simplex infection, and Janus kinases (Jak)-signal transducer and activator of transcription proteins (Stat) signaling pathways were found to be associated with target genes for both gga-mir-34b-5p and gga-mir-34c-5p in the KEGG pathway (Fig. 3.8B).

As shown in Fig. 3.9, four gga-mir-449 family sharing two seeding sequences with gga-miR-34b/c, including gga-mir-449a, gga-mir-449b-5p, gga-mir-449c-5p, gga-mir-449d-5p, targeted genes involved in signal transduction, cell adhesion, argininosuccinate lyase activity, transcription elongation factor complex, regulation of membrane potential, positive regulation of mitotic cell cycle, beta-catenin binding, and aminoacyl-tRNA biosynthesis.

We also analyzed the cluster of all of the miRNAs that shared common seeding sequences GGCAGUGU and GUUAGCUG (Fig. 3.7C) for their target genes and pathways. DAVID functional GO analysis of biological processes enrichment for gga-mir-34b-5p, gga-mir-34c-5p, gga-mir-449a, gga-mir-449b-5p, gga-mir-449c-5p, and gga-mir-449d-5p showed that they all of them targeted genes involved in humoral/innate/adaptive immune response, cytokine-mediate signaling pathway, B cell proliferation and differentiation, natural killer cell and T cell activation involved in immune responses, positive regulation of peptidyl-serine phosphorylation of STAT protein, positive regulation of Notch signaling pathway, regulation of membrane potential, defense response to virus, tissue hemostasis, regulation of Notch signaling pathway, miRNA mediated inhibition of translation and positive regulation of mitotic cell cycles ($P < 0.05$, Fig. 3.10).

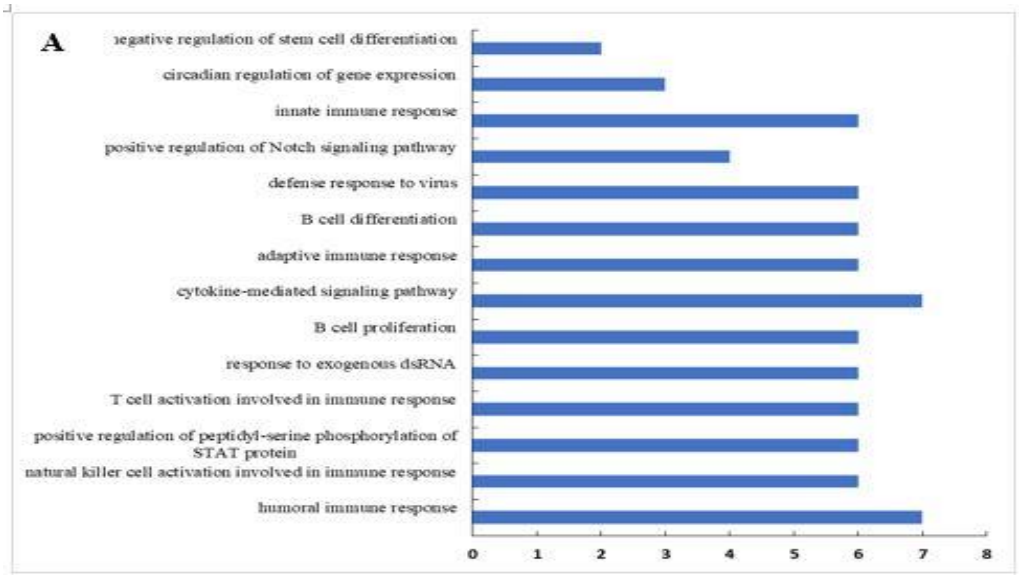

Figure 3.8 DAVID functional GO analysis of biological processes enrichment. (A) and KEGG pathway enrichment (B) for gga-mir-34b-5p and gga-mir-34c-5p. For A, X-axis represents the count of target genes that are involved in the functional annotation (Y-axis). For B, X-axis represents the count of target genes involved in KEGG pathways (Y-axis). $P < 0.05$.

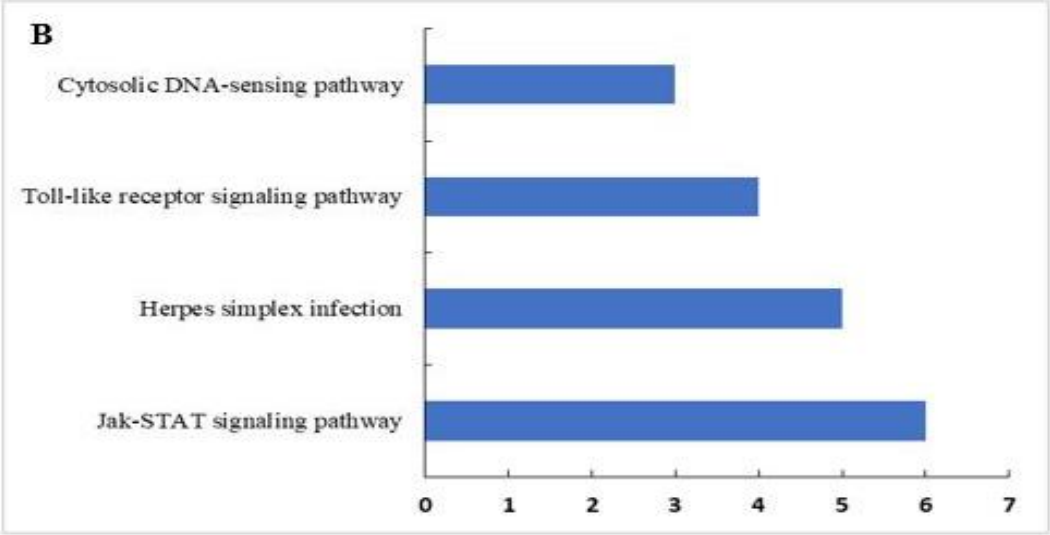

Figure 3.8 Continued.

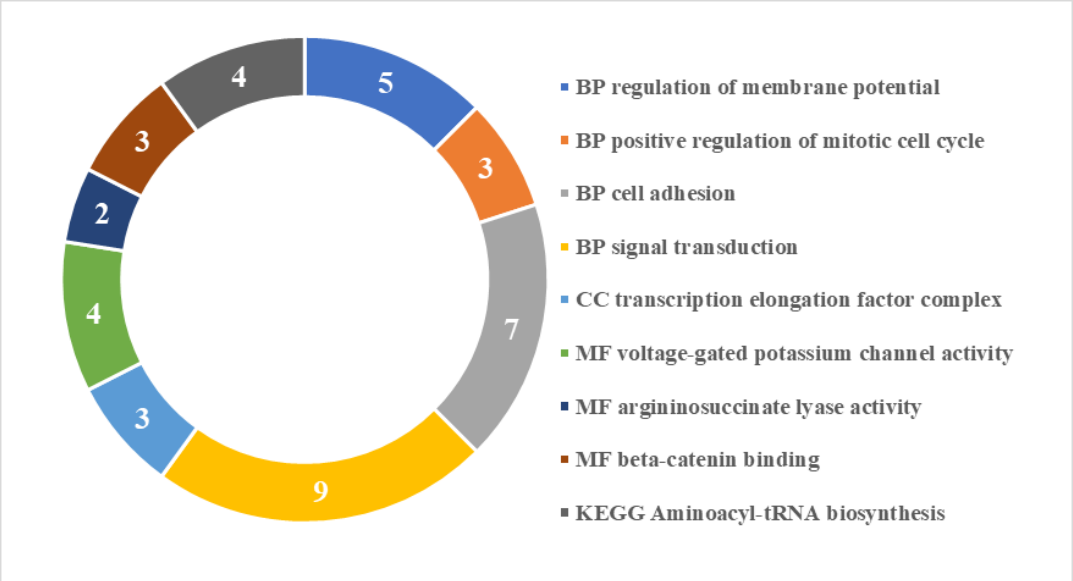

Figure 3.9 DAVID functional GO analysis of biological process (BP), cell component (CC), molecular function (MF), and KEGG pathway of gga-mir-449a, gga-mir-449b-5p, gga-mir-449c-5p, gga-mir-449d-5p. The count of the target gene is labeled in each category. $P < 0.05$.

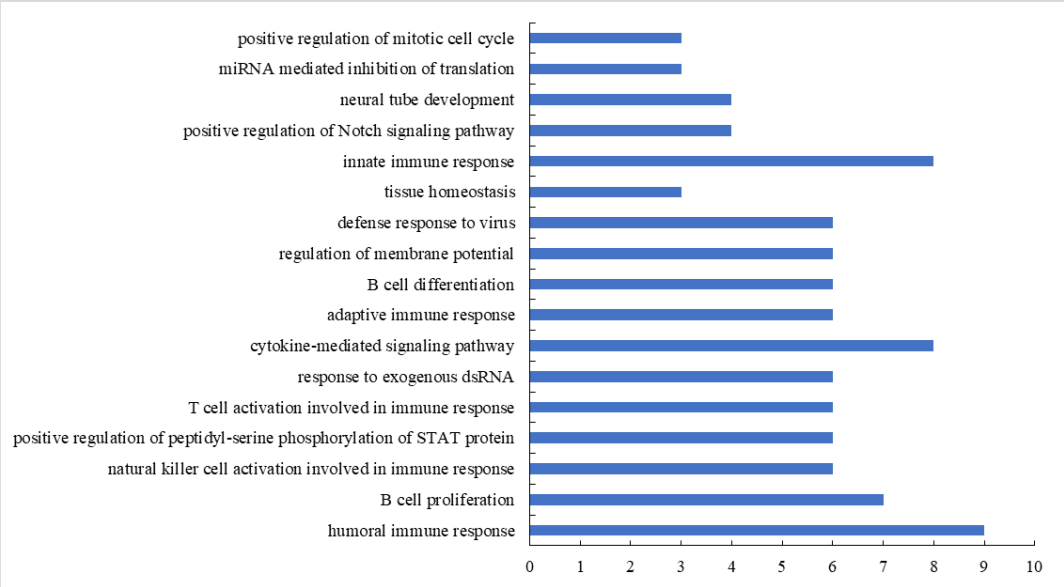

Figure 3.10 DAVID functional GO analysis of biological processes enrichment for gga-mir-34b-5p, gga-mir-34c-5p, gga-mir-449a, gga-mir-449b-5p, gga-mir-449c-5p, and gga-mir-449d-5p. X-axis represents the count of target genes involved in the functional annotation (Y-axis). $P < 0.05$.

3.4. Discussion

The mechanisms underlying the persistence of ST, a causative agent of human food borne illness, are not yet fully understood. MicroRNA has been reported to play important roles in modulating immune responses between host-pathogen interactions (Baltimore et al., 2008; Lodish et al., 2008). Therefore, we studied the miRNA profiles in exosomes from ST-challenged birds and analyzed their potential biological pathways. In this study, we demonstrated DE miRNA expression profiles in serum-derived exosomes from the Con and ST-infected groups. First, we isolated and characterized exosomes derived from serum. The size of the most exosomes in our studies was 30 to 150 nm in diameter, consistent with data obtained by Neerukonda et al. (2019). The mean size (nm), mode size (nm), median size (nm), and concentration (particles / ml) of exosomes were not significantly

different between Con and ST groups, which indicated that the ST infection did not change the size distribution of exosomes in broilers. Several studies demonstrated the alteration in the number of exosomes after pathogen infection. The number of exosomes enriched from *Mycoplasma gallisepticum* infected chicken type II pneumocytes (CP-II) were higher than those from the non-infected cells (Zhao et al., 2020). Exosome concentration was significantly elevated in the culture medium of capsaicin-treated sensory neurons compared to the culture medium of pure sensory neurons by flow cytometry analysis in mice (Simeoli et al., 2017). The amount of exosomes collected from human colon cancer cells were higher than those from normal cells (Ren et al., 2017). This discrepancy could be attributed to the animal model system used, different cell lines, and various concentrations of pathogen used for different lengths of the challenges.

High-throughput small RNA sequencing was utilized to identify DE miRNAs in exosomes. The ST challenge leads to significant regulation of exosome miRNA levels in the serum of broilers. There were 17 miRNAs significantly up-regulated and 12 miRNAs significantly down-regulated in the ST groups than the Con group, which indicated their potential role in the pathogen-host interactions. Exosomal miRNA alterations have also been reported by other pathogen infections. For example, mir-16 and mir-71 were up-regulated in *Heligmosomoides polygyrus* infections in mice (Buck et al., 2014), and mir-21 and mir-29a were up-regulated in exosomes collected from hepatitis B virus-infected human hepatocyte cell lines (Kouwaki et al., 2016). Sixty-two miRNAs related to inflammatory process genes were differentially expressed in the ileum of ST-challenged pigs compared to the Con group after two-day post-infection (Uribe et al., 2016). MicroRNA response to *Salmonella* Enteritidis challenge was investigated in the ceca of

white Leghorn layer chickens, where immune-related genes targeted gga-miR-125b-5p and gga-miR-1416-5p were up-regulated, gga-miR-34a-5p and gga-miR-1662 were down-regulated (Wu et al., 2017). However, DE of miRNAs was not significantly in our study due to the difference in tissues and pathogens studied.

The exosomal miRNAs, gga-miR-1788-5p, gga-miR-3530-5p, and gga-miR-383-5p, only found in ST group, were implicated in positive regulation for apoptotic signaling and FoxO signaling pathways. No reports are found for gga-miR-1788-5p and gga-miR-3530-5p regulation in chicken. However, the exosomal miR-383-5p level was up-regulated in chicken tracheal cells after challenge with LPS and avian influenza virus (O'Dowd et al., 2020).

We are the first to report the largest set of significant cluster miRNA, top 10 up-regulated DE miRNA, all belong to gga-miR-34b/c and gga-miR-449 d/a/b/c family in serum-derived exosomes from ST-challenged broilers. The two seed sequences, GGCAGUGU and GUUAGCUG, of gga-miR-34/449 were conserved among other vertebrates (Lv et al., 2019). Our findings indicate these miRNAs were implicated in the regulation of mitotic cell cycles, which is consistent with other reports that mice lacking miR-34b/c and miR-449a/b/c had activated the cell-cycle machinery (Otto et al., 2017). Our function analyses of miRNAs in this family that share the two seed sequences (Fig. 7C) are predicted to regulate humoral/innate/adaptive immune response (Fig. 10). Similar to our findings, miRNA-34 and miR-449 family has been reported to regulate immune response after viral infection in human and mouse studies (Otto et al., 2017; Lv et al., 2019). Chicken dendritic cells (DC) infected with H9N2 avian influenza virus had significantly increased levels of gga-miR-449c-5p, similar to our report for upregulated

miR-449-5p in exosomes in serum of ST challenged birds (Yang et al., 2020). However, in contrast to our findings, H9N2-infected chicken DC have downregulated levels of gga-miR-34-5p and gga-miR-184-3p and upregulated levels of gga-miR-190a-5p and gga-miR-3535. The expression of miR-34c-3p was significantly downregulated in exosomes from non-small cell lung cancer (NSCLC) patients compared with that of normal controls (Huang et al., 2020), indicating a potential prognostic marker for NSCLC. Regulation of gga-miR-449b/c levels is cell-type specific, depending on the strains of pathogen exposure. For example, gga-miR-449b-5p levels were decreased in avian influenza virus-infected chicken tracheal cells (O'Dowd et al., 2020). However, the expression levels of gga-449c-3p/5p and miR-449b-5p were down-regulated in *mycoplasma gallisepticum*-infected chicken pneumocytes (Zhao et al., 2020). Environmental factors, including heat stress and chronic toxic exposure, can affect the miR-34 and miR-449 expression. Lead exposure increased miR-34b/c levels in mice brains (An et al., 2014). High levels of miR-449c-5p have been reported in the spleen of the broiler under either cold-stress or heat stress (Li et al., 2020).

In conclusion, our study firstly reports DE miRNA in serum-derived exosomes in ST-infected birds. Circulating exosomal cluster miRNAs from gga-miR34b/c and gga-miR-449d/a/b/c/ family could be served as immune-modulators and may provide an opportunity to understand the mechanism of chicken-ST interactions.

3.5. References

Ambros, V. 2004. The functions of animal microRNAs. Nature. 431:350-355.

An, J., T. Cai, H. Che, T. Yu, Z. Cao, X. Liu, F. Zhao, J. Jing, X. Shen, M. Liu, and K. Du. 2014. The changes of miRNA expression in rat hippocampus following chronic lead exposure. Toxicol. Lett. 229:158-166.

Baltimore, D., M. P. Boldin, R. M. O'connell, D. S. Rao, and K. D. Taganov. 2008. MicroRNAs: new regulators of immune cell development and function. Nat. Immunol. 9:839.

Bartel, D. P. 2004. MicroRNAs: genomics, biogenesis, mechanism, and function. Cell. 116:281-297.

Bellingham, S. A., B. Guo, B. Coleman, and A. F. Hill. 2012. Exosomes: vehicles for the transfer of toxic proteins associated with neurodegenerative diseases?. Front. Physiol. 3:124.

Blanchard, N., D. Lankar, F. Faure, A. Regnault, C. Dumont, G. Raposo, and C. Hivroz. 2002. TCR activation of human T cells induces the production of exosomes bearing the TCR/CD3/ζ complex. J. Immunol. 168:3235-3241.

Buck, A. H., G. Coakley, F. Simbari, H. J. McSorley, J. F. Quintana, T. Le Bihan, S. Kumar, C. Abreu-Goodger, M. Lear, Y. Harcus, and A. Ceroni. 2014. Exosomes secreted by nematode parasites transfer small RNAs to mammalian cells and modulate innate immunity. Nat. Commun. 5:1-2.

Caby, M. P., D. Lankar, C. Vincendeau-Scherrer, G. Raposo, and C. Bonnerot. 2005. Exosomal-like vesicles are present in human blood plasma. Int. Immunol. 17:879-887.

Center for Disease Control and Prevention. 2021. *Salmonella*. Accessed Apr. 2021. https://www.cdc.gov/salmonella/

Colombo, M., G. Raposo, and C. Théry. 2014. Biogenesis, secretion, and intercellular interactions of exosomes and other extracellular vesicles. Annu. Rev. Cell Dev. Biol. 30:255-289.

Croce, C. M., and G. A. Calin. 2005. miRNAs, cancer, and stem cell division. Cell. 122:6-7.

da Rocha, I. F., R. F. Amatuzzi, A. C. Lucena, H. Faoro, and L. R. Alves. 2020. Cross-kingdom extracellular vesicles EV-RNA communication as a mechanism for host–pathogen interaction. Front. Cell. Infect. Microbiol. 10:593160.

Das, K., O. Garnica, and S. Dhandayuthapani. 2016. Modulation of host miRNAs by intracellular bacterial pathogens. Front. Cell. Infect. Microbiol. 6:79.

Esquela-Kerscher, A., and F. J. Slack. 2006. Oncomirs—microRNAs with a role in cancer. Nat. Rev. Cancer. 6:259-269.

Fauré, J., G. Lachenal, M. Court, J. Hirrlinger, C. Chatellard-Causse, B. Blot, J. Grange, G. Schoehn, Y. Goldberg, V. Boyer, and F. Kirchhoff. 2006. Exosomes are released by cultured cortical neurones. Mol. Cell. Neurosci. 31:642-648.

Galiş, A. M., C. Marcq, D. Marlier, D. Portetelle, I. Van, Y. Beckers, and A. Théwis. 2013. Control of *Salmonella* contamination of shell eggs—Preharvest and postharvest methods: A review. Compr. Rev. Food. Sci. Food. Saf. 12:155-182.

Guarnieri, D. J., and R. J. DiLeone. 2008. MicroRNAs: a new class of gene regulators. Ann. Intern. Med. 40:197-208.

Hong, Y., J. Lee, T. H. Vu, S. Lee, H. S. Lillehoj, and Y. H. Hong. 2021. Exosomes of lipopolysaccharide-stimulated chicken macrophages modulate immune response through the MyD88/NF-κB signaling pathway. Dev. Comp. Immunol. 115:103908.

Huang, W., Y. Yan, Y. Liu, M. Lin, J. Ma, W. Zhang, J. Dai, J. Li, Q. Guo, H. Chen, and B. Makabel. 2020. Exosomes with low miR-34c-3p expression promote invasion and migration of non-small cell lung cancer by upregulating integrin α2β1. Signal Transduct. Target. Ther. 5:1-3.

Hunter, M. P., N. Ismail, X. Zhang, B. D. Aguda, E. J. Lee, L. Yu, T. Xiao, J. Schafer, M. L. Lee, T. D. Schmittgen, and S. P. Nana-Sinkam. 2008. Detection of microRNA expression in human peripheral blood microvesicles. PLoS One. 3:e3694.

Huotari, J., and A. Helenius. 2011. Endosome maturation. The EMBO J. 30:3481-3500.

Kim, S. I., S. Kim, E. Kim, S. Y. Hwang, and H. Yoon. 2019. Corrigendum: Secretion of *Salmonella* Pathogenicity Island 1-Encoded Type III Secretion System Effectors by Outer Membrane Vesicles in *Salmonella* Enterica Serovar Typhimurium. Front. Microbiol. 10:411.

Kogut, M. H., C. L. Swaggerty, J. A. Byrd, R. Selvaraj, and R. J. Arsenault. 2016. Chicken-specific kinome array reveals that *Salmonella* Enterica serovar Enteritidis modulates host immune signaling pathways in the cecum to establish a persistence infection. Int. J. Mol. Sci. 17:1207.

Kouwaki, T., Y. Fukushima, T. Daito, T. Sanada, N. Yamamoto, E. J. Mifsud, C. R. Leong, K. Tsukiyama-Kohara, M. Kohara, M. Matsumoto, and T. Seya. 2016. Extracellular vesicles including exosomes regulate innate immune responses to hepatitis B virus infection. Front. Immunol. 7:335.

Lai, E. C. 2002. Micro RNAs are complementary to 3′ UTR sequence motifs that mediate negative post-transcriptional regulation. Nat. Genet. 30:363-364.

Lässer, C., V. S. Alikhani, K. Ekström, M. Eldh, P. T. Paredes, A. Bossios, M. Sjöstrand, S. Gabrielsson, J. Lötvall, and H. Valadi. 2011. Human saliva, plasma and breast milk exosomes contain RNA: uptake by macrophages. J. Transl. Med. 9:1-8.

Li, M., E. Zeringer, T. Barta, J. Schageman, A. Cheng, and A. V. Vlassov. 2014. Analysis of the RNA content of the exosomes derived from blood serum and urine and its potential as biomarkers. Philos. Trans. R. Soc. Lond. B. Biol. Sci. 369:20130502.

Li, P., W. Fan, N. Everaert, R. Liu, Q. Li, M. Zheng, H. Cui, G. Zhao, and J. Wen. 2018. Messenger RNA sequencing and pathway analysis provide novel insights into the susceptibility to *Salmonella* Enteritidis infection in chickens. Front. Genet. 9:256.

Li, T., Y. Song, X. Bao, and J. Zhang. 2020. The Mediation of miR-34a/miR-449c for immune cytokines in acute cold/heat-stressed broiler chicken. Animals. 10:2168.

Li, X., A. L. Corbett, E. Taatizadeh, N. Tasnim, J. P. Little, C. Garnis, M. Daugaard, E. Guns, M. Hoorfar, and I. T. Li. 2019. Challenges and opportunities in exosome research—Perspectives from biology, engineering, and cancer therapy. APL Bioeng. 3:011503.

Lodish, H. F., B. Zhou, G. Liu, and C. Z. Chen. 2008. Micromanagement of the immune system by microRNAs. Nat. Rev. Immunol. 8:120-130.

Lv, J., Z. Zhang, L. Pan, and Y. Zhang. 2019. MicroRNA-34/449 family and viral infections. Virus Res. 260:1-6.

Mathivanan, S., J. W. Lim, B. J. Tauro, H. Ji, R. L. Moritz, and R. J. Simpson. 2010. Proteomics analysis of A33 immunoaffinity-purified exosomes released from the human colon tumor cell line LIM1215 reveals a tissue-specific protein signature. Mol. Cell. Proteomics. 9:197-208.

Maudet, C., M. Mano, and A. Eulalio. 2014. MicroRNAs in the interaction between host and bacterial pathogens. FEBS Lett. 588:4140-4147.

Neerukonda, S. N., N. A. Egan, J. Patria, I. Assakhi, P. Tavlarides-Hontz, S. Modla, E. R. Muñoz, M. B. Hudson, and M. S. Parcells. 2019. Comparison of exosomes purified via ultracentrifugation (UC) and Total Exosome Isolation (TEI) reagent from the serum of Marek's disease virus (MDV)-vaccinated and tumor-bearing chickens. J. Virol. Methods. 263:1-9.

Neerukonda, S. N., P. Tavlarides-Hontz, F. McCarthy, K. Pendarvis, and M. S. Parcells. 2019. Comparison of the transcriptomes and proteomes of serum exosomes from Marek's disease virus-vaccinated and protected and lymphoma-bearing chickens. Genes. 10:116.

O'Dowd, K., M. Emam, E. Khili, M. Reda, A. Emad, E. M. Ibeagha-Awemu, C. A. Gagnon, and N. Barjesteh. 2020. Distinct miRNA profile of cellular and extracellular vesicles released from chicken tracheal cells following avian influenza virus infection. Vaccines. 8:438.

Otto, T., S. V. Candido, M. S. Pilarz, E. Sicinska, R. T. Bronson, M. Bowden, I. A. Lachowicz, K. Mulry, A. Fassl, R. C. Han, and E. S. Jecrois. 2017. Cell cycle-targeting microRNAs promote differentiation by enforcing cell-cycle exit. Proc. Natl. Acad. Sci. 114:10660-10665.

Packialakshmi, B., R. Liyanage, J. O. Lay Jr, S. K. Makkar, and N. C. Rath. 2016. Proteomic changes in chicken plasma induced by *Salmonella* Typhimurium lipopolysaccharides. Proteomics Insights. 7:PRI-S31609.

Pisitkun, T., R. F. Shen, and M. A. Knepper. 2004. Identification and proteomic profiling of exosomes in human urine. Proc. Natl. Acad. Sci. 101:13368-13373.

Ren, R., H. Sun, C. Ma, J. Liu, and H. Wang. 2019. Colon cancer cells secrete exosomes to promote self-proliferation by shortening mitosis duration and activation of STAT3 in a hypoxic environment. Cell Biosci. 9:1-9.

Scallan, E., R. M. Hoekstra, F. J. Angulo, R. V. Tauxe, M. A. Widdowson, S. L. Roy, J. L. Jones, and P. M. Griffin. 2011. Foodborne illness acquired in the United States—major pathogens. Emerg. Infect. Dis. 17:7.

Schorey, J. S., Y. Cheng, P. P. Singh, and V. L. Smith. 2015. Exosomes and other extracellular vesicles in host–pathogen interactions. EMBO Rep. 16:24-43.

Simeoli, R., K. Montague, H. R. Jones, L. Castaldi, D. Chambers, J. H. Kelleher, V. Vacca, T. Pitcher, J. Grist, H. Al-Ahdal, and L. F. Wong. 2017. Exosomal cargo including microRNA regulates sensory neuron to macrophage communication after nerve trauma. Nat. Commun. 8:1-7.

Simpson, R. J., S. S. Jensen, and J. W. Lim. 2008. Proteomic profiling of exosomes: current perspectives. Proteomics. 8:4083-4099.

Théry, C., L. Zitvogel, and S. Amigorena. 2002. Exosomes: composition, biogenesis and function. Nat. Rev. Immunol. 2:569-579.

Uribe, J. H., M. Collado-Romero, S. Zaldívar-López, C. Arce, R. Bautista, A. Carvajal, S. Cirera, M. G. Claros, and J. J. Garrido. 2016. Transcriptional analysis of porcine intestinal mucosa infected with *Salmonella* Typhimurium revealed a massive inflammatory response and disruption of bile acid absorption in ileum. Vet. Res. 47:1-10.

Van Niel, G., G. Raposo, C. Candalh, M. Boussac, R. Hershberg, N. Cerf–Bensussan, and M. Heyman. 2001. Intestinal epithelial cells secrete exosome–like vesicles. Gastroenterology. 121:337-349.

Wu, L., J. Guo, Q. Wang, S. Lu, X. Dai, Y. Xiang, and D. Fan. 2017. Sensitivity enhancement by using few-layer black phosphorus-graphene/TMDCs heterostructure in surface plasmon resonance biochemical sensor. Sensor Actuat. B-Chem. 249:542-548.

Yáñez-Mó, M., P. R. Siljander, Z. Andreu, A. Bedina Zavec, F. E. Borràs, E. I. Buzas, K. Buzas, E. Casal, F. Cappello, J. Carvalho, and E. Colás. 2015. Biological properties

of extracellular vesicles and their physiological functions. J. Extracell. Vesicles. 4:27066.

Yang, J., X. Huang, Y. Liu, D. Zhao, K. Han, L. Zhang, Y. Li, and Q. Liu. 2020. Analysis of the microRNA expression profiles of chicken dendritic cells in response to H9N2 avian influenza virus infection. Vet. Res. 51:1-9.

Yates, L. A., C. J. Norbury, and R. J. Gilbert. 2013. The long and short of microRNA. Cell. 153:516-519.

Zhang, J., S. Li, L. Li, M. Li, C. Guo, J. Yao, and S. Mi. 2015. Exosome and exosomal microRNA: trafficking, sorting, and function. Genomics Proteomics Bioinformatics. 13:17-24.

Zhao, Y., Y. Fu, M. Zou, Y. Sun, X. Yin, L. Niu, Y. Gong, and X. Peng. 2020. Analysis of deep sequencing exosome-microRNA expression profile derived from CP-II reveals potential role of gga-miRNA-451 in inflammation. J. Cell Mol. Med. 24:6178-6190.

4. ALTERED EXPRESSION OF LACTATE DEHYDROGENASE AND MONOCARBOXYLATE TRANSPORTER INVOLVED IN LACTATE METABOLISM IN BROILER WOODEN BREAST[*]

4.1. Introduction

Per capita consumption of broilers has increased 290% over the last 58 years in the US (National Chicken Council, 2018). To meet the increasing demand for poultry meat, broilers have been selected based on fast growth rate, a high feed conversion ratio, and high meat yields (Zuidhof et al., 2014; Petracci et al., 2015; Tallentire et al., 2018). However, the fast-growing and heavy weights of broilers have increased the incidence of degenerative myopathies, severely affecting meat appearance and quality (Kuttappan ett al., 2012, Tijare et al., 2016). One muscle myopathy is wooden breast (WB), which affects the pectoralis muscles in fast-growing commercial broilers (Sihvo et al., 2014). It is considered as one of the manifestations of metabolic syndrome in these fast-growing broilers, which makes the Pectoralis major muscle pale, rigid and bulge outwards (Sihvo et al., 2014; Bailey et al., 2015; Tasoniero et al., 2016). Histologically, WB is characterized by myofiber necrosis, fibrosis, and high levels of fibrillar collagen in skeletal muscle tissues (Sihvo et al., 2014; Velleman and Clark, 2015; Kuttappan et al., 2016). Sihvo et al. (2014 and 2017) reported that WB starts to develop at approximately two weeks of age in broiler chickens and estimated that 48 to 73% of commercial broilers had WB. The

[*] This article was published in Poultry Science, Vol 99, Zhao, D., M. H. Kogut, K. J. Genovese, C. Y. Hsu, J. T. Lee, Y. Z. Farnell, Altered expression of lactate dehydrogenase and monocarboxylate transporter involved in lactate metabolism in broiler wooden breast, Page 11-20, Copyright Elsevier (2020).

widespread incidence of WB has caused large economic losses due to poor meat quality, such as low water-holding capacity, reduced product yield, decreased myofibrillar protein content, and poor meat texture (Mazzoni et al., 2015; Mudalal et al., 2015; Aguirre et al., 2018). The causes of WB are still unknown, however, WB is believed to be caused by a combination of genetic and environmental factors (reviewed in Zampiga et al., 2018). Studies have suggested the association of genetic basis of WB in broilers (Macrae et al., 2006; Griffin et al., 2018), environmental factors (Bailey et al., 2015), WB-related gene changes associated localized hypoxia (Mutryn et al., 2015) and inflammation and abnormal (Abasht et al., 2016), metabolisms, increased oxidative stress (Mutryn et al., 2015; Abasht et al., 2016), and decreased capillary density (Hoving-Bolink et al., 2000).

Due to the presence of localized tissue hypoxia (Mutryn et al., 2015; Sihvo et al., 2018) and decreased lactate levels in WB-affected muscle (Abasht et al., 2016), we propose that the expression of key molecules, including lactate dehydrogenase (LDHA and LDHB) enzymes and two major monocarboxylate transporters (MCT1 and MCT4) that regulate the levels of lactate are altered in WB. Lactate dehydrogenase is a cytoplasmic enzyme found in nearly all living animal cells, composed of tetramers derived from two LDH subunits. It is encoded by the LDHA which converts pyruvate to lactate and LDHB gene which converts lactate to pyruvate in the last step of glycolysis (Cahn et al., 1962; Dawson et al., 1964; Pesce et al., 1964). The combination of LDHA and LDHB produce five LDH isoenzymes, categorized as LDH1 (B4), LDH2 (A1B3). LDH3 (A2B2), LDH4 (A3B1) and LDH5 (A4) (Dawson et al., 1964). The altered level of LDH enzyme in human serum indicates damaged cells and tissues and has become a common marker for tissue injuries and disease (Drent et al., 1996; Kato et al., 2006; Ding et al., 2017). Lactates, the

end product of anaerobic glycolysis, are transported by MCT1 and MCT4, which are located on the cell membrane. Translocation of lactate in skeletal muscles is facilitated by MCT1, which facilitates uptake of lactate into cells, and MCT4, which exports lactate out of cells (Roth and Brooks, 1990; Halestrap and Price, 1999; Halestrap and Meredith, 2004). Micro RNAs (miRNAs) are small no-coding RNAs that negatively regulate gene expression. Micro RNA-375 has been reported to be inversely associated with LDHB gene expression in cancer cells including human squamous cell carcinoma, esophageal squamous cancer cells, and merkel cell carcinoma (Kinoshita et al., 2012; Isozaki et al., 2015; Kumar et al., 2018). Therefore, the objectives of this study were to evaluate whether there were changes in the mRNA and protein levels of LDHA and LDHB, MCT2 and MCT4, and miR-375 in WB compared to NB.

We report here in WB tissues, up-regulation of LDHB mRNA and protein that converts lactate to pyruvate was accompanied by an increase in MCT4 mRNA and protein expression, which act as a lactate efflux transporter. Further, we observed the inverse relationship of miR-375 with LDHB in WB tissue. Interestingly, the LDH isoenzyme activity that converts lactate to pyruvate was reduced in WB tissues compared to NB tissues. Future studies will involve isolating individual components of cells from WB tissues which will help us understand the cellular and molecular mechanisms behind WB muscles, leading to the development of new strategies for preventing and/or treating WB condition.

4.2. Materials and methods

4.2.1. Sample collection

A total of 16 commercial high yielding broilers at 49 days of age were used to collect breast tissues, including 8 wooden breasts, which were determined independently by three experienced individuals who followed the methods described by Zotte et al. (2015), and 8 normal breasts. Due to reports that a defective blood supply causes muscle damage and ischemia in the cranial section of WB muscles (Kuttappan et al., 2013; Hoving-Bolink et al., 2000), we collected the tissue samples from the cranial part of the pectoralis major muscles. The breast tissue samples were dissected and immediately snap-frozen in liquid nitrogen. All tissues were then transferred and stored at -80 °C for later total RNA and protein extractions. The animal use protocol was approved by Texas A&M University Animal Care and Use Committee.

4.2.2. Total RNA and small RNA extraction

Total RNA was extracted from NB and WB samples utilizing the RNeasy Mini Kit (Qiagen, Valencia, CA, USA) according to the manufacturer's protocol. Briefly, a small piece of chicken breast was homogenized in buffer RLT using a GEX 130 PB ultrasonic processor (Cole-Parmer, Vernon Hills, IL, USA) at 50% power for 10 sec on ice. The lysate was centrifuged at the speed of 2000 x g for 5 mins, and the supernatant was collected. Then 1 volume of 70% ethanol was added to partially precipitate total RNA. The partially precipitated total RNA bonded to the RNeasy spin column, and treated with DNase to digest the contamination of genomic DNA. Buffer RPE was used to wash the column. The total RNA was eluted in 50 µL DNase/RNase free water. The quantity and

quality of total RNA were evaluated through the NanoDrop 1000 (Thermo Scientific, MA, USA).

Small RNA isolation was performed using the mirVana PARIS kit (Ambion, Austin, TX). The procedure was followed according to the manufacturer's protocol. The concentration of small RNA was confirmed by an Agilent Small RNA kit on the Agilent 2100 Bioanalyzer (Agilent, Palo Alto, CA).

4.2.3. Quantitative reverse transcription polymerase chain reaction (RT-PCR) for mRNAs

One microgram of total RNA from each sample was transcribed into cDNA using SuperScript III First-Strand Synthesis System (Invitrogen, Carlsbad, CA) following the manufacturer's protocol. Briefly, first strand cDNA synthesis was prepared by mixing 1 µg of total RNA, 1 µL of 50ng/µl random hexamers, and 1 µL of 10mM dNTPs mix. The mixture was incubated at 65°C for 5 min to denature RNA, and then placed on ice for at least 1 min. Ten microliters cDNA synthesis mix (2 µL 10× RT Buffer, 4 µL 25 mM $MgCl_2$, 2 µL 0.1 M DTT, 1 µL RNase OUT, and 1 µL SuperScript III RT) was added and incubated at 25°C for 10 min, followed by 50°C for 50 min, and terminated at 85°C for 5 min. One microliter RNase H (2 U/µL) was added and incubated at 37°C for 20 min. The cDNA product was stored at -20°C. The cDNA samples were diluted to the concentration of 1 ng/µL, and 8 µL of the diluted cDNA was subjected to a real-time PCR reaction with PowerUp SYBR Green Master Mix (ThermoFisher Scientific, Waltham, MA) using an ABI 7900H system (ThermoFisher Scientific, Waltham, MA). The oligonucleotide primers for LDHA, LDHB, MCT1, MCT4, and GAPDH were listed in Table 4.1. The conditions of real time PCR amplification were 1 cycle at 50°C for 2 min, 95°C for 10 min, 40 cycles

at 95°C for 15 sec, 60°C for 1 min, followed by a melting curve analysis. The GAPDH was employed as an internal control used to normalize the expression of target transcript (Zambonelli et al., 2016). The values of average cycle threshold (Ct) were determined for each sample, and $2^{-\Delta\Delta Ct}$ values for the comparison of the target gene and GAPDH were used for relative quantification by fold-change (Schmittgen and Livak, 2008). The PCR efficiency test was performed using serial dilutions of cDNA pool and primers. All reactions were performed in triplicates.

Table 4.1. Primer sequences used for qRT-PCR.

Target gene	Primers	Primer Sequence (5' to 3')	(bp)	Reference
LDHA	Forward	CCATGTCTCTCAAGGATCATCTC	295	Imagawa et al., 2006
	Reverse	GCACCAGCAGTGACAATGAC		
LDHB	Forward	TTCCCAGCAACAAGATCACCGT	511	Imagawa et al., 2006
	Reverse	AACACCTGCCACATTAACTCCG		
MCT1	Forward	AGCAGCATCCTGGTGAACAAG	59	Zhang et al., 2017
	Reverse	AGGCACCCACCCACGAT		
MCT4	Forward	GCTGGTCTCAAGTGGGTTAG	107	Current study
	Reverse	CCACCGTAATCGACAGACATAG		
GAPDH	Forward	AGAACATCATCCCAGCGT	182	Guo et al., 2016
	Reverse	AGCCTTCACTACCCTCTTG		

4.2.4. Quantitative RT-PCR for miR-375

A total of 100 ng small RNA was reverse-transcribed for miRNA detection. Complementary DNA (cDNA) synthesis was performed using the miScript II RT kit (Catalog no. 218161; Qiagen, Valencia, CA, USA) following the manufacturer's instruction. Briefly, the RT reaction was conducted in a 20 µL reaction mixture containing 100 ng of small RNA, 4 µL 5x miScript HiFlex Buffer, 2 µL 10x miScript Nucleics Mix and 2 µL miScript Reverse Transcriptase Mix. The reverse transcription was performed at 37°C for 60 min and 95°C for 5 min, and the cDNA product was stored at -20°C. Two

hundred pg of cDNA was used for quantitative RT-PCR reaction using the miScript SYBR Green PCR kit and Custom miScript Primer Assay for miR-375 (Catalog no. MSC0075989; Qiagen, Valencia, CA, USA) and U6 small nucleolar RNA (Catalog no. MSC0075901; Qiagen, Valencia, CA, USA). The following components were combined in a 10 µL reaction using 384-well plates: 5 µL 2x QuantiTect SYBR Green PCR Master Mix, 1 µL miScript Universal Primer, 1 µL of 10x miR-375 primer, and 200 pg of cDNA with nuclease-free water. The conditions of PCR were comprised of denaturation at 95°C for 10 min, followed by 40 cycles of 94°C for 15 sec, 55°C for 30 sec, and 70°C for 30 sec, followed by the melting curve analysis. Data was analyzed using comparative delta delta Ct method ($2^{-\Delta\Delta Ct}$) (Schmittgen and Livak, 2008). Relative miR-375 expression was normalized to U6 small nucleolar RNA. The efficiency test was performed using serial dilutions of cDNA pool and primers. Melting curve analyses were performed for validating the specificity of amplicons.

4.2.5. Western blotting analysis

Frozen tissues were homogenized in radioimmunoprecipitation assay (RIPA) buffer (Thermo Fisher Scientific, Waltham, MA). The protein concentration was quantified by a BCA Protein Assay Kit (Thermo Fisher Scientific, Waltham, MA). Ten micrograms of protein from each sample was loaded onto 4-12% SDS-PAGE gradient gels (Bio-Rad, Hercules, CA). After electrophoresis, proteins were transferred to PVDF membranes by a semi-dry electroblotting system (Cat. #: 170-3940; Bio-Rad, Hercules, CA) at 50mA for 2 hours. Then, the PVDF membranes were blocked in a Tris-buffered saline (TBS) containing 0.1% Tween (TBST) and 5% non-fat milk overnight at 4°C. The membranes were washed 4 times for 20 minutes in TBST, and then incubated with primary antibody

for 4 h. The following primary antibodies were purchased from Abcam, TLC (Cambridge, MA) unless indicated and used at the indicated dilutions: mouse anti-GAPDH (catalog no. ab8245; 1:20,000 dilution), rabbit anti-monocarboxylic acid transporter 1 (MCT1) (catalog no. 93048; 1:1,000 dilution), rabbit anti-LDHA (catalog no. ab135366; 1:1,000 dilution), rabbit anti-SLC16A3 (MCT4) (catalog no. ab74109; 1:500 dilution), rabbit anti-LDHB (catalog no. ab75167; 1:1,000 dilution). The membrane was washed 4 times in TBST, followed by incubation with a secondary antibody for 1 hour at room temperature. The following secondary antibodies were used: HRP-conjugated goat anti-rabbit IgG (catalog no. ab205718; 1:20,000 dilution), HRP-conjugated goat anti-mouse IgG from Life Technology (Carlsbad, CA; catalog no. A16072; 1:5,000 dilution). Enhanced chemiluminescence (ECL) detection reagents (Amersham Pharmacia Biotech, Piscataway, NJ) were employed. The chemiluminescent signals were captured and analyzed by a ChemiDoc^{TM} MP Image System (Bio-Rad, Hercules, CA). Immunoblot images were quantified by Quantity One-4.6.1 software (Bio-Rad, Hercules, CA), and target protein signals were normalized to GAPDH and presented as relative band densities.

4.2.6. Specific LDH enzyme activity assay

Specific LDH activity (conversion from pyruvate to lactate) was determined using a kit made in-house. Briefly, frozen breast muscle tissue was homogenized in the extraction buffer containing 50 mM of Tris-HCl (pH 8.5), 1 mM β-mercaptoethanol, 1 mM phenylmethylsulfonyl fluoride, and 1 mM ethylenediaminetetraacetic acid (EDTA), by a GEX 130 PB ultrasonic processor (Cole-Parmer, Vernon Hills, IL, USA) at 50% power for 10s on ice. The lysate from each sample was centrifugated at 12,000 x g for 5 mins at 4°C. The supernatant was decanted, and snap frozen in liquid nitrogen and stored at -80°C. The

protein concentration for each sample was measured by BCA Protein Assay Kit. The protein samples were diluted to 1 µg in 30 µL extraction buffer and added to 200 µL LDH assay buffer containing 100 mM lithium lactate, 4 mM NAD^+, 3 mM $NaHCO_3$, 166.6 mM NaCl and 8.33 mM Tris-HCl (pH 8.8). The change of NADH absorbance was measured in 51-sec intervals for 10 min at 340 nm absorbance at room temperature using a Synergy H1 multi-mode microplate reader (BioTek, Winooski, VT, USA). The specific activity of LDH was calculated as the ratio of the enzyme activity divided by the protein mass for enzymatic assay. One unit of LDH activity was defined as the amount of enzyme that yielded 1 µM NADH per min. Gen5 3.02 Kinetic v.3.5.1 program (BioTek, Winooski, VT) was used to measure enzyme kinetic activity. Lactate dehydrogenase activities were calculated in the formula below and expressed as units per gram of protein.

Specific activity of LDH = (ΔA/min) x (Assay volume in mL)/εb/mg of protein

Where ΔA = change in absorbance at 340 nm between times

b = 0.725 cm; ε =6220 L/mole x cm

4.2.7. Statistical analysis

Statistical analyses were conducted via a student's T test, using JMP Pro 14 (SAS institute Inc., Cary, NC, U.S.A.). All of the data were presented as mean ± standard error of the mean (SEM). A P-value of < 0.05 was considered significant.

4.3. Results

4.3.1. Expression of the LDHA and LDHB mRNA and protein in WB muscles compared to NB muscles

Since skeletal muscle tissues are the major location for lactate production, we first investigated the impact of WB on expression levels of LDHA, which encodes the LDH

muscle subunit (LDH M), that converts pyruvate to lactate in the last step of fermentative glycolysis (Summermatter et al., 2013). Relative LDHA mRNA levels decreased 1.7-fold ($P < 0.0001$) in WB tissues with respect to those from NB tissues (Fig. 4.1A). In contrast, the LDHA protein levels in WB muscles showed no significant change (Fig. 4.1C and 4.1D). We assessed the mRNA and protein expression levels of LDHB, encoding LDH heart subunit (LDH H) that converts lactate to pyruvate (Dawson et al., 1964). Compared to NB, the mRNA level of LDHB was 8.4-fold higher ($P < 0.0002$) in WB tissues (Fig. 4.1B). Western blot analyses revealed that WB exhibited 13.6-fold higher ($P < 0.003$) LDHB protein levels compared to NB muscles (Fig. 4.1C and 4.1E).

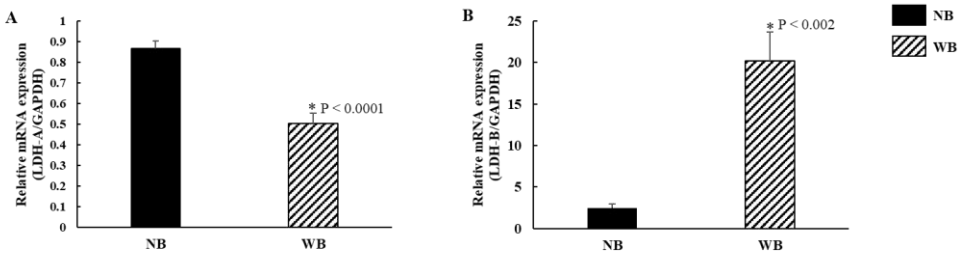

Figure 4.1 The altered mRNA and protein levels of LDHA and LDHB in WB compared to NB tissues. (A) Relative LDHA mRNA expression in NB and WB tissues determined by qRT-PCR with normalization to the reference GAPDH mRNA levels. NB data is represented by the filled bar while the WB data is represented by the hatched bar. Data are represented as means ± SEM of 8 NB and 8 WB tissues. (B) Relative LDHB mRNA level, measured in the same experiment as in (A), was upregulated in WB tissues (N= 8) compared to NB tissue (N = 8). (C) Representative Immunoblots showing protein expression levels of LDHA, LDHB and GAPDH in lysates of NB and WB tissues. GAPDH band is shown as an internal control for sample loading. (D) The graph of immunoblot data shows that there is no significant difference of the levels of LDHA protein between NB (N = 8) and WB (N = 8) tissues. (E) Graphical representation of LDHB immunoblot data, showing greater levels of LDHB protein in WB tissue compared to NB tissue.

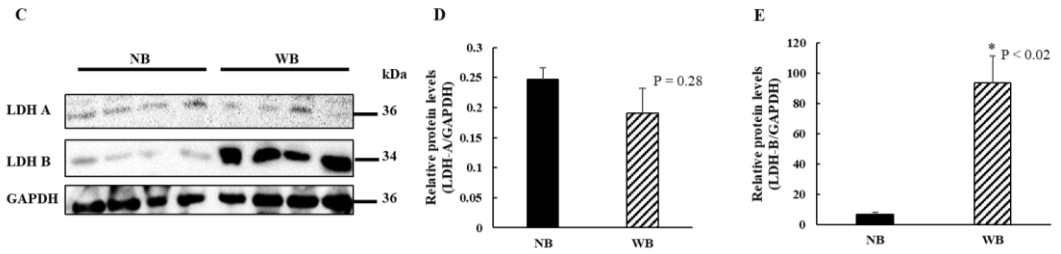

Figure 4.1 Continued.

4.3.2. The levels of miR-375 expression in WB did not differ from those of NB tissues

Levels of miR-375 were reported to be inversely associated with LDHB protein levels in human squamous cell carcinoma (Kinoshita et al., 2012). To test whether the increased LDHB protein levels observed in WB tissue was mediated by miR-375, we performed qRT-PCR analysis on expression of miR-375 in both NB and WB muscles. Wooden breast muscle exhibited a significant reduction of miR-375 (1.4-fold lower levels) compared to NB levels ($P < 0.025$, Fig. 4.2).

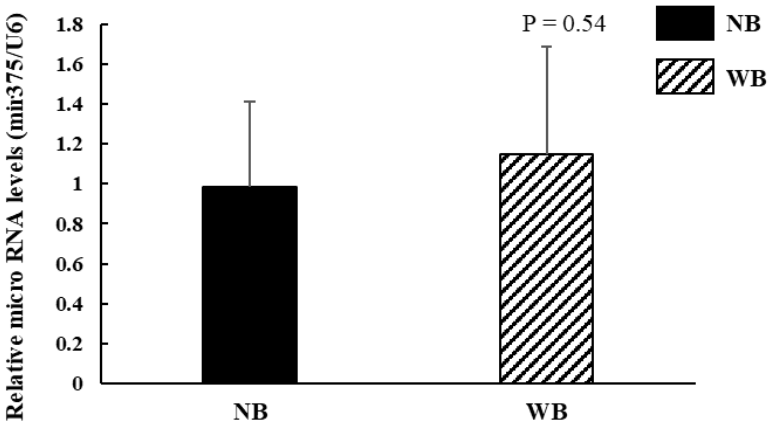

Figure 4.2 The levels of miR-375 expression in WB did not differ from those of NB tissues. Small RNAs from NB and WB were extracted using the mirVana PARIS kit as described in methods. Relative miR-375 expression was quantitated by qRT-PCR. Chicken U6 was used as an endogenous control for normalization. N = 8 per group.

4.3.3. WB has decreased specific LDH enzymatic activities that convert pyruvate to lactate

Given the enhanced LDHB protein expression in WB tissues that converts lactate to pyruvate, we also investigated the enzymatic activity of LDH-mediated lactate-to-pyruvate conversion. In contrast, the special enzymatic activity of LDH that converted pyruvate to lactate was 1.8-fold ($P < 0.01$) lower in WB tissues than NB tissues (Fig. 4.3).

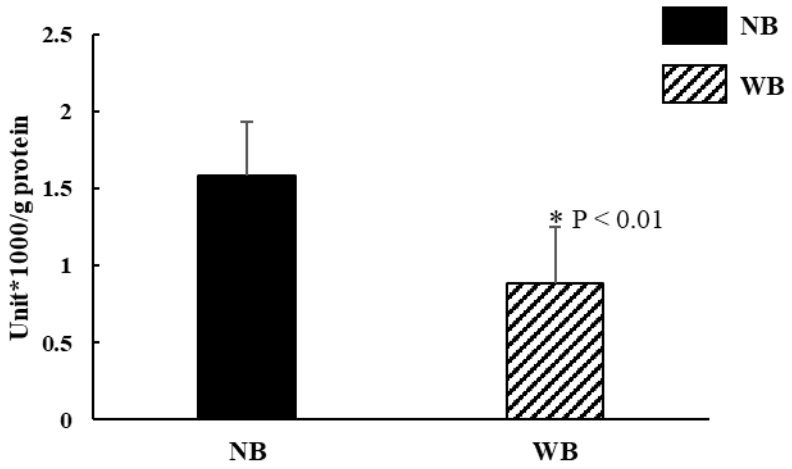

Figure 4.3 LDH enzyme activity that converts lactate to pyruvate is decreased in WB tissue compare to NB tissues. Results of LDH activity were normalized by using the same amount of total protein in the assay. The LDH enzyme activity of WB was significantly lower than NB. P <0.05 is significant different, N = 8 per group.

4.3.4. Gene expression of MCT1 and MCT4

Given the enhanced LDHB mRNA and protein levels in WB muscles compared to NB muscles, we also investigated the mRNA and protein expression of MCT1 and MCT4, which are implicated in lactate import and export in muscles, respectively (Halestrap and Meredith, 2004; Hashimoto et al., 2006; Juel and Halestrap, 1999; Ullah et al., 2006). We found that the relative mRNA levels of MCT1 and MCT4 were 2.3-fold and 2.8-fold

higher in WB muscles than those in NB muscles ($P < 0.02$), respectively (Fig. 4.4A and 4.4B). However, the protein level of MCT1 in WB was not different from that in NB tissues (Fig. 4.4D). Consistent with the up-regulated MCT4 mRNA levels, the expression levels of MCT4 protein were elevated (3.5-fold, $P < 0.005$) in WB tissues compared to NB tissues (Fig. 4.4C and 1.4E).

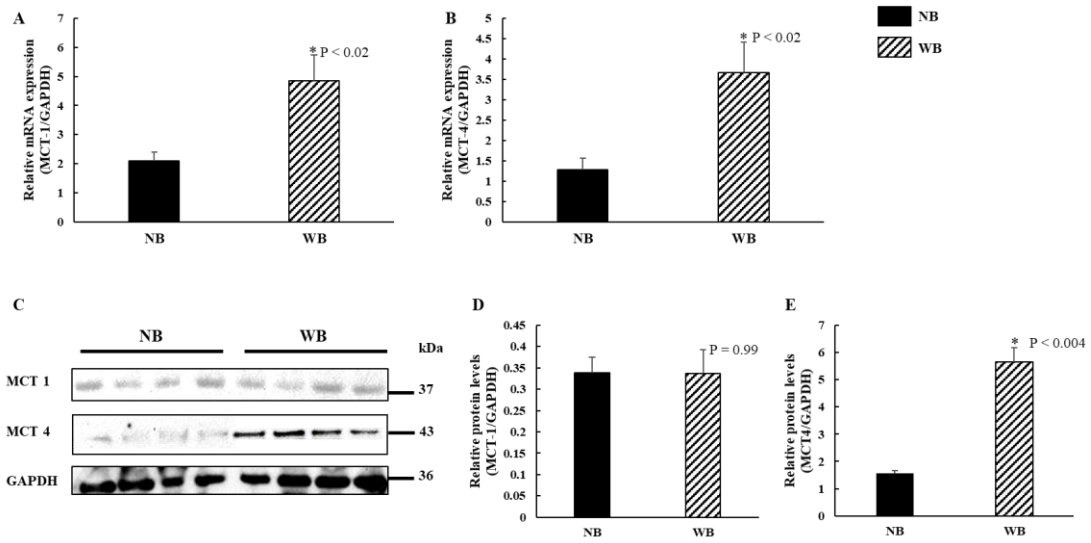

Figure 4.4 The altered mRNA and protein levels of MCT1 and MCT4 in WB compared to NB tissues. Relative levels of MCT1 mRNA (A) and MCT4 mRNA (B) in NB and WB tissues determined by qRT-PCR. (C) Western blot analyses were performed on breast muscle lysates prepared from NB and WB tissues. Protein sample (10 µg) was loaded in each lane. The GAPDH band was shown as internal control for sample loading. (D) Quantification of MCT1 protein level in NB and WB tissues. The protein levels of MCT1 in WB were not different from those in NB tissues. (E) The levels of MCT4 protein were 3.5-fold in WB compared to NB tissues. N = 8 per group.

4.4. Discussion

Wooden breast myopathy causes notable economic loss in the poultry industry and happens in about 48% to 73% of commercial broilers (Sihvo et al., 2014). The molecular mechanisms that cause wooden breast myopathy remain unclear. The presence of localized tissue hypoxia (Mutryn et al., 2015; Sihvo et al., 2018) and decreased lactate concentrations in WB (Abasht et al., 2016) indicate the potential alteration of genes involved in lactate metabolism. Identification of specific molecules that regulate lactate levels will improve our understanding of the mechanisms causing WB myopathy and potentially facilitate us to the development of useful therapeutic targets to eliminate the incidence of WB in broilers. In this study, we tested the hypothesis that the gene expression of the LDHA, LDHB, MCT1, and MCT4, involved in lactate metabolism, in WB muscles would change compared to their levels in NB muscles. Through a combination of qRT-PCR and immunoblotting assays, we have now shown that WB tissues indeed show significant up-regulation of both LDHB and MCT4 mRNA and protein levels, two key players that decrease lactate levels in WB tissues by oxidizing lactate to pyruvate and enhancing lactate efflux, separately (Fig. 4.5).

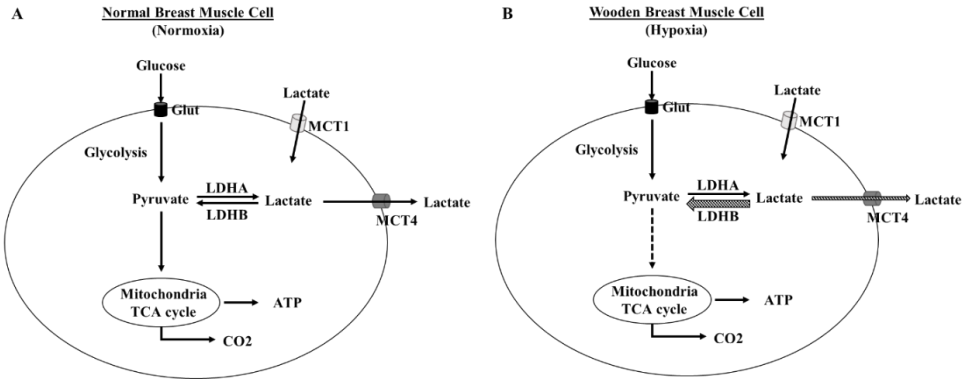

Figure 4.5 Schematic representation of the lactate metabolism pathway of broiler muscle affected with wooden breast (WB) myopathy (B) compared to normal breast muscle (A). Glucose is transported to the cell cytosol by the glucose transporter (Glut), and then is converted to pyruvate, the end product of glycolysis. Under normoxic conditions (A), pyruvate enters the mitochondria and produces 38 ATPs per oxidized glucose molecule, including glycolysis, tricarboxylic acid cycle (TCA cycle) and oxidative phosphorylation. In WB muscle, oxygen delivery is limited (hypoxia, B). The activity of TCA cycle is decreased and the pyruvate switches to the fermentation pathway, resulting in the production of lactate by the action of lactate dehydrogenase A (LDHA). The lactate can be re-oxidized to pyruvate by LDHB activity, or it can be transported out of the cell by the monocarboxylate transporter 4 (MCT4). On the other hand, MCT1 uptakes the lactate from the circulatory system into cells. Hatched arrows denote the possible fates for lactate in WB cells. In this model, increased levels of LDHB and MCT4 are the principal proteins that decrease lactate concentrations in the WB cells (B).

Although transcript levels of two genes, such as LDHA and MCT1, were downregulated and upregulated separately in WB muscles, we did not observe a concomitant reduction of LDHA or increase of MCT1 protein abundances. Both protein levels of LDHA and MCT1 did not change in WB tissues compared to NB tissues, even though their transcript levels significantly differed in WB muscles. Numerous reports have indicated that about 30-40% of the changes in mRNA levels are not correlated to the corresponding protein levels due to multiple factors, including differential turnover rates of transcripts or the presence of post-transcriptional or post-translational control mechanisms (Vogel and Marcotte, 2012; Payne, 2015; Karbownik et al., 2016).

High-throughput technologies such as RNA-seq (Mutryn et al., 2015; Papah et al., 2018; Marchesi et al. 2019) and proteomics (Kuttappan et al., 2017; Cai et al., 2018) have been used to identify differentially expressed molecular components in WB. In accordance with our report, Marchesi et al. (2019) showed the upregulation of LDHB mRNA levels and the reduction of LDHA mRNA levels in a different skeletal muscle myopathy known as white striping. However, there are several conflicting reports describing LDHA protein expression in WB tissues (Soglia et al. 2016; Zambonelli et al., 2016; Kuttappan et al., 2017; Cai et al., 2018). Lactate dehydrogenase A protein levels of WB muscles have been reported to be decreased 2-fold compared to the NB in a proteomic study (Kuttappan et al., 2017). The combination of two-dimensional gel electrophoresis and mass spectrometry by Cai et al. (2018) only identified eight differentially expressed proteins in WB compared to normal breast muscles, and, LDH was not one of them. In fact, sarcoplasmic LDH protein levels in WB have been reported to be higher (ranging from 14% to 22%) in WB than that of NB using an SDS-PAGE method (Soglia et al. 2016; Zambonelli et al., 2016). The positive identification of LDH protein in Soglia et al. (2016) and Zambonelli et al. (2016) was confirmed by expected molecular weight of the protein in SDS-PAGE gel, although it is not known which LDH subunit was involved since immunoblotting methods using specific antibodies were not employed. This discrepancy about the levels of LDHA protein expression could reflect differences in the choice of sample extraction, preparation, and separation methods.

To our knowledge, this is the first report of up-regulation of LDHB protein expression in WB muscles. We confirmed more than 13-fold higher LDHB protein expression in WB tissues than those in NB tissues using western blot analysis. Recent

studies on WB have indicated the changes in several glycolytic proteins (Soglia et al., 2016; Zambonelli et al., 2016; Cai et al., 2018). However, none of the studies found the dramatic change in levels of LDHB protein in WB. These studies provide potential candidate signaling molecules and pathways in WB, however, the challenges with finding a low-abundance of regulatory protein remains to be solved by classical proteomics (Cho, 2007; Chandramouli and Qian, 2009). In fact, LDHA is the most abundant subtype of LDH in pectoralis major muscles of chickens (Dawson et al., 1964; Heinova et al., 1999). Lactate dehydrogenase B, a very low-abundance protein in pectoralis major muscles, may not be detectable without proper pretreatment and handling (Andrecht and Hagen, 2008). Using an immunoblotting method with the specific antibody has enabled us to detect the low-concentration of LDHB in our study.

Despite the lower abundance of LDHB protein compared to LDHA protein in normal skeletal muscle, it is not clear why LDHB protein levels were upregulated more than 13-fold in WB muscles compared to NB muscles. One possible mechanism for upregulating LDHB in WB tissue involves the conversion of lactate to pyruvate. To investigate if LDHB decreases lactate levels in WB, we mined published metabolomic datasets from well-characterized WB and NB of different broiler breeds (Supplementary 2 files in Abasht et al., 2016). We found that upregulation of LDHB protein levels in WB is correlated with reduction of lactate content. The WB muscles showed 0.66 (*P = 0.17*), 0.72 ($P<0.002$) and 0.56-fold ($P<0.005$) reduction in lactate levels from two genetically distinct purebred lines and a commercial breed line, respectively. These data suggest that elevated LDHB protein expression in WB muscles (this study) may contribute to decreased levels of lactate in WB muscles from different broiler breeds (Abasht et al., 2016). The reduction

of lactate contents is correlated with upregulation of LDHB gene expression in WB muscle cells, resulting in an increase in cellular pH value. Tasoniero et al. (2016) reported that the breasts with both white striping and WB exhibited the highest pH values than the normal and white striping groups. Various studies also confirmed increased pH values in WB muscles (Petracci et al., 2013; Dalle Zotte et al., 2014, 2015; Mudalal et al., 2015; Zambonelli et al., 2016). The other possibility for up-regulation of LDHB is through the downregulation of micro RNA, miR-375, which is involved in regulating lactate metabolism in several cancer cells including skin, lung, rectal, and gastric cancers by targeting the LDHB gene (reviewed in Haziapostolou et al, 2013). Isozaki et al. (2012 and 2014) previously revealed that there was an inverse relationship between miR-375 and LDHB using the esophageal squamous cancer cells. In addition, Kinoshita et al (2012) also found the inverse correlation of miR-375 and LDHB with human squamous cell carcinoma. However, the relationship between the miR-375 and LDHB expression was unclear in WB muscles of broilers. In the present study, we found that WB muscles had a higher LDHB mRNA expression and a lower miR-375 expression compared to NB muscles, which is consistent with previous reports of inverse relationship of LDHB and miR-375 from human studies (Haziapostolou et al, 2013).

There is limited information regarding the distribution of isoenzymes of LDH in adult chicken breast tissue. As reviewed by Gallo et al., 2015, LDH isoforms are present in all tissues at different ratios, so that the isoenzymatic profile is tissue-specific. The compositions of LDH isoenzymes in chicken breast muscles have been reported to be regulated depending on the developmental stages (Lindsay, 1963) and pathological conditions (Kaplan and Cahn, 1962). Kaplan and Cahn (1962) reported the complete

changes in LDH isoform enzymes in the chicken breasts from LDH1 (four LDHB subunits) in early embryos to the LDH5 (all four LDHA subunits) in adult chicken. In contrast, Lindsey (1963) indicated the presence of small amounts of LDH4 (3A1B) and that there may be undetectable levels of LDH3 (2A2B) in adult chicken breast muscles due to the poor sensitivity of the method they used. We studied LDH isoenzyme patterns of WB and NB tissues using an electrophoresis of native polyacrylamide gel, which have LDH5 almost exclusively, but levels of LDH5 isoenzyme between WB and NB tissues were undistinguishable (Data not shown). Similar results were reported by Dawson et al (1964), with a different unknown breed of chicken, indicated that that LDH5 enzymatic activity was at least 4,300 times greater than LDH1 in breast muscles. We subsequently evaluated the specific isoenzyme activity of LDH-mediated lactate to pyruvate and found that it was significantly reduced in WB muscles compared to the NB muscles, which agreed with Wieme and Herpol's (1962) report that total LDH activity was decreased in dystrophic human and chicken muscles (Wilson et al., 1988). However, the organization of the LDH subunits in the chicken dystrophic skeletal muscle cells have been changed, resulting in the up-regulation of LDH1 (four LDHB subunits) and the reduction of LDH5 (all four LDHA subunits) compared to normal breast muscles (Kaplan and Cahn, 1962). The majority of studies of LDH enzyme activity in WB muscles of broilers have been focused on the changes of the enzyme activity of LDH-mediating pyruvate-to-lactate conversion in serum or plasma from broilers affected by breast muscle myopathy. For example, serum LDH activity in white striping breast muscles of broilers was elevated (Kuttappan et al., 2013). Recent studies suggested the association of increased plasma total LDH enzyme activity with the severity of WB (Meloche et al., 2018a and b). However, the

distribution of LDH isoenzymes in broiler blood are totally different from those in breast muscles, containing mixing populations of LDH isoenzymes (66%:23%:6%:5%:3% of LDH5, LDH4, LDH3, LDH2, and LDH1) in serum and an exclusive LDH5 in chicken breast muscles, separately (Heinova et al., 1999). Our data suggests that broiler breast muscles contain a majority of LDH5 isoenzyme (all four LDHA subunits) and a very small amount of isoenzyme containing LDHB subunits that function in oxidizing lactate to pyruvate.

In skeletal muscles, MCT1 and MCT4 are the two major MCT isoforms that help the import and export lactate through the cell membrane, respectively (Garcia et al., 1994; Wilson et al., 1998). Little is known about differences of MCT1 and MCT4 protein expression in WB tissues of broilers compared to NB tissues. We found mRNA expression of MCT1 was higher in WB muscles compared to NB muscles. However, the protein levels of MCT1 was not different between WB and NB tissues. In humans, MCT1 gene expression increased in muscles after short-term training (Bonen et al., 1998). Short-term training induced fermentative glycolysis in the skeletal muscle, which is similar to hypoxia in broilers with wooden breast myopathy. Monocarboxylate transporter 4 is highly expressed in white muscles and plays an important role exporting lactate out of cells (Dimmer et al., 2000). Chronic hypoxia has been reported to enhance protein levels of MCT4, not MCT1, in rat skeletal muscles (Py et al., 2005). This selection of upregulation of MCT4 protein, not MCT1 in WB muscles, allows the increased export of lactate out of muscle cells during hypoxia conditions.

In conclusion, the findings of this study demonstrated that WB muscles of broilers exhibited upregulations of LDHB and MCT4 mRNA and protein abundances, decreased

expression of miR-375, and downregulation in specific activity of LDH-mediated lactate to pyruvate. Our results, therefore, provide molecular mechanisms by which enhanced expression of LDHB and MCT4 gene decrease lactate levels in WB muscles of broiler.

4.5. References

Abasht, B., M. F. Mutryn, R. D. Michalek, and W. R. Lee. 2016. Oxidative stress and metabolic perturbations in wooden breast disorder in chickens. PLoS One. 11:e0153750.

Aguirre, M. E., C. M. Owens, R. K. Miller, and C. Z. Alvarado. 2018. Descriptive sensory and instrumental texture profile analysis of woody breast in marinated chicken. Poult. Sci. 97:1456-1461.

Andrecht, S. and von Hagen. 2008. General aspects of sample preparation for comprehensive proteomics analysis in proteomic sample preparation (ed. Jörg von Hagen). Weinheim: WILEY-VCH Verlag: 5-20.

Bailey, R. A., K. A. Watson, S. F. Bilgili, and S. Avendano. 2015. The genetic basis of pectoralis major myopathies in modern broiler chicken lines. Poult. Sci. 94:2870-2879.

Benton, C. R., Y. Yoshida, J. Lally, X. Han, H. Hatta, and A. Bonen. 2008. PGC-1alpha increases skeletal muscle lactate uptake by increasing the expression of MCT1 but not MCT2 or MCT4. Physiol. Genomics. 3:45-54.

Bonen, A., K. J. McCullagh, C. T. Putman, E. Hultman, N. L. Jones, and G. J. Heigenhauser. 1998. Short-term training increases human muscle MCT1 and femoral venous lactate in relation to muscle lactate. Am. J. Physiol. Endocrinol. Metab. 274:102-107.

Cahn, R. D., E. Zwilling, N. O. Kaplan, and L. Levine. 1962. Nature and development of lactic dehydrogenase: the two major types of this enzyme from molecular hybrids which change in makeup during development. Science. 136:962-969.

Chandramouli, K., and P. Y. Qian. 2009. Proteomics: challenges, techniques and possibilities to overcome biological sample complexity. Hum Genomics Proteomics. 2009:239204.

Cho, W. C. 2007. Proteomics technologies and challenges. Genomics Proteomics Bioinformatics. 5:77–85.

Dawson, D. M., T. L. Goodfriend, and N. O. Kaplan. 1964. Lactic dehydrogenases: Functions of the two types rates of synthesis of the two major forms can be correlated with metabolic differentiation. Science. 143:929-933.

Dalle Zotte, A., M. Cecchinato, A. Quartesan, J. Bradanovic, G. Tasoniero, and E. Puolanne. 2014. How does "Wooden Breast" myodegeneration affect poultry meat quality? In: 60th Int. Congr. Meat Sci. Technol., Punta Del Este, Uruguay. 22:476-479.

Dalle Zotte, A., G. Tasoniero, E. Puolanne, H. Remignon, M. Cecchinato, E. Catelli, and M. Cullere. 2017. Effect of "Wooden Breast" appearance on poultry meat quality, histological traits, and lesions characterization. Czech J. Anim. Sci. 62:51-57.

Dawson, D. M., T. L. Goodfriend, and N. O. Kaplan. 1964. Lactic dehydrogenases:functions of the two types rates of synthesis of the two majorforms can be correlated with metabolic differentiation. Science. 143:929-933.

de Fremery, D., and M. F. Pool. 1963. The Influence of Post-mortem Glycolysis on Poultry Tenderness. J. Food Sci. 28:173-176.

Dimmer K. S., B. Friedrich, F. Lang, J. W. Deitmer, and S. Bröer. 2000. The low-affinity monocarboxylate transporter MCT4 is adapted to the export of lactate in highly glycolytic cells.. Biochem J. 350:219-227.

Ding J, J. E. Karp, and A. Emadi. 2017. Elevated lactate dehydrogenase (LDH) can be a marker of immune suppression in cancer: Interplay between hematologic and solid neoplastic clones and their microenvironments. Cancer Biomark. 19:353-363.

Drent M, N. A. Cobben, R. F. Henderson, E. F. Wouters, and M. van Dieijen-Visser. 1996. Usefulness of lactate dehydrogenase and its isoenzymes as indicators of lung damage or inflammation. Eur. Respir J. 9:1736-1742.

Gallo, M., L. Sapio, A. Spina, D. Naviglio, A. Calogero, and S. Naviglio. 2015. Lactic dehydrogenase and cancer: an overview. Front. Biosci. 20:1234-1249.

Garcia, C. K., J. L. Goldstein, R. K. Pathak, R. G. Anderson, and M. S. Brown. 1994. Molecular characterization of a membrane transporter for lactate, pyruvate, and other monocarboxylates: implications for the Cori cycle. Cell. 76:865-873.

Griffin, J. R., L. Moraes, M. Wick, and M. S. Lilburn. 2018. Onset of white striping and progression into wooden breast as defined by myopathic changes underlying *Pectoralis major* growth. Estimation of growth parameters as predictors for stage of myopathy progression. Avian Pathol. 47:2–13.

Guo, Y., P. Zhao, G. Guo, Z. Hu, L. Tian, K. Zhang, Y. Sun, X. Zhang, W. Zhang, and M. Xing. 2016. Effects of arsenic trioxide exposure on heat shock protein response in the immune organs of chickens. Biol. Trace Elem. Res. 169:134-141.

Halestrap, A. P., and D. Meredith. 2004. The SLC16 gene family—from monocarboxylate transporters (MCTs) to aromatic amino acid transporters and beyond. Pflügers Archiv. 447:619-628.

Halestrap, A. P., and N. T. Price. 1999. The proton-linked monocarboxylate transporter (MCT) family: structure, function and regulation. Biochem. J. 343:281-99.

Hatziapostolou, M, C. Polytarchou, and D. Iliopoulos. 2013. miRNA link metabolic reprogramming to oncogenesis. Trends Endocrinol. Metab. 24:361-373.

Hashimoto, T., R. Hussien, and G. A. Brooks. 2006. Colocalization of MCT1, CD147, and LDH in mitochondrial inner membrane of L6 muscle cells: evidence of a mitochondrial lactate oxidation complex. Am. J. Physiol. Endocrinol Metab. 290:1237-1244.

Heinova, D., I. Rosival, Y. Avidar, and E. Bogin. 1999. Lactate dehydrogenase isoenzyme distribution and patterns in chicken organs. Res. in Vet. Sci. 67:309-312.

Hoving-Bolink, A. H., R. W. Kranen, R. E. Klont, C. L. M. Gerritsen, and H. de Greef K. 2000. Fibre area and capillary supply in broiler breast muscle in relation to productivity and ascites. Meat Sci. 56:397-402.

Imagawa, T., E. Yamamoto, M. Sawada, M. Okamoto, and M. Uehara. 2006. Expression of lactate dehydrogenase-A and -B messenger ribonucleic acids in chick glycogen body. Poult. Sci. 85:1232-1238.

Isozaki, Y., I. Hoshino, N. Nohata, T. Kinoshita, Y. Akutsu, N. Hanari, M. Mori, Y. Yoneyama, N. Akanuma, N. Takeshita, T. Maruyama, N. Seki, N. Nishino, M. Yoshida, and H. Matsubara. 2012. Identification of novel molecular targets regulated by tumor suppressive miR-375 induced by histone acetylation in esophageal squamous cell carcinoma. Int. J. Oncol. 41:985–994.

Juel, C., and A. P. Halestrap. 1999. Lactate transport in skeletal muscle - role and regulation of the monocarboxylate transporter. J. Physiol. 517:633-642.

Karbownik, M. S., J. Szemraj, Ł. Wieteska, A. Antczak, P. Górski, E. Kowalczyk, and T. Pietras. 2016. Antipsychotic drugs differentially affect mRNA expression of genes encoding the neuregulin 1-downstream ErbB4-PI3K pathway. Pharmacology. 98:4-12.

Kaplan, N. O., and R. D. Cahn. 1962. Lactic dehydrogenases and muscular dystrophy in the chicken. Proc. Nat. Acad. Sci. 48:2123-2130.

Kato, G. J., V. McGowan, R. F. Machado, J. A. Little, J.Taylor, VI, C. R. Morris, J. S. Nichols, X. Wang, M. Poljakovic, S. M. Morris, Jr, and M. T. Gladwin. 2006. Lactate dehydrogenase as a biomarker of hemolysis-associated nitric oxide resistance, priapism, leg ulceration, pulmonary hypertension, and death in patients with sickle cell disease. Blood. 107:2279–2285.

Kinoshita, T., N. Nohata, H. Yoshino, T. Hanazawa, N. Kikkawa, L. Fujimura, T. Chiyomaru, K. Kawakami, H. Enokida, M. Nakagawa, Y. Okamoto, and N. Seki. 2012. Tumor suppressive microRNA-375 regulates lactate dehydrogenase B in maxillary sinus squamous cell carcinoma. Int. J. Oncol. 40:185-193.

Kumar, S., H. Xie, P. Scicluna, L. Lee, V. Björnhagen, A. Höög, C. Larsson, and W. O. Lui. 2018. *MiR-375* regulation of LDHB plays distinct roles in polyomavirus-positive and -negative Merkel cell carcinoma. Cancers.10: e443.

Kuttappan, V. A., V. B. Brewer, J. K. Apple, P. W. Waldroup, and C. M. Owens. 2012. Influence of growth rate on the occurrence of white striping in broiler breast fillets. Poult. Sci. 91:2677-2685.

Kuttappan, V. A., H. L. Shivaprasad, D. P. Shaw, B. A. Valentine, B. M. Hargis, F. D. Clark, S. R. McKee, and C. M. Owens. 2013. Pathological changes associated with white striping in broiler breasts muscles. Poult. Sci. 92:331-338.

Kuttappan, V. A., B. M. Hargis, and C. M. Owens. 2016. White striping and woody breast myopathies in the modern poultry industry: a review. Poult. Sci. 95:2724-2733.

Kuttappan, V. A., W. Bottje, R. Ramnathan, S. D. Hartson, C. N. Coon, B. W. Kong, C. M. Owens, M. Vazquez-Añon, and B. M. Hargis. 2017. Proteomic analysis reveals changes in carbohydrate and protein metabolism associated with broiler breast myopathy. Poult. Sci. 96:2992-2999.

Kuttappan, V. A., G. R. Huff, W. E. Huff, B. M. Hargis, J. K. Apple, C. Coon, and C. M. Owens. 2013a. Comparison of hematologic and serologic profiles of broiler birds with normal (NORM) and severe (SEV) degrees of WS in breast fillets. Poult. Sci. 92:339–345.

Lindsay D. T. 1963. Isozyme patterns and properties of lactate dehydrogenase from developing tissues of the chicken. J. Exp. Zool. 152:75-89.

Macrae, V. E., M. Mahon, S. Gilpin, D. A. Sandercock, and M. A. Mitchell. 2006. Skeletal muscle fibre growth and growth associated myopathy in the domestic chicken (Gallus domesticus). Br. Poult. Sci. 47:264-272.

Marchesi, J. A. P., A. M. G. Ibelli, J. O. Peixoto, M. E. Cantão, J. R. C. Pandolfi, C. M. M. Marciano, R. Zanella, M. L. Settles, L. L. Coutinho, and M. C. Ledur. 2019. Whole transcriptome analysis of the pectoralis major muscle reveals molecular

mechanismsinvolved with white striping in broiler chickens. Poult. Sci. 98:590-601.

Mazzoni, M., M. Petracci, A. Meluzzi, C. Cavani, P. Clavenzani, and F. Sirri. 2015. Relationship between pectoralis major muscle histology and quality traits of chicken meat. Poult. Sci. 94:123-130.

Meloche, K. J., B. I. Fancher, D. A. Emmerson, S. F. Bilgili, and W. Dozier. 2018a. Effects of quantitative nutrient allocaiton on myopathies of the Pectoralis major muscles in broiler chickens at 32, 43, and 50 days of age. Poult. Sci. 97:1786-1793.

Meloche, K. J, B. I. Fancher, D. A. Emmerson, S. F. Bilgili, and W. Dozier. 2018b. Effects of reduced dietary energy and amino acid density on Pectoralis major myopathies in broiler chickens at 36 and 49 days of age. Poult. Sci. 97:1794-1807.

Mudalal, S., M. Lorenzi, F. Soglia, C. Cavani, and M. Petracci. 2015. Implications of white striping and wooden breast abnormalities on quality traits of raw and marinated chicken meat. Animal. 9:728-734.

Mutryn, M. F., E. M. Brannick, W. Fu, W. R. Lee, and B. Abasht. 2015. Characterization of a novel chicken muscle disorder through differential gene expression and pathway analysis using RNA-sequencing. BMC Genomics. 16:399.

National Chicken Council 2018 Statistics and research: Per capita consumption of poultry and livestock, 1965 to Estimated 2019, in Pounds https://www.nationalchickencouncil.org/about-the-industry/statistics/per-capita-consumption-of-poultry-and-livestock-1965-to-estimated-2012-in-pounds/ Accessed December 2018

Papah, M. B., E. M. Brannick, C. J. Schmidt, and B. Abash. 2018. Gene expression profiling of the early pathogenesis of wooden breast disease in commercialbroiler chickens usin g RNA-sequencing. PLoS One. 13:e0207346.

Payne, S. H. 2015. The utility of protein and mRNA correlation. Trends Biochem. Sci. 40:1-3.

Pesce, A., R. H. McKay, F. Stolzenbach, R. D. Cahn, and N. O. Kaplan. 1964. The comparative enzymology of lactic dehydrogenases: I. properties of the crystalline beef and chicken enzymes. J. Biol. Chem. 239:1753-1761.

Petracci, M., S. Mudalal, A. Bonfiglio, and C. Cavani. 2013. Occurrence of white striping under commercial conditions and its impact on breast meat quality in broiler chickens. Poult. Sci. 92:1670-1675.

Petracci, M., S. Mudalal, F. Soglia, and C. Cavani. 2015. Meat quality in fast-growing broiler chickens. Worlds Poult. Sci. J. 71:363-374.

Py, G., N. Eydoux, K. Lambert, R. Chapot, N. Koulmann, H. Sanchez, L. Bahi, A. Peinnequin, J. Mercier, and A. X. Bigard. 2005. Role of hypoxia-induced anorexia and right ventricular hypertrophy on lactate transport and MCT expression in rat muscle. Metabolism. 54: 634-644.

Roth, D. A. and G. A. Brooks. 1990. Lactate transport is mediated by a membrane-bound carrier in rat skeletal muscle sarcolemmal vesicles. Arch. Biochem. Biophys. 279:377-385.

Schmittgen, T. D. and K. J. Livak. 2008. Analyzing real-time PCR data by the comparative C_T method. Nat. Protoc. 3:1101.

Sihvo, H. K., K. Immonen, and E. Puolanne. 2014. Myodegeneration with fibrosis and regeneration in the pectoralis major muscle of broilers. Vet. Pathol. 51:619-623.

Sihvo, H. K., J. Lindén, N. Airas, K. Immonen, J. Valaja, and E. Puolanne. 2017. Wooden breast myodegeneration of pectoralis major muscle over the growth period in broilers. Vet. Pathol. 54:119-128.

Sihvo, H. K., N. Airas, J. Lindén, and E. Puolanne. 2018. Pectoral vessel density and early ultrastructural changes in broiler chicken wooden breast myopathy. J. Comp. Pathol. 161:1-10.

Soglia, F., S. Mudalal, E. Babini, M. Di Nunzio, M. Mazzoni, F. Sirri, C. Cavani, and M. Petracci. 2016. Histology, composition, and quality traits of chicken Pectoralis major muscle affected by wooden breast abnormality. Poult. Sci. 95:651-659.

Summermatter, S., G. Santos, J. Pérez-Schindler, and C. Handschin. 2013. Skeletal muscle PGC-1α controls whole-body lactate homeostasis through estrogen-related receptor α-dependent activation of LDH B and repression of LDH A. Proc. Natl. Acad. Sci. U. S. A. 110:8738-8743.

Tallentire, C. W., I. Leinonen, and I. Kyriazakis. 2018. Artificial selection for improved energy efficiency is reaching its limits in broiler chickens. Sci. Rep. 8:1168.

Tasoniero, G., M. Cullere, M. Cecchinato, E. Puolanne, and A. Dalle Zotte. 2016. Technological quality, mineral profile, and sensory attributes of broiler chicken breasts affected by white striping and wooden breast myopathies. Poult. Sci. 95:2707-2714.

Tijare, V.V., F. L. Yang, V. A. Kuttappan, C. Z. Alvarado, C. N. Coon, and C. M. Owens. 2016. Meat quality of broiler breast fillets with white striping and woody breast muscle myopathies. Poult. Sci. 95:2167-2173.

Ullah, M. S., A. J. Davies, and A. P. Halestrap. 2006. The plasma membrane lactate transporter MCT4, but not MCT1, is up-regulated by hypoxia through a HIF-1alpha-dependent mechanism. J. Biol. Chem. 281:9030-9037.

Velleman, S. G., and D. L. Clark. 2015. Histopathologic and myogenic gene expression changes associated with wooden breast in broiler breast muscles. Avian Dis. 59:410-418.

Vogel, C., and E. M. Marcotte. 2012. Insights into the regulation of protein abundance from proteomic and transcroptomic analyses. Nat. Rev. Genet. 13:227-232.

Wieme, R. J., and J. E. Herpol. 1962. Origin of the lactate dehydrogenase isoenzyme pattern found in the serum of patients having primary musclular dystrophy. Nature. 194:287-288.

Wilson, B. W., W. R. Randall, G. T. Patterson, and R. K. Entrikin. 1979. Major physiologic and histochemical characteristics of inherited dystrophy of the chicken. Ann. N. Y. Acad. Sci. 317:224-246.

Wilson, B. W., H. Abplanalp, R.J. Buhr, R. J.Entrikin, M. J. Hooper, and P. S. Nieberg. 1988. Inbred crosses and inherited muscular dystrophy of the chicken. Poult. Sci. 67:367-374.

Wilson, M. C., V. N. Jackson, C. Heddle, N. T. Price, H. Pilegaard, C. Juel, A. Bonen, I. Montgomery, O. F. Hutter, and A. P. Halestrap. 1998. Lactic acid efflux from white skeletal muscle is catalyzed by the monocarboxylate transporter isoform MCT3. J. Biol. Chem. 273:15920-15926.

Zampiga, M., J. Flees, A. Meluzzi, S. Dridi, and F. Sirri. 2018. Application of omics technologies for a deeper insight into quali-quantitative production traits in broiler chickens: A review. J. Anim. Sci. Biotechnol. 9:61.

Zambonelli, P., M. Zappaterra, F. Soglia, M. Petracci, F. Sirri, C. Cavani, and R. Davoli. 2016. Detection of differentially expressed genes in broiler pectoralis major muscle affected by white striping - wooden breast myopathies. Poult. Sci. 95:2771-2785.

Zhang, S., B. Saremi, E. R. Gilbert, and E. A. Wong. 2017. Physiological and biochemical aspects of methionine isomers and a methionine analogue in broilers. Poult. Sci. 96:425-439.

Zuidhof, M. J., B. L. Schneider, V. L. Carney, D. R. Korver, and F. E. Robinson. 2014. Growth, efficiency, and yield of commercial broilers from 1957, 1978, and 20051. Poult. Sci. 93:2970-2982.

5. CONCLUSIONS

Salmonella Typhimurium contamination in poultry products is still a major concern for human health. The lack of available *in vivo* intestinal models is a limitation for researchers to investigate the molecular mechanisms of *Salmonella* persistence in the avian intestine. To date, there are no chicken intestinal epithelia cell lines available. Therefore, establishing an avian intestinal organoid model (IO) not only represents a valuable *in vitro* model for study of the avian intestinal system in health and disease and but also has the potential to reduce the use of animals in animal testing studies. *In vivo* animal experiments are also important to our understanding of the mechanism of *Salmonella* infection. Molecular signatures present in circulating exosomes, especially microRNAs (miRNA), play important roles in intercellular communication and have been implicated as novel mediators in host-pathogen interactions. Wooden breast (WB), which is one novel myopathy that happens in fast-growing broilers, causes huge economic losses in the poultry industry due to poor meat quality. However, the causes of WB are still not completely understood. The aims for my work in this dissertation were to (1) establish and characterize an avian intestinal *in vitro* model for a host-pathogen interaction studies, (2) elucidate the functional role of exosomes in circulatory system in host immunity to *Salmonella* infection, and (3) evaluate if altered lactate homeostasis was present in WB muscles of broilers.

In the first experiment, crypt-derived organoids were successfully grown and propagated to form 3D sphere-like structures that were cultured for up to three weeks. We demonstrated that organoids can be derived from intestines from any age of chicken,

consisting of enterocytes, stem cells, enteroendocrine cells, Paneth cells, goblet cells and stem cells, recapitulating the structure and function of the avian intestine *in vivo*. Furthermore, OGM supplemented with both valproic acid and CHIR99021, a glycogen synthase kinase 3β inhibitor and a histone deacetylase inhibitor, increased the size of the avian IO ($P < 0.001$). To our knowledge, this work was the first comprehensive report for establishing long-term, organoid cultures from small intestines and ceca of layer and broiler chickens, which will help us to better understand host-pathogen interactions, eventually leading to the discovery of pathogen intervention strategies in poultry. Furthermore, we anticipate the organoid model will play important roles to advance our knowledge in antimicrobial drug screening, molecular mechanism of cross talk between gut epithelial and immune cells, dietary supplement screening to improve gut health in poultry, and vaccine development.

Recent studies have identified host-derived exosomes that are associated with immune response; however, the role of chicken serum-derived exosomes in host immunity to *Salmonella* infection remains unclear. We successfully characterized a total of 292 exosomal miRNAs in serum of control and ST-challenged birds. The miRNA profiles in exosomes of serum in the ST group were significantly different from those in the Con group. Significantly, 17 miRNAs were up-regulated, and 12 miRNAs were down-regulated in the ST infected birds compared to the Con birds ($P < 0.05$), which suggests that exosomal miRNA act as important modulators for host-pathogen interaction in broilers. The top 6 upregulated exosomal miRNAs, from the same family of gga-miR34b/c and gga-miR-449d/a/b/c, containing two conservative seed sequences, in ST birds were implicated in target genes involved in modulating humoral, innate, and adaptive immune response,

cytokine-mediate signaling pathway, B cell proliferation and differentiation, natural killer cells and T cell activation involved in immune responses, positive regulation of peptidyl-serine phosphorylation of STAT protein, and Notch signaling pathway. Our study firstly reports the DE miRNA in serum-derived exosomes extracted from the ST-infected birds. Circulating exosomal cluster miRNAs from gga-miR34b/c and gga-miR-449d/a/b/c/ family could be served as immune-modulators and may provide an opportunity to understand the mechanism of chicken-*ST* interactions.

In the third experiment of this dissertation, the expression levels of the major signaling molecules that control lactate metabolism, including lactate dehydrogenases (LDHA & B) and monocarboxylate transporters (MCT1 & 4) were analyzed in WB. Our current findings suggest the potential roles of LDHB and MCT4 on lactate metabolism and provide a unique molecular elucidation for altered lactate homeostasis in WB muscles of broilers. Future studies will involve isolating individual components of cells from WB tissues which will help us understand the cellular and molecular mechanisms behind WB muscles, leading to the development of new strategies for preventing and/or treating WB conditions.